Function of Titin in Striated Muscles in Health and Disease

Inaugural-Dissertation

To obtain the German academic degree

Doctor rerum naturalium (Dr. rer. nat.)

Submitted to the Department of Biology, Chemistry and Pharmacy

of the Freie Universität Berlin

by

Christopher Polack

from Eberswalde (Germany)

2015

I completed my doctorate studies from September 01, 2010 to March 31, 2015 under the supervision of Prof. Dr. M. Gotthardt at the Max Delbrück Center for Molecular Medicine, Berlin-Buch.

1st Reviewer: Prof. Dr. Simone Spuler

2nd Reviewer: Prof. Dr. Michael Gotthardt

Date of defense: Berlin-Dahlem; 15.10.2015

Table of contents

1 Abstract

Titin forms a continuous filament along the myofibril and is essential for the development, the maintenance and the passive stiffness of the sarcomere. It contains the cardiac specific elastic N2B, and differentially spliced elastic PEVK region, as well as a titin kinase domain. Mutations of titin have been associated with severe cardiac and skeletal myopathies such as dilated cardiomyopathy (DCM) or hereditary myopathy with early respiratory failure (HMERF). To understand the role of titin's functional domains in striated muscle health and disease, we created diverse knockout mice (KO). They demonstrated the importance of M-band titin for the structural integrity of the sarcomere and the relation of the N2B and PEVK domains to cardiac trophic signaling and ventricular filling. To eliminate the holoprotein, we have generated a complete Titin knockout (TiEx2MCK) flanking the exon containing the ATG with lox sites and expressing the CRE recombinase in striated muscle. The comparison of the Z-disc to the M-band KO mouse included phenotypic, morphologic, ultrastructural, transcriptomic and proteomic analyses. Both KO models developed a severe skeletal muscle atrophy caused by the disassembly of the sarcomere which led to a decreased body weight, strength endurance, and survival. The same sarcomere disassembly was present in cardiomyocytes of both models but led to the development of DCM in the TiEx2MCK KO whereas M-band titin deficiency led to cardiac atrophy. These cardiac abnormalities can contribute to the decreased survival of the Z-disc KO animals. The proteomic analysis of both KO models revealed the differential expression of atrophy and hypertrophy associated proteins such as FHL2. We concluded that in both animal models, the skeletal muscle atrophy was caused by sarcomere disassembly, which also contributed to the cardiac phenotype. Additionally, titin's N-terminus affects trophic signaling in the heart. This study validated titin's role as an essential sarcomeric protein that does not only serve as an elastic scaffold, but also contributes to the regulation of striated muscle size.

2 Zusammenfassung

Titin bildet ein kontinuierliches Filament entlang der Myofibrille und ist wichtig für den Aufbau, den Erhalt und die passive Steifheit des Sarkomeres. Das Protein enthält die herzspezifische elastische N2B Domäne und die differenziell gespleißte PEVK-Region, sowie eine Kinase-Domäne. Titin-Mutationen können zu schweren Herz- und Skeletmuskel-Erkrankungen wie dilatative Kardiomyopahtie oder der hereditären Myopathie mit frühem respiratorischem Fehler (HMERF) führen. Um die Rolle der unterschiedlichen Titindomänen in Funktion und Erkrankung der gestreiften Muskulatur zu untersuchen, haben wir unterschiedliche Knockout-Mausmodelle generiert. Diese demonstrierten die Relevanz der M-Bande für die strukturelle Integrität des Sarkomeres und die Rolle der N2B- and PEVK-Domänen in der kardialen trophischen Reizweiterleitung und der Füllung des Ventrikels. Um das Gesamtprotein zu entfernen, haben wir das ATG-Exon mit lox Rekombinationssequenzen flankiert und die Cre Rekombinase in gestreiftem Muskel exprimiert (TiEx2MCK). Der Vergleich der Z-Scheiben- und M-Banden- Knockout- Maus umfasste phänotypische, morphologische, ultrastrukturelle, transkriptomische und proteomische Analysen. Beide KO-Modelle entwickelten eine schwere Skeletmuskelatrophie die durch eine Auflösung der Sarkomerstruktur verursacht wurde und zu Gewichtsverlust, reduzierter Kraftausdauer und hoher Mortalität führte. Die Auflösung der Sarkomerstruktur betraf gleichermassen Kardiomyozyten beider KO Modelle, führte jedoch zur Ausbildung einer DCM im TiEx2MCK KO und einer kardialen Atrophie bei titin-M-Banden-Defizienz. Diese kardialen Veränderungen können zur erhöhten Mortalität der Z-Scheiben KO Tiere beitragen. Die Analyse des Proteoms beider KO Modelle zeigte die differenzielle Expression von Atrophie- und Hypertrophy-assoziierten Proteinen wie FHL2. Entsprechend scheint die Skeletmuskelatrophie vorwiegend durch den Zusammenbruch der Sarkomerstruktur ausgelöst zu werden, die ebenfalls zum kardialen Phänotyp beiträgt. Zusätzlich führt der Verlust des Titin N-Terminus zu veränderter trophischer Signaltransduktion im Herzen. Diese Studie validierte Titins Rolle als essentielles Sarkomerprotein, welches nicht nur als elastisches Gerüst fungiert, sondern auch an der Regulation des Wachstums der gestreiften Muskulatur beteiligt ist.

3 Introduction

3.1 Structure and function of striated muscles

Muscle is a specialized tissue essential for generating force and movement exemplified by the controlled contraction of skeletal muscle, the regular beating of the heart and peristalsis of the intestine. There are two types of muscle: (a) the smooth muscles which are not under conscious control and mainly located in the walls of hollow organs such as the gastrointestinal tract, uterus, urinary bladder, and blood vessels; and (b) the striated muscles are subdivided into the voluntary controlled skeletal and the involuntary controlled cardiac muscles. Skeletal muscle consists of multiple fiber bundles with a diameter of approximately 100-1000 µm. These bundles contain long multinuclear myofibers whit a diameter of approximately 10-100 µm and a length of up to 15 cm. These myofibers are formed by the fusion of several myoblasts (precursor cells) and are restricted by the sarcolemma, containing the mitochondria, the nuclei, the sarcoplasmic reticulum (SR) and the myofibrils. The latter are composed of the basic contractile elements - the sarcomeres. Unlike skeletal myofibers, cardiac cells are branched and connected by intercalated discs which are protein complexes important for the Ion flux between adjacent cells.

3.1.1 Myofibrillogenesis

Myofibrillogenesis describes the arrangement and the interaction of muscular proteins resulting in a mature myofibril with a highly ordered sarcomeric structure. The three-step pre-myofibril model (Figure 1, p.: 4) explains the myofibril formation through a pre-myofibril and a nascent myofibril (Dabiri et al., 1997; Rhee et al., 1994; Sanger et al., 2000). The pre-myofibril mainly consists of Z-bodies and non-muscle myosin IIB associated with sarcomeric α-actinin and actin filaments, which build a complex close to the plasma membrane (Dlugosz et al., 1984; Kelly, 1969; Rhee et al., 1994). Thereupon a mini-sarcomere develops, initialized by the shift of the Z-bodies to the boundaries of the pre-myofibril and the recruitment of troponin and tropomyosin to the actin filaments (Siebrands et al., 2004). At this early stage non-muscle myosin IIB serves as a ruler for

the alignment of the thin filament (Du et al., 2003; Sanger et al., 2004; Wang et al., 2005). The nascent myofibril formation starts with the lateral alignment of the Z-bodies and the integration of titin (Dabiri et al., 1997; Rhee et al., 1994; Schultheiss et al., 1990; Turnacioglu et al., 1997). Titin supports the alignment of muscle myosin II filaments which subsequently replace the non-muscle myosin IIB (Du et al., 2003; Rhee et al., 1994; Sanger et al., 2004; Wang and Wright, 1988; Wang et al., 2005; Whiting et al., 1989). The formation of the mature myofibril is initiated by the simultaneous fusion of the Z-bodies to solid Z-discs and the drift of the Z-discs along the filament structure (Dabiri et al., 1997; van der Loop et al., 1996). This process stretches and elongates titin and enables the binding of other sarcomeric proteins to their target sites (van der Loop et al., 1996). Finally the mature myofibril is composed of the thin filaments anchored at the Z-disc, the thick filaments aligned at the A-band and the titin filament with two antiparallel titin-molecules anchored at the Z-disc and overlapping at the M-Band (Gregorio et al., 1999). The importance of titin as template for sarcomere assembly and molecular ruler is based on the early appearance in myofibrillogenesis and the interaction with α-actinin, myosin, and actin filaments, as well as its unique domain structure that contains various binding sites for several proteins (McElhinny et al., 2000).

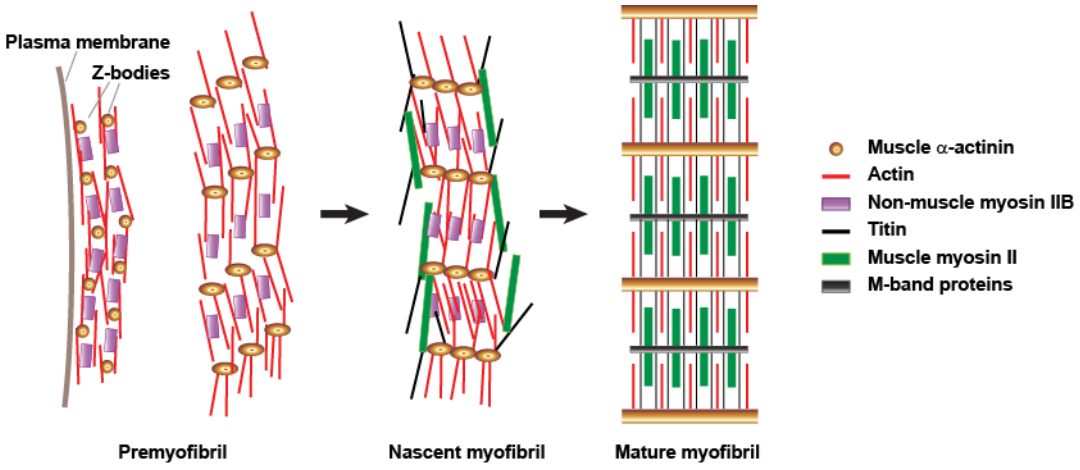

Figure 1: The premyofibril model. The pre-myofibril formation starts with the assembly of actin and muscle α-actinin into Z-bodies. Thereafter Z-bodies align laterally and, titin is integrated into the sarcomere to form the nascent myofibril. The mature myofibril develops as non-muscle myosin IIB is replaced with muscle myosin II and Z-bodies fuse into the Z-disc. Modified from (Du et al., 2003).

3.1.2 Structure and function of the sarcomere

The myofibril consists of adjacent sarcomeres which are the smallest contractile units of striated muscle with a slack length of 2 μm. In the light microscope sarcomeres appear as periodic light and dark bands (Figure 2, p.: 6). The lateral borders of the sarcomere are defined by dark lines, the Z-discs, where the thin- respectively actin filaments are anchored (Drabikowski and Nowak, 1973). Actin filaments consist of two twisted actin polymers, each containing 400 globular actin molecules. The length and the position of these polymers are adapted by the 600-900 kDa long nebulin proteins (Wegner, 1979). Furthermore the capping proteins tropomodulin and CapZ which cover the ends of the actin filament, regulate the polymerization and depolymerization (Caldwell et al., 1989). Tropomyosin is an important element of the thin filament and interacts with the Ca^{2+}-sensitive troponin complex in regular intervals. The area around the thin filament appears isotropic in polarized light and is determined as I-Band (Caldwell et al., 1989; Drabikowski and Nowak, 1973; McElhinney et al., 2003; Wang and Wright, 1988; Wegner, 1979). The thick filament contains about 300 myosin II dimers and spans from the A-band (anisotropic in polarized light) to the M-band. Each myosin II dimer has two globular heads, connected by a joint to the rest of the molecule. The myosin binding protein-C (MyBP-C) is a component of the thick filament and links the thick to the titin filament. Titin, the third filament system, spans half the sarcomere (~1 μm) and is integrated into the Z-disc by α-actinin and into the M-band by myomesin and M-protein. and interacts with the thin and thick filament (Bennett et al., 1986; Furst et al., 1988; van der Loop et al., 1996; Maruyama and Ebashi, 1965; Obermann et al., 1997; Sorimachi et al., 1997). The contractile force of the sarcomere is produced by the interaction of the thin- with the thick-filaments at the A-band region. An intracellular increase of Ca^{2+} leads to a conformational change of troponin within the thin filament to expose myosin binding sites. The hydrolysis of adenosine tri-phosphate (ATP) at the motor domain of a myosin head induces its binding to the actin filament. Accordingly adenosine di-phosphate (ADP) and pyro-phosphate is produced causing a conformational change in the joint region and initiating interaction of actin and myosin. The binding of a new ATP molecule disassociates actin and the myosin head completing the cycle. Titin operates as a passive spring which provides resistance during contraction and supports the structure of the sarcomere (Granzier and Irving, 1995).

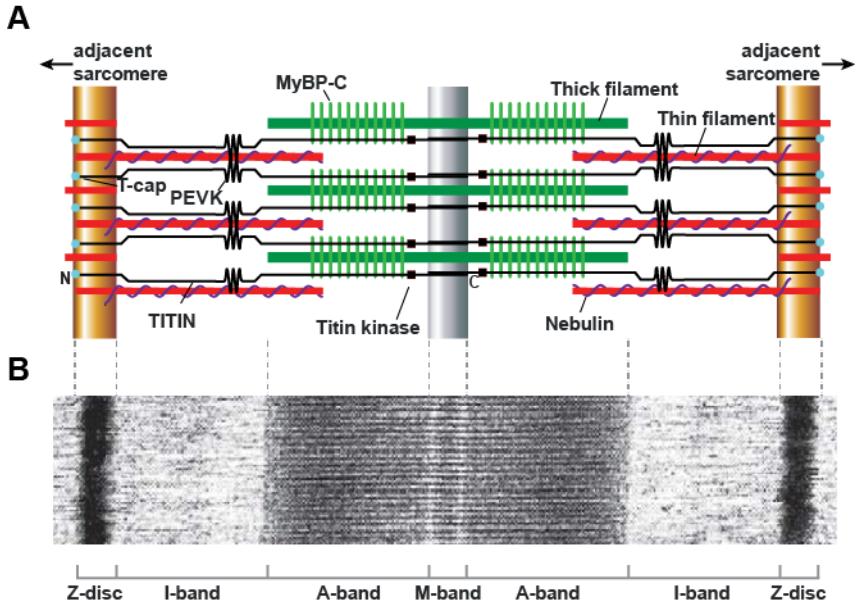

Figure 2: Structure of the sarcomere. (A) The sarcomere includes the thin filaments (red), thick filaments (green), nebulin (purple) and T-CAP (light blue). Titin (black) spans half the sarcomere, and integrates with its N-terminus into the Z-disc and with the C-terminus into the M-band. It forms a continuous filament by overlapping at the Z-disc and the M-band. Titin interacts with myosin binding protein-C (light green) at the A-band. Its elastic PEVK domain resides at the I-band and the kinase domain (black square) at the M-band. Modified from Gregorio et al., 1999. (B) Electron micrograph of skeletal muscle with the Z-disc (dark lines) the isotropic I-band, the anisotropic A-band (dark band) and the M-band in the middle of the sarcomere. Modified from (Agarkova and Perriard, 2005).

3.2 Titin

At the end of the 70's two giant elastic proteins, connectin (1977) and titin (1979) were purified from skeletal and cardiac muscles (Maruyama et al., 1977; Wang et al., 1979). Electrophoretic mobility experiments of both proteins identified connectin and titin as the same proteins (Maruyama et al., 1981). With a size of up to 3.7 MDa titin is the largest known protein. It represents 10% of the muscle mass. With a length of 1 µm, titin extends from the I-band to the A-band and forms a continuous filament system along the myofibril as titin N-termini from adjacent sarcomeres integrate in the Z-disc and the C-termini overlap within the M-band (Figure 2, p. 6) (Furst et al., 1988; Labeit et al., 1997; Wang et al., 1991). Titin mainly consists of repeating immunoglobulin (Ig) and fibronectin-III (FN III) domains which represent approximately 90% of its mass. These super repeats contain multiple binding sites for sarcomeric proteins (Figure 3 andFigure 4, p. 8 and 10) (Gautel et al., 1996; Labeit et al., 1990). Titin's unique sequences contain the skeletal muscle specific N2A, the PEVK and the cardiac specific N2B domains, which reside in the I-band, as well as the titin kinase domain

located at the M-band (Greaser et al., 2000; Sebestyen et al., 1996). The N-terminal 90 kDa of titin contain nine Z-disc Ig elements (Z1-Z9) and up to seven repeating sequence motifs (Z-repeats) which are differentially included into the mature titin protein depending on the muscle type (Gautel et al., 1996; Gregorio et al., 1998). The mechanically active I-band region of titin starts 100 nm from the center of the Z-disc and undergoes muscle type specific alternative splicing (Linke et al., 1999). Four spring-like elements located in the I-band produce passive tension during the stretch of the sarcomere. These spring elements include tandem Ig modules of variable length and the PEVK motifs (enriched in proline (P), glutamic acid (E), valine (V), and lysine (K) residues). Cardiac titin differs in the expression of the cardiac specific N2B region and the skeletal N2A domain (Figure 3, p. 8) (Granzier and Labeit, 2006; Greaser et al., 2000; Linke et al., 1999). When the sarcomere stretches, the tandem Ig segments extend first, followed by the PEVK, N2B and N2A elements. This produces a passive tension and resting force (Watanabe et al., 2002). The largest part of titin (~2 MDa) contains the A-band which consists of 70% Ig- and FN III motifs. The latter are exclusively found in the A-band region of titin (Figure 3, p. 8) (Labeit et al., 1992; Linke et al., 1996; Tskhovrebova and Trinick, 2004). A-band titin is tightly associated with the thick filament forming a stabile complex which regulates the length of the thick filament (Whiting et al., 1989). The approximately 200 kDa large C-terminus of titin is encoded by 6 exons (MEx1-MEx6) and contains 10 Ig motifs (M1-M10) as well as 7 specific interdomains (is1-is7) of variable length (Figure 3, p. 8) (Gautel et al., 1993; Kolmerer et al., 1996). The exon MEx1 encodes a serine/threonine kinase like domain. This domain contains a catalytic core that binds ATP and the substrate as well as an inhibitory regulatory domain, which has been suggested to be mechanically activated (Gautel et al., 1995; Labeit et al., 1992). Recently the catalytic activity of titin kinase has been questioned and proposed to act as a pseudo kinase scaffold for the E3 ubiquitin ligase MURF1 (Bogomolovas et al., 2014).

3.2.1 Titin isoforms

The gene locus of human and mouse titin have been mapped to the long arm of chromosome 2. The human titin gene consists of 363 exons and encodes for proteins of up to 38,138 amino acids with a predicted size of ~4.2 MDa. Titin mRNA is alternatively spliced to generate multiple isoforms (Figure 3, p. 8), which determine the elasticity of

the sarcomere and vary between muscle types (Bang et al., 2001; Freiburg et al., 2000; Muller-Seitz et al., 1993; Pelin et al., 1997; Rossi et al., 1994).

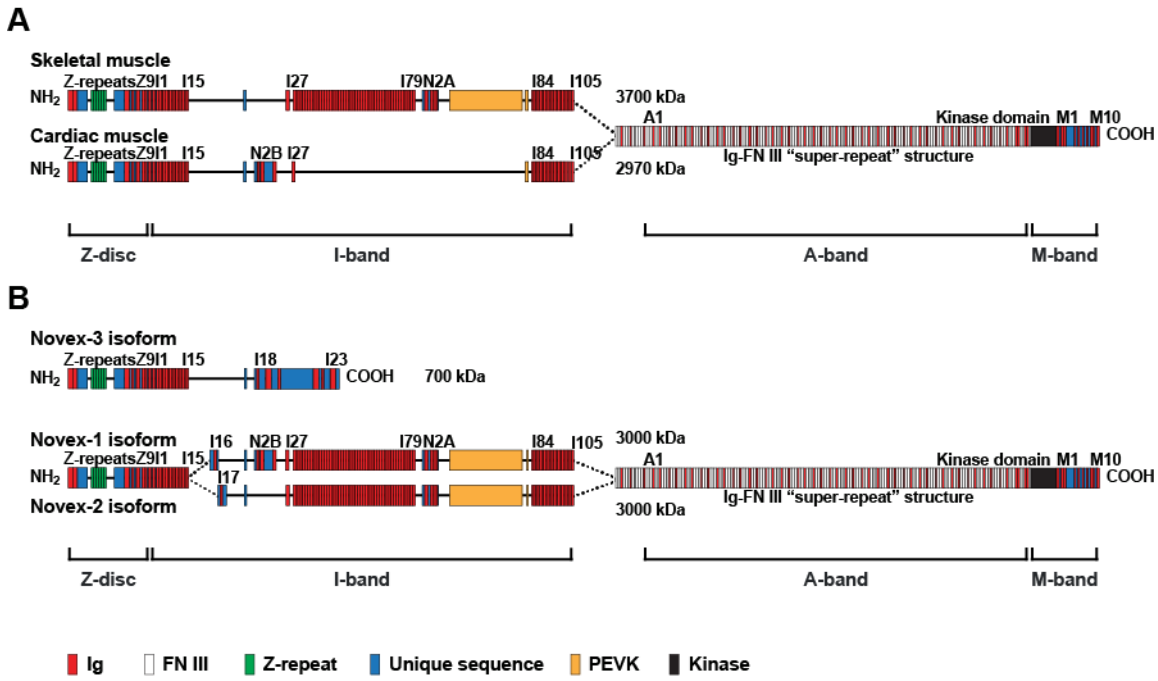

Figure 3: Titin isoforms and domain composition. Titin contains immunoglobulin (Ig, red) and fibronectin-III (FN III, white) domains as well as Z-repeats (green), unique sequences (blue), the PEVK elements (yellow), and a the kinase domain (black). (A) The 3.7 MDa skeletal muscle titin isoform is characterized by the N2A domain and a large PEVK region. The embryonic and neonatal cardiac titin with a size of ~3.8 MDa contains the N2A as well as the N2B domain (not shown). The major cardiac isoform (2.97 MDa) contains the N2B domain and a short PEVK region. (B) Cardiac and skeletal muscle express three unique I-band splice variants in addition to the main titin isoforms which are termed novex 1-3. The smallest novex-3 titin (625 kDa) excludes the A-band region and contains of an alternative C-terminus. Modified from (Bang et al., 2001).

The Z-disc region of titin contains Z-repeats with repetitive motifs of 45 amino acids (AS). These Z-repeats provide binding sites for α-actinin. The thickness and the mechanical strength of the Z-disc correlates with the number of Z-repeats (Gautel et al., 1996; Sorimachi et al., 1997). Both Z-disc and I-band composition are determined by alternative splicing. This affects predominantly the skeletal N2A, the cardiac N2B and the PEVK domains of titin (Neagoe et al., 2003; Prado et al., 2005). Three classes of titin isoforms are known in the heart: the N2B, the N2BA, and fetal N2BA titin isoform. All three contain differentially expressed tandem-Ig, PEVK, and N2B elements. The expression of titin's exon 49 and the simultaneous repression of the exons 51-218 generates the relatively small (~2.97 MDa) cardiac N2B isoform (Bang et al., 2001; Freiburg et al., 2000). The larger (~3.3-3.5 MDa) cardiac N2BA isoform is derived from the additional expression of the exons 102-109 which encode for the N2A element. N2BA

titin includes the long PEVK element (600-800 AS) as well as a variable number of Ig domains (Bang et al., 2001; Casoria et al., 2000; Freiburg et al., 2000). The third cardiac isoform is the large (~3.6-3.8 MDa) embryonic/neonatal titin, which includes additional tandem-Ig and PEVK domains (Lahmers et al., 2004; Opitz et al., 2004). Perinatally the ratio of N2BA and N2B changes dramatically as the long N2BA titin is replaced by the shorter N2B isoform. Thus alternative splicing determines the elasticity of the cardiac sarcomere (Greaser et al., 2005; Lahmers et al., 2004; Opitz et al., 2004). The skeletal N2A titin isoforms range from ~3.3 up to 3.7 MDa with the largest isoform known in the diaphragm (Freiburg et al., 2000; Prado et al., 2005). Muscle specific N2A-titin is expressed as a single isoform with the exception of musculus adductor magnus, gluteus medius, psoas major, quadriceps femoris and tibialis anterior where two N2A titin isoforms have been described (Ottenheijm et al., 2009a; Prado et al., 2005). Additionally, three unique I-band titin isoforms are expressed in heart and skeletal muscle (Figure 3B, p. 8). The cardiac novex-1/N2B and novex-2/N2BA titin are co-expressed with the N2B and the N2BA titin (Bang et al., 2001; Cazorla et al., 2000; Freiburg et al., 2000). The small (~700 kDa) novex-3 titin has also been described in *Xenopus laevis*, where *Xtn3* is developmentally expressed in cardiac and skeletal muscles (Brown et al., 2006). Novex-3 titin integrates into the Z-disc and provides an alternative C-terminus, which connects the Z-disc and the I-band (Bang et al., 2001). Unlike the I-band exons, A-band and the M-band of titin are not alternatively spliced, except for MEx5 (Freiburg et al., 2000; Kolmerer et al., 1996).

3.2.2 Titin binding proteins

Titin's unique domain structure provides several binding sites for structural, regulatory, and contractile proteins. The resulting interactions make titin an essential component of the myofilament and relate to signaling, scaffolding, and mechanical functions.

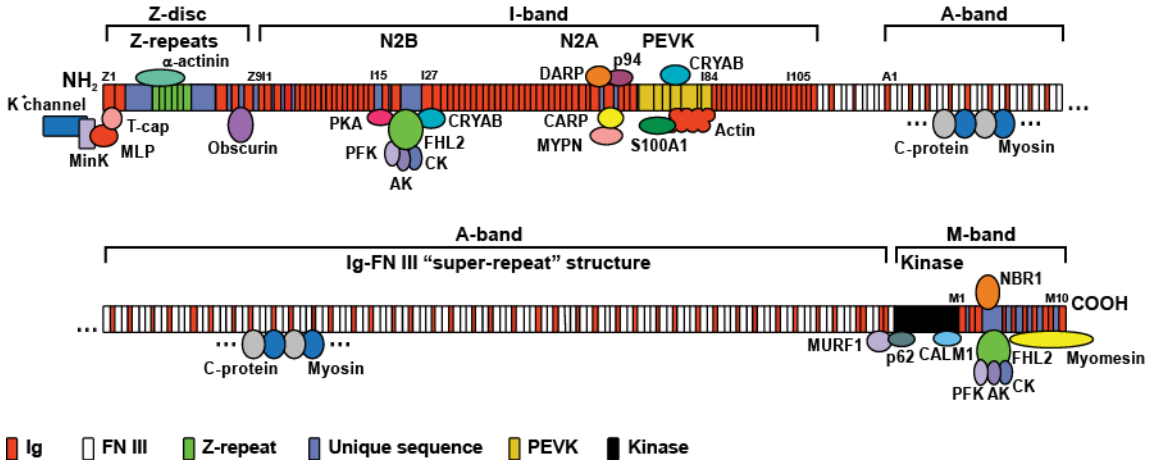

Figure 4: Binding partners of cardiac N2BA titin. Titin contains multiple binding sites for structural and signaling proteins. The proteins α–actinin, obscurin, small ankyrin 1 (sANK1), T-CAP, the muscle LIM protein (MLP) and the potassium voltage-gated channel subfamily E member 1 (MinK) interact with the Z-disc region of titin. The I-band consists of three functional domains (N2B, N2A, and PEVK). The N2B region interacts with αB-crystalline (CRYAB), the four and a half LIM domain protein (DRAL/FHL2), the protein kinase A (PKA), the phospho fructo kinase (PFK), the adenylate kinase (AK) and the creatin kinase (CK). The N2A domain binds to the cardiac ankyrin repeat protein (CARP), to calpain 3 (p94), to the diabetes related ankyrin repeat protein (DARP) and to myopalladin (MYPN). Actin, the S100 calcium binding protein A1 (S100A1) and αB-crystalline (CRYAB) are binding partner of the PEVK domain. The A-band of titin manly binds to myosin and the myosin binding protein C. The E3 ubiquitin ligase MURF1, sequestosome 1 (p62), calmodulin 1 (CALM1), the neighbor of BRCA1 (NBR1), myomesin, FHL2, PFK, AF and CK bind to titin's M-band. Modified from (Bang et al., 2001).

3.2.2.1 Z-Disc interactions

The 19 kDa small T-CAP (titin-cap or telethonin) is expressed in skeletal and cardiac muscles and localizes at the periphery of the Z-disc (Figure 4, p.10) (Gregorio et al., 1998; Mues et al., 1998; Valle et al., 1997). T-CAP binds to the Ig domains Z1 and Z2 at the very N-terminal part of titin and promotes titins integration into the Z-disc (Gregorio et al., 1998; Zou et al., 2006). Additionally, T-CAP recruits the potassium voltage-gated channel subfamily E member 1 (MinK) to titin. This interaction may contribute to a stretch-dependent regulation of potassium flux in cardiac muscle, providing a "mechano-electrical feedback" system (Furukawa et al., 2001). T-CAP also binds to the muscle LIM protein (MLP) which is associated with the sarcolemma by interacting with the beta-spectrin network. This interaction may stabilize the association of the contractile apparatus with the sarcolemma (Flick and Konieczny, 2000). The sarcoplasmic reticulum (SR) transmembrane protein small ankyrin 1 (sANK1) binds to titin's Ig domains Z1 and Z2 as well as to the M-band of titin (Kontrogianni-Konstantopoulos and Bloch, 2003; Zhou et al., 1997). Both T-CAP and sANK1 can simultaneously bind to titin and mediate the interaction between the Z-disc and the surrounding SR

(Kontrogianni-Konstantopoulos and Bloch, 2003). The Z1 and Z2 Ig domains of titin are followed by the Z-repeats, whose number is regulated by alternative splicing dependent on the type of the muscle. The Z-repeats 1-7 provide binding sites for the C-terminus of α-actinin. This interaction is important for the assembly and the maintenance of the Z-disc and cross-links titin to the thin filament system. The variations of the number Z-repeats determine the binding sites and regulate the interaction of the thin filament and titin (Ohtsuka et al., 1997; Peckham et al., 1997; Sorimachi et al., 1997; Young et al., 1998). α-actinin also binds distal of titin's Z-repeats and in an interdomain sequence of Z-disc titin (Labeit et al., 2006; Young et al., 1998). The latter also contains a binding site for filamin C. This interaction may coordinate the connection between membranes and myofibrils during early myofibrillogenesis (van der Ven et al., 2000). Other binding partner of titin's Z-disc region are the giant muscle proteins obscurin (~720-900 kDa) and nebulin (600-900 kDa) (Bang et al., 2001; Labeit et al., 2006; Young et al., 2001). Nebulin is known to regulate the length of the actin polymers and the interaction of titin and nebulin suggest specifying the width of the Z-disc in striated muscles. The association of titin and obscurin indicates a significant function of titin in signal transduction (Witt et al., 2006; Young et al., 2001). The interaction of Z-disc titin with sarcomeric and membrane-associated proteins has been implied in the assembly and the maintenance of the sarcomere.

3.2.2.2 I-Band interactions

The I-band of titin contains the cardiac N2B, the skeletal N2A and the PEVK region which provide multiple binding sites for proteins related to contraction, metabolism, and regulation of gene expression (Figure 4, p. 10) (Greaser et al., 2000; Sebestyen et al., 1996). The cardiac N2B domain of titin interacts with the four and a half LIM domain protein (FHL2). FHL2 has multiple functions. It interacts with the mitogen-activated protein kinase MAPK1 and inhibits its nuclear accumulation after signal induction. That inactivates the transcriptional responsiveness of MAPK1 for the ETS domain-containing protein (ELK-1), the GATA binding protein 4 (GATA4), and the atrial natriuretic factor promoter. These proteins are members of the MAPK signaling pathway which is associated with cardiac hypertrophy (Purcell et al., 2004). FHL2 binds non-phosphorylated CREB (cAMP responsive element binding protein 1), which initiates the transcription of cAMP-responsive genes like the MAP kinases. This interaction

suggests an additional FHL2 dependent activation of transcription (Johannessen et al., 2006). FHL2 also interacts with the potassium voltage-gated channel subfamily E member 1 (MinK), linking titin to the repolarization of cardiac cells (Furukawa et al., 2001). Other interaction partners of FHL2 are the phospho fructo kinase (PFK), the adenylate kinase (AK) and the creatin kinase (CK). These proteins are important metabolic enzymes which provide energy for muscle contraction (Lange et al., 2002). Additionally titin's N2B region binds to another four and a half LIM domain protein 1 (FHL1) which initiates titin's response to biochemical stress and plays an important role in the general mechanism of pathological hypertrophy (Sheikh et al., 2008). The N2B domain of titin also interacts with αB-crystalline (CRYAB) and the protein kinase A (PKA). The first operates as heat shock protein and increases the stability of titin during stress (Bullard et al., 2004). Furthermore αB-crystalline influences the protein kinase C α (PKCα) which is a member of the RAF/MEK/ERK signal pathway, associated with cardiac hypertrophy (Braz et al., 2002; Liu et al., 2004). The PKA regulates the stiffness of the N2B domain by phosphorylation responding to β-adrenergic signaling (Yamasaki et al., 2002). The skeletal N2A domain of titin can be bound by the non-lysosomal calcium-dependent cysteine protease calpain-3 (p94). This interaction inhibits the proteolytic auto activation of the protease and regulates the activity of calpain-3 (Sorimachi et al., 1995). Calpain-3 significantly controls the protein degradation of sarcomeric proteins like myosin binding protein C (MyBP-C), tropomyosin (TPM), nebulin, troponin T (TnT), troponin I (TnI) and titin (Huang and Forsberg, 1998). Other binding partners of the N2A domain are muscle-ankyrin-repeat proteins (MARPs), the cardiac ankyrin repeat protein (ANKRD1/CARP), the diabetes related ankyrin repeat protein (ANKRD23/DARP) and the skeletal muscle ankyrin repeat protein (Ankrd2). These proteins respond to stretch and regulate transcription and may link stretch-induced signaling pathways and muscle gene expression (Miller et al., 2003). Myopalladin (MYPN) interacts to titin's N2A region and influences the integrity of the sarcomere (Bang et al., 2001). Titin's I-band overlaps with the thin filament system and provides two binding sites for sarcomeric actin. The first site locates at the Z-disc/I-band junction and anchors the I-band region of titin into the sarcomere (Linke et al., 1997). The second binding site arranges in the third important domain of I-band titin, the PEVK domain. This interaction regulates the generation of passive force and is controlled by the binding of the calcium-binding protein S100A1 (Linke et al., 1998; Yamasaki et al., 2001).

Additionally the PEVK domain provides binding sites for αB-crystalline (CRYAB) and nebulin. The latter interaction mediates the proper integration of nebulin into the I-band (Ma and Wang, 2002).

3.2.2.3 A-Band interactions

The structure of titin's A-band is characterized by multiple Ig and FN III domains, arranged in super-repeats. They provide regularly spaced binding sites for the thick filament system, especially for myosin and myosin binding protein C (MyBP-C; Figure 4, p. 10; Furst et al., 1992; Houmeida et al., 1995; Wang et al., 1992). MyBP-C binds to the Ig-FN III -super-repeats of titin as well as to the myosin heavy chain (MHC) of myosin, an interaction important for the assembly and stability of the sarcomere (Freiburg and Gautel, 1996; Furst et al., 1992). Furthermore MyBP-C controls the formation and cycling of cross-bridges and therefore it is involved in the regulation of muscle contraction (Oakley et al., 2007). Myosin, especially the MHC, binds to titin's FN III motifs, integrating titin into the thick filament system. This interaction determinates the length of myosin and enables titin to act as a protein-ruler for the assembly and the organization of the sarcomere (Houmeida et al., 1995). An additional binding partner of the A-band titin is the muscle-specific RING finger protein 1 (MURF1). This E3-ubiquitine ligase binds close to the M-band region to the A-band domains A168-170. MURF1 interacts with multiple muscle proteins including troponin T (TnT), troponin I (TnI), myosin, T-CAP and nebulin. It controls proteasome-dependent protein degradation. Overexpression of MURF1 leads to disruption of the M-band structure what indicates an important role in the assembly and maintenance of the thick filament (Centner et al., 2001; McElhinny et al., 2002; Witt et al., 2005). MURF1 also operates in the nucleus where it interacts with transcription factors like the glucocorticoid modulatory element binding protein-1 (GMEB-1) suggesting an essential role in the regulation of cardiac hypertrophy (Gregorio et al., 2005; McElhinny et al., 2002; Willis et al., 2007). Muscle-specific RING finger proteins, MURF2, also binds to the A-band motifs A164-169 (Centner et al., 2001) and binds MURF1 in addition to several other muscle proteins and has a role in maintaining the M-band structure (McElhinny et al., 2004; Witt et al., 2005). The interaction of the MURF's and titin implicates a link of the contractile system to mechanisms regulating protein synthesis and degradation (McElhinny et al., 2004; Tskhovrebova and Trinick, 2003; Witt et al., 2005).

3.2.2.4 M-Band interactions

The M-band provides several binding sites for structural, regulatory, and contractile proteins (Figure 4, p. 10). Within the M-band, titin binds to myomesin 1, 2 and 3 (M-proteins), to obscurin and to the tumor suppressor protein bridging integrator protein 1 (BIN1). Myomesin 1 binds the Ig domain M4 of titin in a phosphorylation-dependent manner and cross-bridges titin's M-band region with the thick filament system by interacting with the heavy chain of myosin (Nave et al., 1989; Obermann et al., 1996, 1997). The M-proteins 2 and 3 also contains binding sites for both titin and myosin and act as elastic cross-linkers in postnatal cardiac and fast-twitch myofibrils (Obermann et al., 1996; Vinkemeier et al., 1993). Furthermore M-band titin interacts with BIN1 which assembles mature sarcomeres coordinating the differentiation of skeletal muscle cells (Fernando et al., 2009). The interaction of obscurin and titin's Ig domain M10 promotes the stability of the sarcomeric M-band region which implicates a significant function of titin in signal transduction (Fukuzawa et al., 2008; Witt et al., 2006; Young et al., 2001). This hypothesis is supported by the interaction with FHL2 at the Ig domains M3-M4 of M-band titin (Lange et al., 2002). The protease calpain-3 (p94) binds I-band and M-band, where it interacts with the M-band exon 5 (MEx5) and links to protein quality control mechanisms in skeletal muscles (Kinbara et al., 1997; Sorimachi et al., 1995). Importantly the M-band region of titin contains a kinase domain, encoded by the exon 358 (M-band exon 1 = MEx1; Figure 4, p. 10). This serine/threonine kinase domain is 42% similar to the smooth muscle myosin light-chain kinase (MLCK) and the invertebrate muscle protein twitchin kinase (Labeit et al., 1992). Similar to MLCK the titin kinase consists of a catalytic core, able to bind ATP and a substrate and a regulatory auto-inhibitory domain, which binds calcium/calmodulin (Gautel et al., 1995) indicating an intrasteric regulation. The activation of the kinase has been suggested to involve the phosphorylation of the auto inhibitory tyrosine in the catalytic core (Y170) and the binding of the calcium/calmodulin complex. This changes the conformation of the regulatory domain and releases the ATP-binding site (Mayans et al., 1998). In 1998 Mayans et al. postulated the phosphorylation of the Z-disc protein T-CAP by the titin kinase *in vitro*, suggesting an important role of the titin kinase in sarcomere assembly (Mayans et al., 1998). Recent studies from the same authors indicate that the titin kinase may indeed act as a pseudo kinase and scaffold for signaling proteins (Bogomolovas et al., 2014). This hypothesis is supported by the interaction of the titin kinase with the

zinc-finger protein neighbor of Brca1 gene (NBR1) and the NBR1-related zinc finger protein sequestosome 1 (p62) (Lange et al., 2005). The latter is known as multivalent scaffolding platform controlling the ubiquitin proteasome-mediated degradation and interacts with multiple kinase pathways (Geetha and Wooten, 2002; Seibenhener et al., 2004). Mechanical stimulus acting on the kinase domain induces a conformational change which uncovers the catalytic core and enables the binding of NBR1. P62 binds to NBR1 and recruits the RING/B-box protein muscle-specific ring finger protein 2 (MURF2). MURF2 is an E3 ubiquitin protein ligase which binds with specific sarcomeric proteins and promotes protein degradation during muscle atrophy. The NBR1-p62-MURF2 complex is able to translocate to the nucleus suppressing the transcriptional activity of the serum response factor (SRF). The SRF is important for a normal development of the heart by regulating hypertrophic signal transduction. Any alterations or mechanical instability of the titin kinase consequently leads to NBR1-p62-MURF2 mislocalization, implicating severe diseases like hereditary myopathy with early respiratory failure (HMERF) (Lange et al., 2005; Linke, 2008).

3.3 Clinical relevance

Several independent studies have linked titin to sarcomere formation and the mechanical properties of striated muscle and mechanotransduction Granzier and Labeit, 2006; Trinick, 1996, Linke, 2008) Accordingly, mutations of titin have been linked to severe diseases of the heart and the skeletal muscles.

3.3.1 Titin mutations in cardiomyopathies

Dilated cardiomyopathy (DCM) (2015 ICD-10-CM I42.0) is characterized by the enlargement (dilation) of the chambers of the heart (ventricles) and leads to a diastolic and systolic dysfunction, predominantly of the left ventricle. The resulting effect on circulation leads to heart failure with edema of the lung and the lower extremities, arrhythmia, and an increased risk of thrombus formation as serious consequences for patients (Hershberger and Morales, 1993; Richardson et al., 1996; Towbin and Lorts, 2011). The large size of the titin gene increases the chance of mutations of the N2B, N2A, PEVK or M-band domain, which can affect titins function. Mutations that substantially disrupt the structure of full-length titin are the most common known genetic cause of

dilated cardiomyopathy (Herman et al., 2012). In 2002 researchers identified a nonsense mutation (p.G4053ter) which affects the N2B domain of titin leading to a non-functional titin molecule (Itoh-Satoh et al., 2002). Another mutation at the A-M-band junction of titin leads to a 2-bp insertion of exon 326 which causes a frame shift and truncates titin to a 1.14 MDa sub fragment (Gerull et al., 2002). Four years later the same group discovered a heterozygous 1-bp deletion (c.62890delG) in an Australian family. This mutation also affects the A-band titin, as it causes a premature stop-codon (p.E20963K) and the addition of ten novel amino acid residues (Gerull et al., 2006). Other mutations found in DCM patients affect the M-band exons (MEx) of titin. Therefore a homozygous 1-bp deletion in exon 360 (MEx3; g.291297delA) and an 8-bp deletion near the 3′ end of exon 358 (MEx1; g.289385-289392delACCAAGTG) were identified. The first causes a frame shift, affecting 21 amino acids and generates a stop-codon resulting in a deletion of the most C-terminal 447 amino acids of titin. The latter produces a premature stop-codon besides the addition of 8 novel amino acids and introduces a loss of the last 808 C-terminal residues downstream of the kinase domain (Carmignac et al., 2007). The truncated titin proteins are most likely degraded by RNA- and protein-surveillance pathways what decreases the titin level and affects sarcomere formation. This haploinsufficiency impairs the titin interactions and several structural, regulatory, and contractile proteins like calpain-3 (Carmignac et al., 2007; Herman et al., 2012). In addition to the truncations, amino acid changes are known to modify the binding affinity of titin to the thin or the thick filaments as well as to its interacting partners. The missense mutations p.V54M and p.A743V in the Z-disc region affect the binding of T-CAP and α-actinin. That influences the sarcomeric integrity and thereby the stability of striated muscles (Itoh-Satoh et al., 2002). The mutation W930R impacts the binding of α-actinin to the Z4 Ig-domain but additionally it disrupts a highly conserved hydrophobic core sequence located in the Z-disc I-band transition zone (Gerull et al., 2002). Furthermore the amino acid exchange p.R25618Q modifies the electrical charge from basic to neutral affecting the binding capability of FHL2 which seems to be involved in hypertrophic signal transduction (Matsumoto et al., 2005). Titin does not only relate to DCM by mutations in its coding region but also through secondary changes in titin gene expression, for example splicing. In patients with DCM significantly increased N2BA:N2B expression ratios are identified. The overexpression of long cardiac N2BA titin generates a loss of the passive tension in the myocardium and initiates an increased expression of titin binding proteins like ANKRD1/CARP, ANKRD23/DARP and

ANKRD2. These proteins especially bind to the N2A region which is not existent in the adult cardiac N2B titin isoform (Nagueh et al., 2004). Hypertrophic cardiomyopathy (HCM) (2015 ICD-10-CM I42.2) is characterized by the increase of the wall thickness of the ventricles. This pathological modification of the heart leads to a diastolic and systolic dysfunction characterized by arrhythmias such as atrial fibrillation or ventricular tachycardia. Furthermore, patients describe chest pain, shortness of breath and fatigue and syncope. The severest consequence of the HCM is the sudden cardiac death (Berenji et al., 2005). Several mutations of the Z-disc and I-band regions of titin are associated with HCM. Researchers described a G to T transversion, replacing the amino acid arginine with leucine. This mutation (p.R740L) affects the Z-repeat 7 which increases the binding affinity of α-actinin and potentially influences the integrity of the Z-disc (Satoh et al., 1999). The mutations p.S3799Y and p.S4465N, located in the N2B-domain of titin, alter the binding of FHL2 which is associated with the MAPK signal transduction, the cAMP response and the contraction dependent metabolism (Itoh-Satoh et al., 2002; Johannessen et al., 2006; Lange et al., 2002; Matsumoto et al., 2005; Purcell et al., 2004).

3.3.2 Titin mutations in muscular dystrophies

A muscular dystrophy associated with mutations of titin is the tibial muscular dystrophy (TMD) (2015 ICD-10-CM Q74.2). TMD is an autosomal dominant late-onset distal myopathy and characterized by muscle weakness and atrophy, predominantly developed in the tibialis anterior muscle. The mutations mainly affect the M-band exons (MEx5 and MEx6) and are caused by amino acid substitutions as well as frame shifts generating premature stop-codons. The mutations p.I293329N, p.L293357P, p.H33378P and p.Q33396X modify the MEx6 and thereby the binding affinity of the protease calpain-3 which significantly controls the protein degradation of sarcomeric proteins (Van den Bergh et al., 2003; Hackman et al., 2002; Huang and Forsberg, 1998; Pollazzon et al., 2010). Two additional frame shift mutations in MEx5 (g.292998delT and g.293376delA) lead to a premature stop in the M-band region of titin and provoke a more severe phenotype with earlier onset (Hackman et al., 2008). Mutations of titin are associated with the hereditary myopathy with early respiratory failure (HMERF) (2015 ICD-10-CM G71.9). The HMERF is a slowly progressive myopathy beginning in the third to fifth decades of life. Patients develop distal and proximal as well as respiratory muscle weaknesses what causes gait disturbances and respiratory problems

(Ohlsson et al., 2012; Pfeffer et al., 2014a). Several missense mutations (p.P22859L, p.C30071D, p.W30088L, p.P30091L, p.N30145K and p.G30150D) were identified in the 119th FN III-domain (A150) of A-band titin. At least eight different mutations associated with HMERF are associated with this hot spot. Consequently this domain undergoes conformational changes which affect the binding of myosin and myosin binding protein C (Izumi et al., 2013; Ohlsson et al., 2012; Palmio et al., 2014; Pfeffer et al., 2014b; Toro et al., 2013; Vasli et al., 2012). This interaction is important for the assembly and the stability of the sarcomere (Freiburg and Gautel, 1996; Furst et al., 1992).

3.4 Aims of the study

The giant titin proteins are associated with sarcomere formation during myofibrillogenesis. This structure is important for the development and adaptation of striated muscle and determines the passive properties. In addition to the involvement in contraction and relaxation titins serine/threonine (Ser/Thr) kinase domain at the M-band is believed to act as stretch sensor (Granzier and Labeit, 2006; Linke, 2008; Trinick, 1996). Investigations on patients with severe cardiac and skeletal myopathies like DCM, HCM, TDM or HMERF identified mutations of titin as cause to the disease (Herman et al., 2012; Johannessen et al., 2006; Ohlsson et al., 2012; Pollazzon et al., 2010). This clinical relevance leads to the generation of multiple knockout animal models which were used for detailed structural and functional investigations of the titin N2A, N2B and PEVK domains (Labeit et al., 2006; Lips et al., 2004; Ma and Wang, 2002; Miller et al., 2003). In addition titins kinase domain especially became in focus. The identification of the kinase dependent phosphorylation of T-CAP predicted an association of titins M-band with stretch dependent signal transduction (Mayans et al., 1998). In order to investigate the function of M-band titin Gotthardt and colleagues generated a M-band deficient mouse strain and demonstrated the critical role of the M-band titin for the structural integrity of the sarcomere, the regulation of the expression of genes involved in skeletal muscle contraction and the induction of proteasome activity (Gotthardt et al., 2003; Ottenheijm et al., 2009b; Peng et al., 2006, 2007; Weinert et al., 2006). In addition the investigations of the PEVK deficient strain as well as the N2B deficient strain simultaneously disclosed the importance of the titin I-band for sarcomeric passive stiffness as well as for the signal transduction associated with FHL2 (Granzier et al., 2009; Radke et al., 2007). Both investigations lead to the hypothesis that the titin kinase is

maybe not the only stretch dependent signaling domain of titin which regulates muscle development. We believe that the I- and the M-band domains of titin potentially interact in signaling thereby influencing the force dependent development and adaptation of the striated muscles. Furthermore M-band deficiency leads to a loss of the integrity of the sarcomere which could be the main reason for the observed phenotype of the M-band KO. In order to answer the questions if the sarcomeric disruption or if the titin M-band mediated signaling is the cause of the changes in the M-band deficient animals as well as if there are other domains of titin important for muscle development we generated a novel CRE inducible titin deficient mouse model. These mice lack the 2nd exon of titin which contains the translational start-codons (mus musculus, chr2 76980180-76980183, chr2 76980162-76980164, complement). The deletion of this exonic sequence leads to the loss of titin and its isoforms. This titin deficient animal model (TiEx2MCK) was compared to the already described M-band deficient mouse strain (TiMexMCK) which expresses all important titin domains except of the M-band and its titin kinase domain. The differences of both animal strains should be analyzed on phenotypic, morphologic, ultrastructural, transcriptomic and proteomic levels. The respective results should be arranged into the previous research and should help to address the structural function of titin in more detail. Furthermore we tried to specify the order and the responsibility of the signalling pathways activated by the I-band and/ or the M-band domains of titin.

4 Material and methods

4.1 Material

Chemicals were purchased from GE Healthcare, Invitrogen, Carl Roth GmbH & Co. KG, Sigma-Aldrich Chemie GmbH or Life Technologies™ if not stated otherwise.

4.1.1 Chemicals and kits

Table 1: Kits

Kit	Manufacturer
100mM dNTP Set	Invitrogen
Glutaraldehyde Solution	Sigma-Aldrich
Illumina Total Prep 96 RNA Amp Kit	Life Technologies
MouseRef-8 v2.0 Expression BeadChip Kit	Illumina
PCR Purification Kit	QIAGEN
RNA-to-cDNA Kit	Applied Biosystems
RNeasy Micro Kit	QIAGEN
Roti®-Histol	Carl Roth
Supersignal West Pico/Femto Chemiluminescence-Substrate	Pierce Chemical Co.
Taq DNA Polymerase Kit	Invitrogen
Trichrome Stain (Masson) Kit (HT15-1KT)	Sigma-Aldrich
TriZol™	Invitrogen

4.1.2 Enzymes

Table 2: Enzymes

Enzyme	Manufacturer
DNase I	QIAGEN
Proteinase K	Roche
Taq DNA polymerase	Invitrogen

4.1.3 Oligonucleotides

Table 3: Primer for genotyping

Primer	Sequence
3'neoflox-rev	5'-TCGACTAGAGGATCAGCTTGGGCTG-3'
NBfP1Ex2-for	5'-CACTGGCTTACAGACAGGAAAA-3'
NBrP2Ex2-rev	5'-CATTAAAGGGCAGGCTCTGA-3'
MRZE2 5'-for	5'-ACTTTGATTCCCTATCTTCCTGG-3'
MRZE2 3'-rev	5'-GGGGATACATCCTATAATCAGCC-3'
MG Ti-SL1-for	5'-GTGTCTGGCACTGCTTCCTTGGAAGTG-3'
MG Ti-SL2-rev	5'-ACCGCTCCCATGCCTTCGAGAGTCTTG-3'
Ti-FRTr2-rev	5'-AAGTTCGCTATACAACTGAGGCTAAG-3'
MG-FLP1-for	5'-GTCACTGCAGTTTAAATACAAGACG-3'
MG-FLP-rev	5'-GTTGCGCTAAAGAAGTATATGTGCC-3'
Cre800-for	5'-GCTGCCACGACCAAGTGACAGCAATG-3'
Cre1200-rev	5'-GTAGTTATTCGGATCATCAGCTACAC-3'

for: forward; rev: reverse.

Table 4: Primer-probe set for quantitative real-time PCR (RT-qPCR)

Set	Order number	Manufacturer
AKT1	Mm00437443_m1	Applied Biosystems
Atrogin1	Mm01207878_m1	Life Technologies
DARP (ANKRD23)	Mm00463265_m1	Applied Biosystems
MURF1 (TRIM63)	Mm01185221_m1	Applied Biosystems

Table 5: Primers and probes for quantitative real-time PCR (RT-qPCR)

Primer and probe	Sequence
18S RNA-for	5'-CGCCGCTAGAGGTGAAATTC-3'
18S RNA-rev	5'-TGGGCAAATGCTTTCGCTC-3'
18S RNA-probe	6-FAM-TGGACCGGCGCAAGACGGAC-TAMRA
CP-Ex2/3 for	5'-CGTTACAAAGCGTTGTGGTACT-3'
CP-Ex2/3-rev	5'-GGCAGAGTGGAAGTTGAAATC-3'
CP-Ex2/3-probe	6-FAM-TCACGTTAGTGGTTCCCCAGTTCCTG-TAMRA
NB fExon 357- 358 for	5'-CCGATGGACTCAAGTACAGGATT-3'
NB fExon 357- 358 rev	5'-CCCATGCCTTCGAGAGTCTT-3'
NB fExon 357- 358 probe	6-FAM-TCCTTGGAAGTGGAAGTTCCAGCTAAGATACAC-TAMRA
Mouse-ANP-for	5'-CATCACCCTGGGCTTCTTCCT-3'
Mouse-ANP-rev	5'-TGGGCTCCAATCCTGTCAATC-3'
Mouse-ANP-probe	6-FAM-ATTTCAAGAACCTGCTAGACCACCTGGA-TAMRA
Mouse-BNP-for	5'-AGCTGCTGGAGCTGATAAGAGAA-3'
Mouse-BNP-rev	5'-GTGAGGCCTTGGTCCTTCAA-3'
Mouse-BNP-probe	6-FAM-AGTCAGAGGAAATGGCCCAGAGACAGCTA-TAMRA
Mouse-ß-MHC-for	5'-ATGTGCCGGACCTTGGAA-3'
Mouse-ß-MHC-rev	5'-CCTCGGGTTAGCTGAGAGATCA-3'
Mouse-ß-MHC-probe	6-FAM-CAGCGTTCTGTCAATGACCTCACCAG-TAMRA
Mouse-SERCA2-for	5'-TCCATGAGCAAGATGTTTGTGAA-3'
Mouse-SERCA2-rev	5'-TCCCGAATGACAGACACATAATCTTCT-3'
Mouse-SERCA2-probe	6-FAM-CATCCGAGTTGGAAGTACCAAGGTCCC-TAMRA
Mouse-TNFα-for	5′-CATCTTCTCAAAATTCGAGTGACAA-3′
Mouse-TNFα-rev	5′-CCAGCTGCTCCTCCACTTG-3′
Mouse-TNFα-probe	6-FAM-CCTGTAGCCCACGTCGTAGCAAACCA-TAMRA
Mouse-CARP-for	5′-TGGTGCGGACCTCAA-3′
Mouse-CARP-rev	5′-CCAGTGCAACACCAGATC-3′
Mouse-CARP-probe	6-FAM-TCAAGAACTGTGCTGGGAAGACCC-TAMRA

For: forward; rev: reverse; 6-FAM: 6-carboxyfluorescein; TAMRA: 6-carboxytetramethylrhodamine.

4.1.4 Antibodies

Table 6: Antibodies used for Western Blotting (WB)

Antibody	Species	Dilution	Manufacturer
ANKRD1 (CARP)	rabbit	1:1000	Thermo Scientific
ANKRD23 (DARP)	rabbit	1:500	Abcam
CAMKII	rabbit	1:200	Santa Cruz
CREB1	mouse	1:1000	Cell Signaling /NEB
CryAB	rabbit	1:1000	Calbiocham
FHL1	mouse	1:200	Abcam
FHL2	mouse	1:1000	MBL
GAPDH	mouse	1:8000	Calbiochem
MAPK 1/3 (ERK1/2)	rabbit	1:1000	Millipore
MURF1	mouse	1:1000	Prof. Siegfried Labeit
MURF2	goat	1:1000	Abcam
MYOM1	goat	1:250	Santa Cruz
NBR1	mouse	1:1000	Abcam
NFκB1	rabbit	1:1000	Sigma
NFκB2	rabbit	1:1000	Cell Signaling
p62/SQSTM1	mouse	1:1000	Abcam
TBP	rabbit	1:1000	Cell Signaling
T-CAP	rabbit	1:1000	Eurogentec AGG
TRAF6	rabbit	1:1000	Abcam
Anti-goat-HRP	donkey	1:5000	Santa Cruz
Anti-mouse-HRP	sheep	1:5000	GE Healthcare
Anti-rabbit-HRP	donkey	1:5000	GE Healthcare

4.1.5 Equipment

Table 7: Equipment

Equipment	Company, Type
Agarose gel electrophoresis system	Cosmo Bio Co, Mupid 21
Bioanalyzer	Agilent, Bioanalyzer 2100
Centrifuge	Eppendorf, centrifuge 5804
Centrifuge (Well-Plates)	Sigma, 4K15, Rotor: 09100
Chemiluminescence detection system	PeqLab, Fusion Fx7
Camera / lens	Canon, EOS40D / Canon, EFs 17-85mm
Cooling plate	Leica, EG 1140 C
Desktop centrifuge	Eppendorf, Centrifuge 5415R
Drying hotplate	Thermo Scientific, Raymond A Lamb
Freezer & fridges	Sanyo-biomedical, MDF-U74V / Liebherr, CNP3913
Homogenizer	Qiagen, TissueLyzer II
Microscope	Olympus, CK30/Leica, DMI 6000 B
Microtome	MICROM, HM355S
Paraffin dispensing unit	Leica, EG 1140 H
Paraffin tissue processor	Leica, TP 1020
PCR-system	MJ Research, PTC-225
pH meter	Mettler Toledo, Seven Easy pH
Pipettes	Eppendorf / Gilsen
Plate-Reader	Tecan Infinite M200
Power supply	Biometra, 105BIO-LVD
Real-time PCR system	Applied Biosystems, 7900HT
SDS-P. electrophoresis system	BioRad, Mini-PROTEAN Tetra Cell
Sonicator	Hielscher, UIS250V
Spectrophotometry	NanoDrop ND-1000
Thermo mixer	Eppendorf, Thermomixer comfort
Trans illuminator	Biometra, UVsolo
Water bath	Haake, DC10
Western blot-equipment	BioRad, Mini Trans. Blot Cell

4.1.6 Software

Table 8: Software

Software	Company
Adobe Bridge CS6	Adobe®
Adobe Illustrator CS6	Adobe®
Adobe Photoshop CS6	Adobe®
Aida Array Compare v.4.23	Raytest
Cytoscape 3.2.0	Cytoscape
GraphPad Prism 5.0	GraphPad Inc.
MS Excel 2013	Microsoft
MS Word 2013	Microsoft

4.2 Methods

4.2.1 Animal procedures and experiments

Animals were maintained at the animal facility of the MDC, Berlin-Buch. The mice were bred individually in ventilated cages (IVC) with free access to food and water as well as a regular 12 h day and night rhythm. The animal experiments were performed following the rules for Animal Welfare of the German Society for Laboratory Animal Science (LaGeSo Berlin).

Titin deficient animals were generated previously. The titin M-band deficient mouse strain (TiMexMCK) was produced and published by Michael Gotthardt (Gotthardt et al., 2003). The complete titin deficient mouse strain (TiEx2MCK) was generated by my colleague Nora Bergmann.

The TiEx2MCK knockout strain is referred to as Ex2 KO or titin null and the TiMexMCK knockout strain was termed as M-band KO or M-band deficient strain. The genotypes of the wild-type animals (WT) are lox/lox, cre- or lox/+, cre-. The genotypes of the heterozygous animals (HET) are lox/+, cre+ and the genotypes of the knockout animals (KO) are lox/lox, cre+.

4.2.1.1 Animal and heart photography

Age and gender matched knockout and wild type litter mates were positioned on a white and well illuminated surface and photographed with a Canon EOS40D. The hearts were dissected and rinsed with PBS (Phosphate Buffered Saline). Photos were taken of hearts submerged in PBS with the dish positioned on a white surface. The pictures were analyzed and processed with the software Adobe Bridge / Camera RAW, Adobe Photoshop, and Adobe Illustrator (Table 8, p. 25).

4.2.1.2 Survival analysis

The males of multiple offspring of titin null and M-band deficient breedings were observed over 7 weeks. The pups were weaned at an age of 21 days. Premature death was recorded and a tail biopsy of the corresponding animal was used for genotyping. The surviving animals were tailed and genotyped after 7 weeks.

4.2.1.3 Weight analysis

Different complete titin deficient and M-band deficient knockout, heterozygote and wild-type male littermates were observed over a time range of 7 weeks. The pups were genotyped with an age of 15 days but stayed by the dam until they were weaned with an age of 21 days. The weight was determined every 7 days. Data was collected and tested for outlier by Grubb's test.

4.2.1.4 Force measurements (Grid holding)

The same animals described for the weight analysis were used for the four limb wire grid holding test (Carlson et al., 2010). The force performance was determined every 7 days. Therefor a box of 27 x 27 x 30 cm, filled with wood chip bedding up to 3 cm was used. The wire grid used had a netting of 0.25 cm^2. The animals were set on the grid and accumulated to the environment for a few seconds before the experiments started. The grid was flipped, positioned over the box and the time the mice are able to hold their own body weight was measured. Each animal was tested 3 times with a break of 10 min in between. Data was collected and tested for outlier by Grubb's test.

4.2.1.5 Harvesting mouse tissue

Age and gender matched wild-type, heterozygous and homozygous Ex2 KO and M-band KO males were balanced after shading by cervical dislocation. The hearts and the skeletal muscles of the lower extremities were dissected and the weights were determined. The tissues were collected and snap frozen in liquid nitrogen for protein preparation and DNA or RNA isolation. Furthermore the tibia bone was dissected and the length was measured to determine the weight tibia length ratio. Animals planned for paraffin and electron microscopy sections were sacrificed by cervical dislocation and perfused by different fixation buffers. The hearts and the quadriceps muscle were dissected and processed accordingly to the specific protocols.

4.2.2 Molecular methods

4.2.2.1 Isolation of genomic DNA

4.2.2.1.1 HotSHOT genomic DNA preparation

The HotSHOT method was mainly used to prepare short fragments of genomic DNA for genotyping (Truett et al., 2000). Therefor the mouse tail snips (1-2 mm) were incubated in 50 µl alkaline lysis buffer at 95 ºC and 300 rpm for 30 min. Subsequently the samples were placed on ice for 5 minutes followed by the neutralization of the reaction with 50 µl neutralization buffer. The DNA was directly used for PCR analysis or frozen at --20 ˚C for later analysis.

Alkaline lysis buffer
25 mM NaOH, 0.2 mM EDTA pH 8.0
Neutralization buffer
40 mM Tris-HCl

4.2.2.1.2 Preparation of genomic DNA from mouse skeletal muscles

Mouse skeletal muscle tissues were incubated in 700 µl tail buffer supplemented with 25 µl proteinase K (10 mg/ml) at 52ºC and 700 rpm overnight. Afterwards the proteinase K was inactivated by a 10 min incubation at 95 ºC. The separation of DNA and proteins was initiated by adding 700 µl of phenol/chloroform/isoamyl alcohol. The reaction was continuously inverted for 5 min and centrifuged at 13,000 rpm for another

5 min. After the transfer of the upper phase to a new reaction tube, 1250 µl of precooled 99% ethanol was added. For the DNA precipitation the solution was incubated for 30 min at -20 ºC. Subsequently, the samples were centrifuged for 30 min at 4ºC and 13.000 rpm. The pellet was washed with 70% ethanol, air-dried for 10 min and resuspended in 100 µl Tris-EDTA (TE) buffer. The prepared genomic DNA was used for PCR or frozen at -20 ˚C for later experiments.

Tail buffer

20 mM Tris-base pH 8.0, 5 mM EDTA pH 8.0, 0.2% SDS, 400 mM NaCl

TE buffer

10 mM Tris-HCl, 1 mM EDTA, pH 8.0

4.2.2.2 Isolation of total RNA

For the extraction of total RNA the heart and skeletal muscles of titin null and M-band deficient wild-type, heterozygous and homozygous animals were dissected and snap frozen in liquid nitrogen. The samples were stored at -80 °C. The frozen tissue was prepared for homogenization by pounding with mortar and pestle. During this procedure the tissue and the material were cooled by liquid nitrogen and dry ice to guarantee the stability of the RNA. 50 mg of the powder as well as a ceramic ball were transferred to a 2 ml reaction tube and 1 ml TriZol^{TM} was added. The further solubilization was done in the TissueLyzer (TissueLyzer II, QIAGEN) using a frequency of 20 hits per second for 2 min. Subsequently the reaction was centrifuged for 10 min at 12.000 g and 4 °C. The supernatant was taken and dislocated with 200 µl phenol/chloroform/isoamyl alcohol. After 2 min of inverting the reaction incubated 3 min at RT followed by centrifugation at 12.000 g and 4 °C for 15 min. The RNA containing phase was transferred to a new 1.5 ml reaction tube and incubated with 500 µl of isopropanol for 10 min at RT. The additional centrifugation at 12.000 g and 4 °C for 10 min precipitated the RNA which was washed with 75% ethanol and centrifuged for 10 min at 7.500 g and at 4 °C. The supernatant was discarded and the RNA pellet was dried at room temperature (RT) before resuspending in 89 µl DEPC-H_2O.

4.2.2.2.1 RNA-cleanup

The isolated RNA still contained contaminating DNA which was digested by incubation with DNase I (QIAGEN) for 10 min at RT. Continuously the RNA was purified with the

RNeasy Mini Kit (QIAGEN) following the manufacturer's instructions. RNA was stored at -80 °C.

4.2.2.2.2 Analysis of RNA-integrity

The quality of the RNA was determined by the Bioanalyzer 2100 (Agilent) which uses a chip based gel electrophoresis method. The RNA was processed using the RNA 6000 Nano Kit (Agilent) following the manufacturer's instructions.

4.2.2.3 Determination of nucleic acid concentration

The DNA and RNA concentrations were determined at 260 nm with the NanoDrop ND-1000 spectrophotometer (Thermo scientific).

4.2.2.4 Complementary DNA (cDNA) synthesis

The cDNA synthesis was required for the implementation of a quantitative real-time Polymerase chain reaction (RT-qPCR). Therefor 3 µg of the RNA was transcribed using the RNA-to-cDNA Kit (Applied Biosystems) following the manufacturer's protocol. The cDNA synthesis was performed in a thermocycler for 1 h at 37 °C. The inactivation of the reverse transcriptase occurred at 95 °C for 5 min and the cDNA was stored at -80 °C.

4.2.2.5 Polymerase chain reaction (PCR) for mouse genotyping

The genotyping PCR's were performed in a PTC-225 Thermo Cycler (MJ Research) using the Taq DNA Polymerase Kit as well as the 100 mM dNTP set from Invitrogen. One µl of HotSHOT or 20 50 ng/µl of genomic DNA served as template for the PCR reactions. Primer used and the expected PCR products sizes are listed in Table 3Table 9Table 10 (p.21, 30 and 30). Table 10 illustrates the pipetting and Table 11 (p. 30) explains the cycling of the performed genotyping PCR's.

Table 9: Primers for genotyping and sizes of PCR products

Mouse model	PCR name	Analysis	Forward primer	Reverse primer	Product size
TiMEx2MCK	Neo	Integration	MRZE2 5'-for	3'neoflox-rev	345bp
	RecFlp	Genotype	NBfP1Ex2-for	NBrP2Ex2-rev	256 bp WT
					540 bp RECf
	RecCre	Recombination	MRZE2 5'-for	MRZE2 3'-rev	500 bp
	Flp	Flp	MG-FLP1-for	MG-FLP2-rev	400 bp
	Cre	Cre	Cre800-for	Cre1200-rev	480 bp
TiMexMCK	TiMlox	Genotype	MG Ti-SL1-for	MG Ti-SL2-rev	200 bp WT
					300 bp RECf
	TiMrec	Recombination	MG Ti-SL1-for	Ti-FRTr2-rev	370 bp
	Cre	Cre	Cre800-for	Cre1200-rev	480 bp

MCK: MCK-Cre; WT: wild-type; KO: knockout; RecCre or TiMrec: deleted allele; RecFlp or TiMlox: floxed allele; Flp: flippase recombination enzyme; Cre: causes recombination; for: forward; rev: reverse.

Table 10: Pipetting scheme of the genotyping PCR's

Components	Final concentration		
	Cre, Neo	RecFlp	Flp, TiMlox, TiMrec
10x *Taq* DNA polymerase buffer	1x	1x	1x
50 mM $MgCl_2$	1.5 mM	2 mM	3mM
10 µM dNTP	0.2 mM	0.2 mM	0.2 mM
10 µM Primer mix	0.4 mM	0.4 mM	0.4 mM
5 U/µl *Taq* DNA polymerase	0.03 U/µl	0.03 U/µl	0.03 U/µl
DNA	1 µl	1 µl	1 µl
ddH_2O	Ad to 25 µl	Ad to 25 µl	Ad to 25 µl

Table 11: Genotyping PCR programs

Temperature	Time / Anealing Temperature		
	Neo	Cre, Flp, TiMlox, TiMrec	RecFlp
Initial denaturation 94 ºC	2 min	2 min	3 min
Denaturation 94 ºC	15 sec	15 sec	15 sec
Anealing Temperature	15 sec / 54 ºC	15 sec / 55 ºC	15 sec / 58 ºC
Elongation 72 ºC	45 sec	45 sec	45 sec
Cycles	35 x	35 x	35 x
Final elongation 72 ºC	8 min	8 min	8 min
Storage 10 ºC	∞	∞	∞

The MCK-cre is a striated muscle specific recombinase, active from day E13. In order to control the proper exclusion of our targets we performed the TiMrec and RecCre PCR's on muscle tissue. For the RecCre PCR we needed a specialized protocol described in Table 12 (p. 31). The separation of the PCR products was performed by DNA agarose gel electrophoresis.

Table 12: RecCre PCR pipetting and conditions

Final concentration of components	**PCR conditions**		
	Step	**Temperature**	**Time**
1 x Gitschier buffer	1. Initial denaturation	94 ºC	3 min
10% DMSO	2. Initial annealing	58 °C	5 min
0.4 µM primer mix	3. Initial elongation	65ºC	5 min
0.5 mM dNTP	4. Denaturation	93ºC	30 sec
0.08 mg/ml BSA	5. Annealing	58 °C	1 min
0.025 U/µl *Taq* DNA polymerase	6. Elongation	65ºC	1 min
	7. Final elongation	65°C	10 min
	8. Storage	4ºC	∞
	Repeat steps 4-6: 45 x		

10 x Gitschier buffer

166 mM $(NH_4)_2SO_4$, 670 mM Tris-HCl pH 8.8, 67 mM $MgCl_2$, 50 mM β-mercaptoethanol, 67 mM EDTA pH 8.0

4.2.2.6 Quantitative real-time PCR

Quantitative real-time PCR (RT-qPCR) was used to analyze the transcription of specific genomic sequences in heart, gastrocnemius and quadriceps muscle (Table 5, p. 22). Therefor we dissected 5 weeks old titin null as well as M-band deficient wild-type and knockout animals. The RNA was extracted and transcribed into cDNA. The RT-qPCR was performed with the TaqMan probe based chemistry as well as the Sequence Detection System 7900 HT from Applied Biosystems. The method relies on a fluorophore labeled probe enabling the detection of a specific PCR product as it accumulates during RT-qPCR cycles. Primer and probes used are listed in Table 5 (p. 22). The reaction mix was prepared following the manufacturer's instructions with adaptation to a reaction volume of 10 µl (Table 13, p. 32). Thermal cycling was performed like described in Table 14 (p. 32).

Table 13: RT-qPCR PCR pipetting scheme

qPCR MasterMix Plus (Eurogentec)	1 x
Forward primer	900 nM
Reverse primer	900 nM
Probe	250 nM
cDNA	25 ng

Table 14: RT-qPCR program

1. UNG incubation	50°C	2 min
2. *Taq* activation, UNG inactivation	95°C	10 min
3. Denaturation	95°C	10 sec
4. Elongation	60°C	1 min
Repeat steps 3-4: 50 x		

Data was collected and analyzed with the Sequence Detection System 2.3 software (Applied Biosystems). The comparative CT Method ($\Delta\Delta C_T$ Method) was used as described in the User Bulletin 2: ABI PRISM 7700 Sequence Detection System. Values were normalized to 18S RNA. MS Excel was used to calculate the significances, the fold change and the SEM.

4.2.2.7 DNA agarose gel electrophoresis

Agarose gel electrophoresis was used for separation and analysis of amplified PCR products. Therefor UltraPure™ agarose powder (Invitrogen) was completely melted in 0.5 x Tris-acetate EDTA (TAE) electrophoresis buffer. Ethidium bromide (final concentration 0.5 µg/ml) was added for DNA visualization. The samples were mixed with 3 µl loading buffer before loading the gel. Electrophoresis chambers from Cosmo Bio Co (Mupid-21) were used to separate the DNA at 100 V for 20 min. The utilized ultraviolet transilluminator UVsolo (Biometra) visualized the amplified PCR products. Sizes were determined using 5 µl of GeneRuler™ 50 bp DNA ladder (Fermentas).

0.5 x TAE buffer

20 mM Tris-base, 0.05% acetic acid, 0.5 mM EDTA pH 8.0

Loading buffer

0.5% orange G, 50% glycerol, 25 mM EDTA pH 8.0

4.2.3 Biochemical methods

4.2.3.1 Protein preparation for vertical SDS-agarose gel electrophoresis (VAGE)

The hearts and the quadriceps muscles of 5 weeks old titin null and M-band deficient wild-type and homozygous animals (n = 3) were dissected and snap frozen in liquid nitrogen. The samples were stored at -80 °C. Cooled mortar and pestles were used to prepare a tissue powder which was balanced and lysed in 20 volumes of VAGE sample buffer. The suspension was placed into a Dounce homogenizer (Wheaton) and processed for 5 min at 60 °C. Subsequently 50% glycerol buffer was added (final concentration 12%) and the samples were processed for another 5 min at RT. After a cooling period of 5 min on ice a centrifugation for 5 min at 13.000 rpm occurred. The supernatant was taken and stored at -80°C. Protein concentration was determined by the colorimetric amido black method and the samples were analyzed using VAGE.

VAGE sample buffer

8 M urea, 2 M thiourea, 3% SDS, 0.03% bromphenol blue, 0.05 M Tris-HCl, 75 mM DTT, pH 6.8

50% Glycerol buffer

50 ml H2O, 50 ml Ultrapure Glycerol, 1 Tablet protease inhibitor cocktail (Roche)

4.2.3.2 Protein preparation for SDS polyacrylamide gel electrophoresis (PAGE)

The hearts and skeletal muscles of 5 weeks old titin null and M-band deficient wild-type (n = 4) and homozygous (n = 5) animals were dissected and snap frozen in liquid nitrogen. The samples were stored at -80 °C. Tissue powder was prepared, using a mortar and pestles cooled by liquid nitrogen and dry ice. 50 mg of the powder as well as a ceramic ball were transferred to a 2 ml reaction tube and 500 ml PIPA buffer containing protease inhibitor complex (Invitrogen) were added. The decomposition occurs in the Tissuelyzer (Tissuelyzer II, QIAGEN) at a frequency of 20 for 30 seconds. After an incubation of 30 min on ice the samples were centrifuged at 4 °C for 15 min and 12.000 g. The supernatant was transferred into a new reaction tube and the protein concentration was determined by the colorimetric amido black method.

RIPA-Buffer

50 mM Tris pH 8; 150 mM NaCl; 1% IGPAL; 0.1% Na-DOC; 5 mM EDTA; 0.1% SDS; 0.2 mM PMSF; 0.01 mM Leupeptin

4.2.3.3 Determination of protein concentration

The total protein concentration of the prepared samples was determined by the colorimetric amido black method (Schaffner and Weissmann, 1973). The protein standards were prepared by diluting bovine serum albumin (BSA) in VAGE sample buffer. Equal sized pieces of a nitrocellulose membrane (GE Healthcare) were utilized for protein spotting. The spotted membranes were incubated for 1 min in 0.1% amido black stain solution and subsequently transferred into destaining solution. Destaining was repeated until the protein dots were clearly visible. The elution occurred in 500 µl elution of buffer and shaking for 30 min. Absorbance was measured at 630 nm with the Tecan Infinite M200 spectrophotometer.

Amido black stain solution

45% methanol, 10% acetic acid, 0.1% amido black

Destaining solution

90% methanol, 2% acetic acid

Elution buffer

50% ethanol, 0.05 mM EDTA pH 8.0, 25 mM NaOH

4.2.3.4 Vertical SDS-agarose gel electrophoresis

The vertical SDS-agarose gel electrophoresis (VAGE) was performed on left ventricle and quadriceps muscle tissue of 5 weeks old wild-type and knockout animals (n = 3) according to the protocol of Warren et al., 2003 (Warren et al., 2003). A 1% agarose gel (SeaKem Gold Agarose; Vambrex) was prepared and transferred to the HoeferTM SE600 Ruby (Amersham Bioscience) electrophoresis unit. 1 x running buffer in the lower chamber and 1 x running buffer supplemented with 10 mM β-mercaptoethanol in the upper chamber were utilized for VAGE. Proteins were separated for ~4 h at 4°C and 15 mA / gel or 3 mA / gel overnight. For visualization of the proteins Coomassie staining was used.

5x running buffer

250 mM Tris-base, 1.92 M glycerol, 0.5% SDS

Agarose gel solution

1% agarose, 30% glycerol, 1 x running buffer

4.2.3.5 Coomassie staining

After the VAGE the SDS-agarose gels were fixed with a sufficient volume of fixation solution for 1 h and smooth rocking. Afterwards the gels were dried at 37 °C overnight and rehydrated by washing 3 times for 20 min with ddH_2O. Subsequently the gels were stained with colloidal Coomassie solution for 5 h or overnight (Neuhoff et al., 1988). The destaining was realized by washing the gels with ddH_2O minimal 3 times for 10 min. Pictures were developed by scanning the wet gels and quantified with the AIDA software.

Fixation solution

50% methanol, 12% acetic acid 5% glycerol, ddH_2O

Colloidal Coomassie stock solution

0.1% (w/v) Coomassie Brilliant Blue G250, 2% (w/v) ortho-posphoric acid, 10% (w/v) ammonium sulfate

Colloidal Coomassie working solution

80% (v/v) Stock solution, 20% (v/v) methanol

4.2.3.6 SDS-polyacrylamide gel electrophoresis (PAGE)

The separation of proteins occurs by PAGE (Laemmli, 1970). Therefor 25 µg of total protein were mixed with 4x Laemmli buffer and incubated for 5 min at 95 °C. Samples were loaded onto SDS-polyacrylamide gels with different percentages of polyacrylamide depending on the size of the proteins of interest. The electrophoresis was performed with the Mini-PROTEAN Tetra Cell system (BioRad) at 80 V. Protein size was determined by using 5 µl of PAGE Ruler Prestained Protein Ladder (Fermentas).

SDS-Gel Buffer

1% SDS; 0.2 M glycine; 25 mM Tris-HCl, pH 7.5

4 x Laemmli Buffer

0.08% bromphenol blue; 50% glycerin; 5% ß-mercaptoethanole; 4% SDS

4.2.3.7 Western blotting

After the SDS-PAGE the proteins were transferred to a PVDF-membrane (GE-Healthcare). Therefor the Mini-PROTEAN Tetra Cell (BioRad) was used. Blotting was performed at 200 mA for 3 h. followed by a separate probing with antibodies

4.2.3.8 Immunodetection

The plotted proteins were analyzed by immunodetection. Unspecific binding of the antibody was reduced by incubating the membranes with superblotto for 1 h at RT while shaking. Specific primary antibodies (Table 6, p. 23), diluted in superblotto were used for incubation at 4°C overnight. Unbound antibodies were removed by washing the membranes 3 times with Tris-buffered saline Tween 20 (TBS-T). Secondary antibodies conjugated with horseradish peroxidase (HRP), necessary for visualization, were diluted in superblotto and used for incubation for 2 h at RT. The blots were washed 3 times with TBS-T and developed by chemiluminescence staining with ECL (Supersignal West Femto Chemiluminescent Substrate; Pierce Chemical Co.). Images were taken on the FUSION Fx7 imaging system (PeqLab) and quantified using the Aida Image Analyzer v.2.23 software (Raytest). The signals were normalized to GAPDH and tested for outlier by Grubbs test. The fold-change (F.C.) and the SEM were calculated with MS Excel. The figures were assembled with Adobe Photoshop and Adobe Illustrator CS6.

Superblotto

10 mM Tris-HCl pH 8.0, 150 mM NaCl, 0.1% Tween 20, 0.5% BSA, 2.5% skim milk

TBS-T

50 mM Tris-HCl, 150 mM NaCl, 0.1% Tween 20, pH 7.4

4.2.3.9 Quantitative mass spectrometry

The analysis of the proteome occurred by quantitative mass spectrometry performed at the MDC mass spectrometry facility, managed by Dr. Gunnar Dittmar (MDC, Berlin-Buch). The protein lysates were prepared, following the procedure of protein preparation for SDS-polyacrylamide gel electrophoresis (PAGE). Protein concentration was determined by the colorimetric amido black method (Schaffner and Weissmann, 1973). For the analysis 1.5 mg of total protein was needed. Therefore the quadriceps and heart samples of 5 weeks old Ex2 and M-band knockout (n = 7) and wild-type (n = 10) animals

were pooled, decreasing the variance in each sample. The stable isotope dimethyl labeling method for quantitative analysis was performed for 3 technical replicates (Paul et al., 2011; Trinkle-Mulcahy et al., 2008). Collected data was preprocessed, analyzed by MS Excel and filtered for significance ($p < 0.05$) and fold-change (20%). The gene ontology analysis was performed with the Cytoscape 3.2.0 software. The visualization and the alignment occurred with Adobe Illustrator CS6 (Adobe®).

4.2.4 Histological methods

4.2.4.1 Preparation of paraffin sections

Titin null and M-band deficient knockout and wild type animals were sacrificed by cerebral dislocation and perfused with 15 ml phosphate buffered saline buffer (PBS) followed by 15 ml 4% paraformaldehyde (PFA) in PBS. The hearts and the quadriceps muscles were dissected and incubated in 4% PFA in PBS at 4 ºC overnight. The tissues were shacked in ddH_2O for several hours and placed in embedding cassettes. For dehydration and coating with paraffin the Leica TP 1020 automated tissue processor was used.

Table 15: Dehydration and coating program

70% ethanol	1 x 1 h
90% ethanol	1 x 1 h
96% ethanol	2 x 1 h
100% ethanol	3 x 1 h
Roti®-Histol	3 x 1 h
Paraffin	2 x 1 h

Tissue was embedded in paraffin with the Leica EG 1140 H embedding station and bonded on a cooling plate (Leica EG 1140 C). Paraffin blocks were sectioned using the microtome HM 355S (Microm). Five µm sections floating on a water bath were transferred on HistoBond glass slides (Marienfeld) and dried on a Raymond A Lamb Drying Hotplate (Thermo Scientific). Histological staining of the slides occurred with Masson's trichromatic staining.

4.2.4.2 Masson's trichromatic staining

Masson's trichromatic histology staining (HT15-1KT Kit) was performed to colorize the paraffin sections. Therefore the slides were deparaffinized in Roti®-Histol (3 x 5 min) and rehydrated in a descending alcohol series:

Table 16: Descending alcohol series

100% ethanol	2 x 5 min
96% ethanol	1 x 5 min
80% ethanol	1 x 5 min
70% ethanol	1 x 5 min
50% ethanol	1 x 5 min

Staining occurred in Bouin's solution overnight at RT. Excess stain was removed in running tap water. Subsequently the slides were washed in ddH_2O followed by nuclei staining (black-blue) with working Weigert's iron hematoxylin solution (solution A:B 1:1) for 3 min. Continuously the slides were washed in running tap water as well as ddH_2O for 7 min. The cytoplasm was stained red by incubating with Biebrich Scarlet-Acid Fuchsin solution for 4 min. Afterwards the sections were washed several times with ddH_2O. The collagen staining was facilitated by incubation with phosphotungstic/phosphomolybdic acid solution for 3 min and performed with Aniline Blue staining solution for 5 min. Slides were rinsed with ddH_2O and dehydrated in an ascending alcohol series. For mounting the Roti®-Histo kit was used. The slides dried overnight at room temperature. Pictures were recorded with the Leica DMI 6000 B Microscope. Images were taken with the LAS 3.4.0software. Adobe Bridge, Adobe Photoshop and Adobe Illustrator CS6 were used for assembling the pictures.

Phosphotungstic/phosphomolybdic acid solution

Phosphotungstic acid solution: phosphomolybdic acid solution: dH_2O (1:1:2)

4.2.4.3 Electron microscopy

The ultra-structural analysis of Ex2 KO and M-band KO hearts as well as quadriceps muscles of wild-type, heterozygote and knockout animals was performed by Dr. B. Purfürst from the "Electron Microscopy (EM) Core Facility" (MDC, Berlin). For this experiment the animals were sacrificed by cerebral dislocation and perfused with 15 ml phosphate buffered saline buffer (PBS) followed by 15 ml of EM fixation solution.

The tissues were dissected and transported to the facility in EM fixation solution. After treatment with 1% OsO_4 for 2 h at RT, the samples were dehydrated in an ascending alcohol series and propylene oxide. Embedding of the tissues occurred in Poly/Bed® 812 (Polysciences Inc.) followed by cutting ultra-thin sections. These sections were contrasted with uranyl acetate and lead citrate. The ZEISS 910 electron microscope with a CDD camera (Proscan) and iTEM Software (Olympus Soft Imaging Solutions) were utilized for the examining. Figures of a magnification of 8900x were assembled with Adobe Bridge, Adobe Photoshop and Adobe Illustrator CS6.

EM fixation solution

2% formaldehyde, 2% glutaraldehyde, 0.1 M phosphate buffer

4.2.5 Bioinformatics

4.2.5.1 Data analysis

The data depicted in graphs was preprocessed in MS Excel. The significances were calculated and the graphs were prepared using the GraphPad Prism software. The pictures were formatted by the Adobe Illustrator software.

4.2.5.2 Gene-ontology-analysis

Cytoscape 3.2.0 Plugin ClueGO v1.4 was used for the analysis of the gene ontology (Bindea et al., 2009; Smoot et al., 2011). Parameters: significance = $p < 0.05$, specificity = medium, Minimum number of identifiers and minimum percentage of mapped identifiers = 1, Kappa Score = 3 at 10% involvement of the genes in the pathway.

4.2.6 Statistical analysis

The software MS Excel as well as GraphPad Prism 5.0 were utilized for statistical analysis. Student's t-test was used to assess significant differences between 2 data sets. Data with 3 different groups were analyzed by one-way ANOVA. Groups affected by two independent variables were assessed by two-way ANOVA. The results were represented as mean ± standard error of the mean (SEM). Significances were set at a probability value of 0.05 and are depicted as * $p \leq 0.05$; ** $p \leq 0.01$;*** $p \leq 0.001$.

5 Results

In order to investigate titin in striated muscle physiology and signal transduction we used a morphological and functional approach. A complete titin knockout animal model was established to differentiate the role of Z-disc and M-band titin.

5.1 Generation and validation of the titin Ex2 knockout (TiEx2MCK)

5.1.1 Generation of the titin exon 2 knockout

The titin start-codon (chr2 76980180-76980183, chr2 76980162-76980164, complement), is localized in exon 2 (chr2 76980092-76980195, complement) of the gene. A deletion of this codon is expected to result in a complete loss of titin and all of its isoforms.

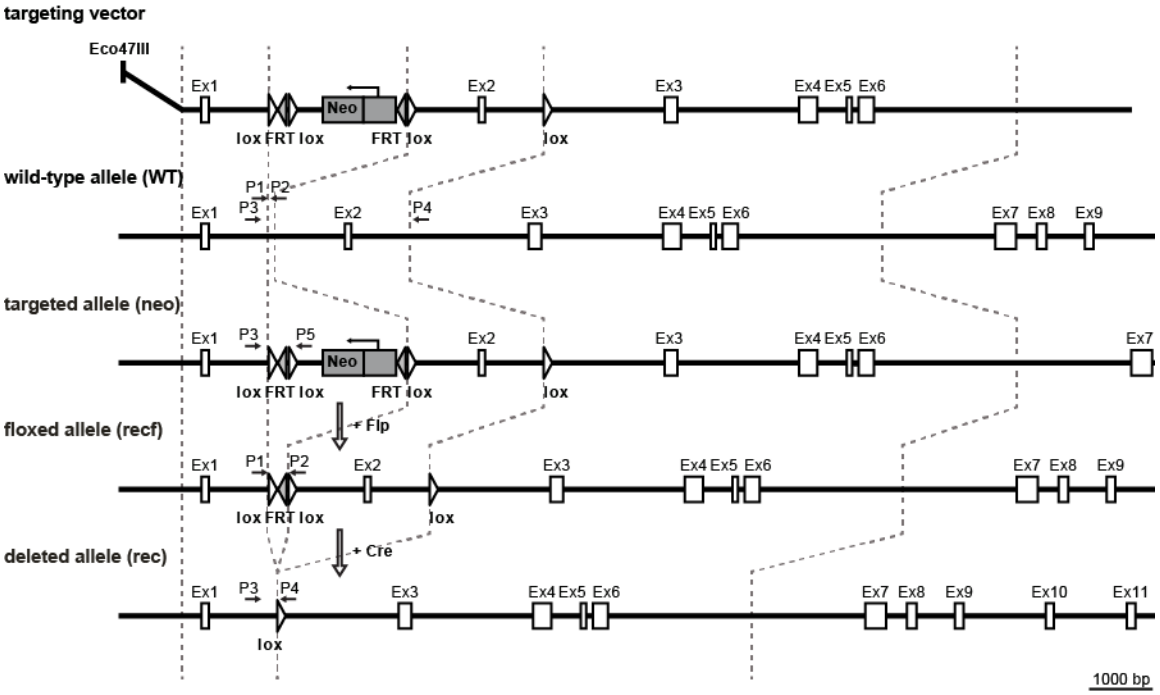

Figure 5: Targeting strategy to generate the Ex2 knockout. Exon/intron (boxes/lines) structure of titin's 5'- exons. Exon two encodes the translational start of titin and was flanked by two lox-sites (white triangle) and 5' a neomycin cassette (grey box) was inserted, which was flanked by two FRT-sites (grey triangle; targeted allele). The neomycin cassette was removed by breeding the animals with a transgenic mouse expressing the Flp recombinase in the germline to obtain the floxed allele. The floxed region was deleted (deleted allele) by breeding to a transgenic mouse expressing the cre-recombinase under control of the muscle creatine kinase promotor (MCKcre) which is active in striated muscle from day E13. Primers for genotyping of the titin alleles are indicated as black arrows (P1: NBfP1Ex2, P2: NBrP2Ex2, P3: MR Z E2 5'F, P4: MR Z E2 3'R, P5: 3'neoflox).

To investigate the function of titin in muscle development and function, we generated a novel titin exon 2 knockout mouse. We designed a targeting vector with titin exon 2 followed by flippase recognition target (FRT) sites flanked by a neomycin (Neo) resistance cassette. This cassette was flanked by two loci of recombination (lox) sites (Figure 5, p. 40). After electroporation of the targeting vector and neomycine- selection, embryonic stem cells (ES) were analyzed by polymerase chain reaction (PCR) to evaluate for the integration of the targeted exon 2 into the titin locus (Figure 6, p. 41). Positive ES-cells were injected into blastocysts and offspring was analyzed for germline transmission by PCR genotyping. The exon 2 floxed positive animals were bred with a flippase recombinase (FLP) expressing strain to avoid potential effects from the Neo cassette (Kaul et al., 2000). FLP mediates the recombination of the two FRT-sites as depicted in Figure 5 (p. 40). The excision of the Neo resistance cassette and the expression of the FLP were tested by the Flp-PCR and the RecFlp-PCR (Figure 6, p. 41). Homozygous TiEx2 animals were back-crossed to 129/S6 mice (Taconic). The NEO and FLP negative offspring were bred to transgenic animals expressing the CRE recombinase under control of the muscle creatin kinase promotor (MCKcre). MCKcre is active from day E13 and drives expression in striated muscle only, leading to the muscle specific excision of Exon 2 in the conditional knockout.

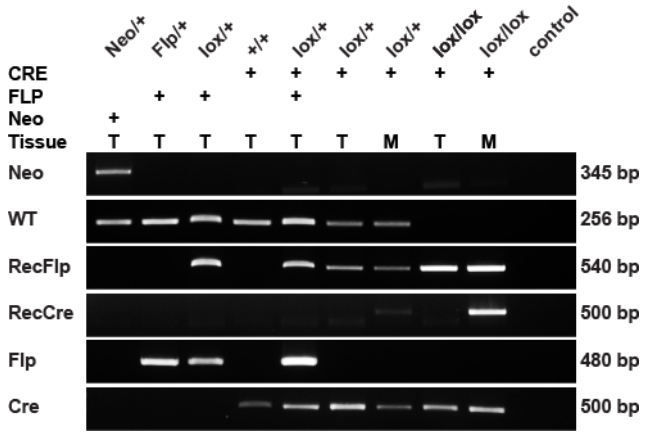

Figure 6: Genotyping of the Ex2 deficient strain. PCR analysis of the phenotypes (Neo/+, wild type Flp/+, heterozygous lox/+ Flp+, wild-type +/+ Cre+, heterozygous lox/+ Flp+ Cre+, heterozygous lox/+ Cre+, homozygous lox/lox Cre+) to determine the exclusion of titin's Ex2 in our mouse model. The targeting allele flanked neomycin cassette of the Neo/+ animals (Neo PCR: MR Z E2 5'F, 3'neoflox) was deleted by mating these animals with an Flp recombinase transgene strain (Flp/+) (Flp PCR: MG-FLP1, MG-FLP2). The Flp recombined offspring (RecFlp PCR: NBfP1Ex2, NBrP2Ex2) was bred with MCKcre transgenic mice (Cre PCR: CRE 800, CRE 1200). Flp- Cre+ heterozygous mice were used to generate homozygous and Cre+ animals. The RecCre PCR (MR Z E2 5', FMR Z E2 3'R) determines the exclusion of titin's Ex2 in striated muscle (T = tail, M = muscle, bp = Base pairs).

The Cre-PCR was performed to test for the MCKcre transgene. Its activity and the deletion of the exon 2 were evaluated by the RecCre-PCR on quadriceps muscle tissue (Figure 6, p. 41). The differences between heterozygous and homozygous TiEx2MCK animals are reflected in the partial and total excision of titin exon 2 (Figure 6, p. 41). The primers and genotyping procedure are provided in the methods section, tablesTable 9,Table 10,Table 11 and Table 12 (p. 30 - 31). The early activity of the MCKcre transgene did not lead to an embryonic phenotype, as offspring from heterozygous males (lox/+, cre+) and floxed females (lox/lox, cre-) resulted in a normal mendelian distribution of the genotypes. We used four litters from a breeding of one male and two females and obtained offspring with an expected sex ratio of 44% female (n = 16) and 56% male (n = 20) and a mendelian distribution of 22% homozygous knockout (lox/lox, cre+; n = 8), 28% homozygous wild-type (lox/lox, cre-; n = 10), 25% heterozygous wild-type (lox/+, cre-; n = 9) and 25% heterozygous (lox/+, cre+; n = 9) animals. Moreover no differences in heart weight (HW), body weight (BW) and the HW/BW ratio of fifteen-day-old complete titin deficient animals were determined (Figure 7, p. 42).

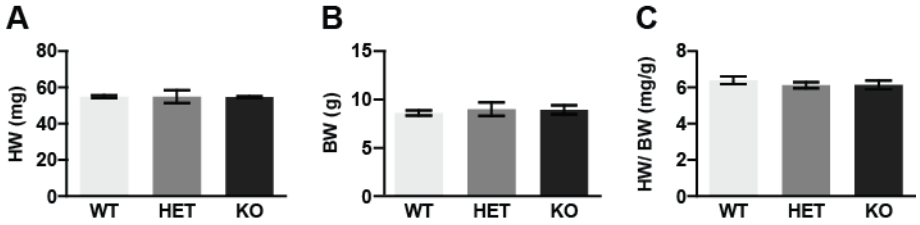

Figure 7: HW and BW comparison of Ex2 KO animals. (A) The heart weight (HW), **(B)** body weight (BW) and **(C)** heart to body weight ratio of 15 days old animals was not different between genotypes. Ex2 wild-type (WT), heterozygous (HET) and KO animals (n = 3, mean with SEM, One-way ANOVA).

5.1.2 Validation of Ex2 knockout

The correct integration of the targeting vector as well as the excision of exon 2 were determined by RT-qPCR on left ventricle (LV) and quadriceps muscle (Q) tissue of complete titin deficient wild-type (WT) and knockout (KO) animals. The corresponding primer/probe set was designed to detect the regions 3' of exon 2 and 5' of exon 3. The forward primer binds to exon 2. The reverse primer binds to the sequence of exon 3 and the probe recognizes the overlapping RNA/ cDNA sequence of exon 2 and 3. An exclusion of exon 2 in the knockout animals prevents the amplification and leads to a loss

of signal. A primer probe set detecting the M-band exons 358 and 359 (Mex1/2) was used as an internal control. In KO mice transcription of exon 2 was significantly decreased in the left ventricle (LV) as well as in the quadriceps (Q; Figure 8, Ex2/3, p. 43). The transcription of the titin M-band region was unaffected (Figure 8, MEx1/2, p. 43).

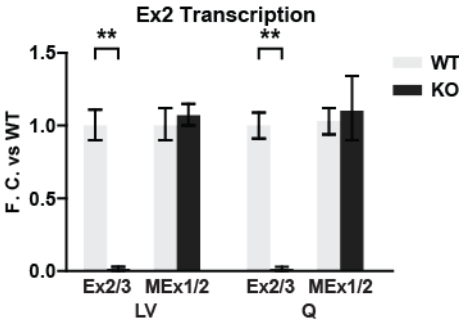

Figure 8: Titin mRNA expression in Exon 2 deficient animals. RT-qPCR of left ventricle (LV) and the quadriceps (Q) of knockout (KO) and wild-type (WT) mice. Transcript levels were significantly decreased after loss of titin exon 2 (Ex 2/3) in the left ventricle and the quadriceps. Transcription of the internal control (MEx 1/2) was unchanged (n = 5, Mean +/- SE, two tailed T-test, $p < 0.01$ **).

In order to verify our finding on the protein level we determined the expression of titin isoforms by SDS-agarose gel electrophoresis (VAGE) using heart and quadriceps tissue (Figure 9, p. 43).

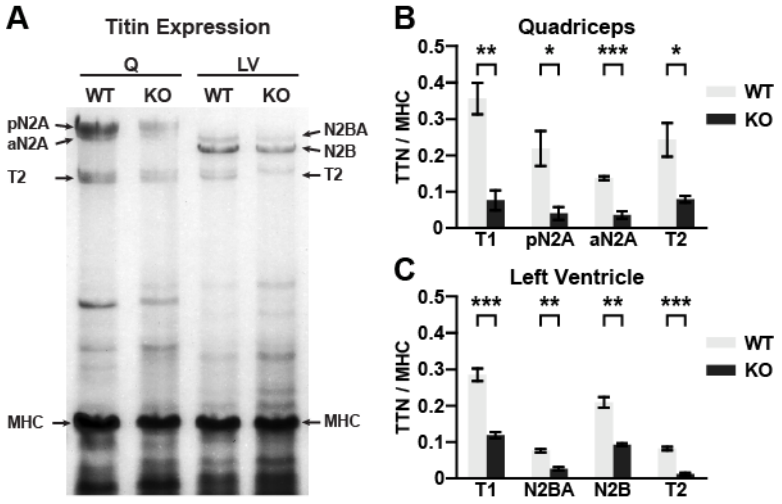

Figure 9: Titin expression in Ex2 KO heart and quadriceps. (A) Coomassie stained VAGE of Ex2 deficient wild-type (WT) and knockout (KO) left ventricle (LV) and quadriceps (Q). Expression of all titin isoforms and degradation products were decreased. This includes the pN2A (3.5 MDa, postnatal) and aN2A (3.4 MDa, adult) isoform in skeletal muscle and the cardiac titin N2BA (3.3 MDa) and N2B (3 MDa) isoforms as well as the degradation products (T2, left and right). **(B, C)** All changes in quadriceps and heart were significant. T1 titin is the combination of the isoforms that are not proteolytically degraded. (n = 3, Mean with SEM, significances calculated by a two tailed T-test, $p < 0.05$ *, $p < 0.01$ **, $p < 0.001$ ***).

In the striated muscle specific knockout, expression of the two skeletal muscle isoforms pN2A (3.5 MDa, postnatal) and aN2A (3.4 MDa, adult) was reduced (summarized as skeletal T1 functional titin). We found a similar reduction of the cardiac titin isoforms N2BA and N2B, summarized as cardiac T1 functional titin (Figure 9 A, left and right, p. 43). The corresponding skeletal and cardiac titin degradation products (T2) were similarly reduced (Figure 9 A, T2 left and right, p. 43). The quantification of the corresponding bands confirmed this observation (Figure 9 B and C, p. 43). The significant reduction of total skeletal muscle titin in Ex2 KO animals (Figure 9 B, T1, p. 43) affected both skeletal N2A titin isoforms (Figure 9 B, pN2A and aN2A, p. 43). Furthermore, the N2A titin degradation products were significantly reduced (Figure 9, T2, p. 43). Similar results were obtained using cardiac samples. Total cardiac titin was significantly depleted (Figure 9 C, T1, p. 43) and both cardiac titin isoforms were affected (Figure 9 C, N2BA and N2B, p. 43). Similar to the skeletal muscle the N2BA and N2B titin degradation products were also reduced (Figure 9 C, T2, p. 43). The signals of the specific isoforms were normalized to myosin heavy chain (MHC) and a two tailed t-test was used to determine significance. In order to investigate if protein stability was altered in knockout animals, we determined the ratios of T1 to T2 titin (Figure 10 A and B, left, p. 44), the ratios of the skeletal muscle specific isoforms pN2A and aN2A (Figure 10 A, right, p. 44), and the cardiac titin isoforms N2BA and N2B (Figure 10 B, right, p. 44). No significant changes in the expression of the different titin isoforms were present in quadriceps muscle (Figure 10 A, p. 44).

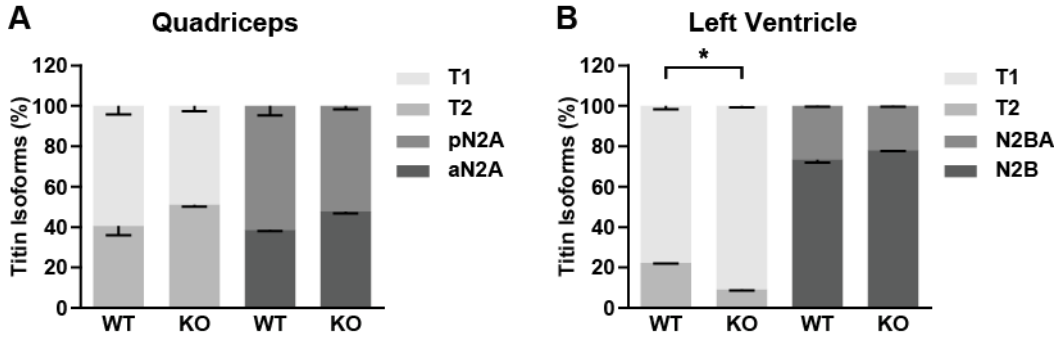

Figure 10: Titin isoforms ratio in Ex2 KO heart and quadriceps. Titin isoform ratios in wild-type (WT) and knockout (KO) heart and quadriceps muscle. **(A)** There was no significant difference in the ratios of functional titin (T1) to degraded titin (T2) (left) or in the ratios of pN2A (3.5 MDa) to aN2A (3.4 MDa) (right) titin in WT vs. KO. **(B)** The ratio of T1 to T2 in the left ventricle was significantly changed, unlike the cardiac N2BA and N2B isoforms. (Mean with SEM, significances calculated by a two tailed T-test, $p < 0.05$ *).

In the heart, the ratio of the functional (T1) and degraded (T2) titin was significantly different with increased intact titin (Figure 10 B, left, p. 44). The ratio of cardiac N2BA and N2B titin was unaffected (Figure 10 B, right, p. 44). These results suggested the global decrease of titin in the Ex2 knockout, which does not affect the expression of titin isoforms.

5.2 Generation and validation of the titin M-band knockout (TiMexMCK)

5.2.1 Generation of the M-band knockout

To study the titin holoprotein in striated muscle, we compared the Exon 2 titin knockout mouse (TiEx2MCK) to the M-band titin knockout (TiMexMCK; Figure 11, p. 45; Gotthardt et al., 2003).

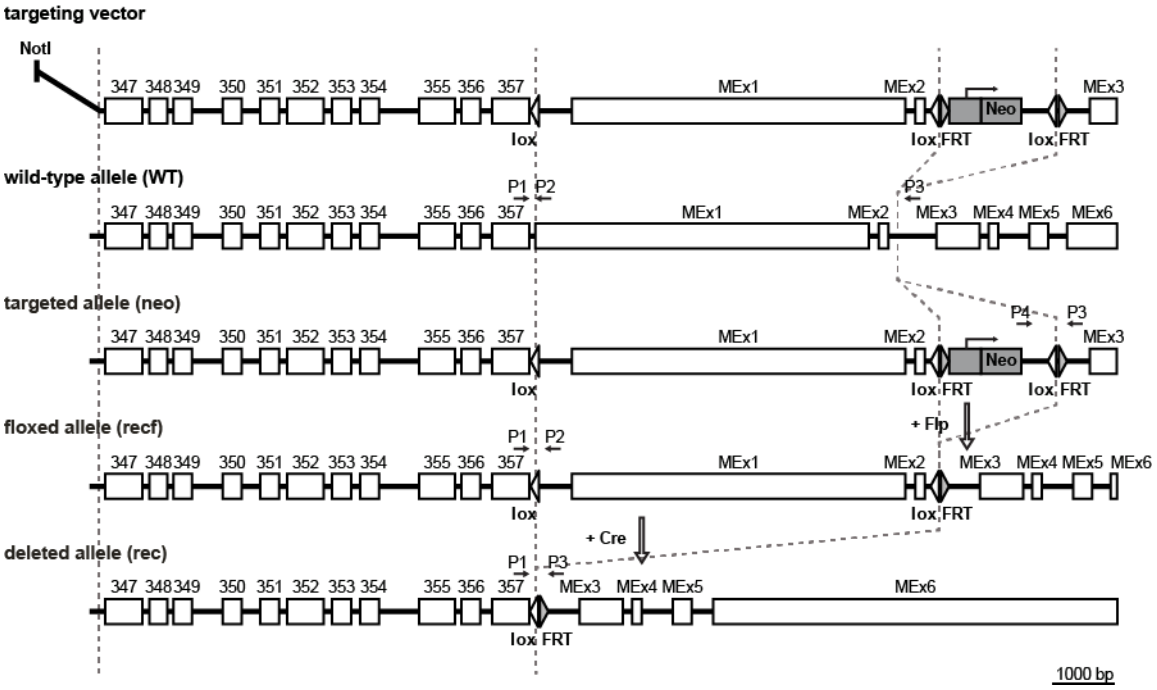

Figure 11: Targeting strategy to generate the M-band knockout. Exon/intron (boxes/lines) structure of titin's 3'- exons. Titin's M-band Ex1 and 2 (MEx1 and 2) were flanked by two lox-sites (white triangle) and 3' a neomycin cassette (grey box was inserted, which was flanked by two FRT sites (grey triangle; targeted allele). The neomycin cassette was removed by breeding the animals with a transgenic mouse expressing the Flp recombinase in the germline to obtain the floxed allele. The floxed region was deleted (deleted allele) by breeding to a transgenic mouse expressing the cre recombinase under control of the muscle creatine kinase promotor (MCKcre) which is active in striated muscle from day E13. Primers for genotyping the titin alleles are indicated as black arrows (P1: Ti-SL 1, P2: Ti-SL 2, P3: Ti FRTr2, P4: MG-neo-2) (Modified from Gotthardt et al., 2003).

In the latter, the floxed M-band exons 358 and 359 (MEx1 and 2) are excised in striated muscle resulting in a truncation of titin that prevents its proper integration of titin into the M-band region of the sarcomere. We performed polymerase chain reaction (PCR) to genotype the TiMexMCK mice (Figure 12, p. 46). The excision of the Neo resistance cassette was determined by the TiMlox-PCR. To detect the MCKcre we used the Cre-PCR. The activity of the striated muscle specific MCKcre recombinase was tested using the TiMrec-PCR and DNA extracted from quadriceps muscle (Figure 12, P. 46; Table 9,Table 10,Table 11 and Table 12, p. 30 - 31).

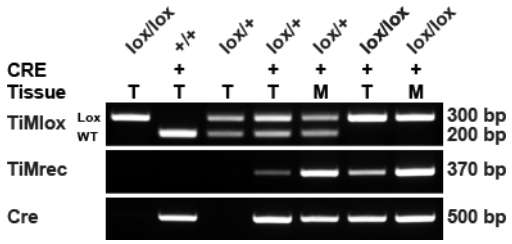

Figure 12: Genotyping of titin M-band deficient mice. PCR analysis of the phenotypes (homozygous lox/lox, wild type Cre+, heterozygous lox/+, heterozygous lox/+ Cre+, homozygous lox/lox Cre+). The floxed targeting allele was recognized by the TiMlox PCR (MG Ti-SL1-for, MG Ti-SL2-rev) The MCKcre allele was detected by the Cre PCR (CRE 800, CRE 1200). The TiMrec PCR (MG Ti-SL1-for, Ti-FRTr2-rev) determines the excision of MEx1-2 in striated muscle (T = tail, M = muscle, bp = Base pairs).

5.2.2 Validation of the M-band knockout

The proper excision of the titin MEx 1 and 2 on RNA level was tested by RT qPCR, similar to the analysis of the complete titin deficient strain. The forward primer was designed to bind in titin's exon 357 and the reverse primer recognizes a sequence in exon 358 (MEx1). The probe was designed to bind the 3' sequence of exon 357 and the 5' sequence of MEx1. The absence of MEx1 leads to a decreased signal. As a control for titin mRNA transcription we used the Ex2/3 primers and probe set. Transcription of exons 358 and 359 (MEx1 and 2) was significantly decreased in KO left ventricle and quadriceps (Figure 13, MEx1/2, p. 47). Transcription of titin exons 2 and 3 was unchanged (Figure 13, Ex2/3, p. 47).

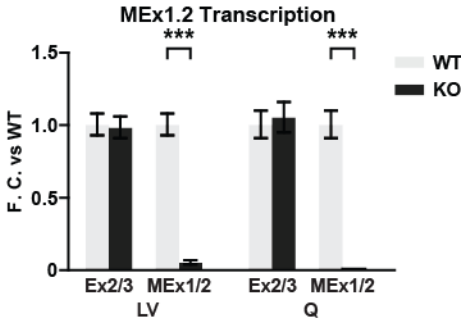

Figure 13: Titin mRNA transcription in MEx1/2 deficient animals. RT-qPCR wild-type (WT) and knockout (KO) left ventricle (LV) and quadriceps (Q). The transcription of titin M-band exons 1 and 2 (MEx1/2) were significantly decreased in LV and Q in the M-band KO. The transcription of the exons 2 and 3 (Ex2/3) was unaffected (n = 5, Mean +/- SE, significances calculated by a two tailed T-test, $p < 0.001$ ***).

The level of titin and titin isoform expression was determined by a SDS agarose gel electrophoresis (VAGE). The postnatal isoform of titin (pN2A) was reduced in skeletal muscle. The deletion of MEx1 and 2 additionally leads to a third T1-band reflected by M-band deficient adult N2A titin (Figure 14 A, N2A-M, p. 48). This observation was verified by the quantification of the bands (Figure 14 B, p. 48). The total amount of titin (T1) was unchanged, but the skeletal muscle specific titin isoform pN2A was significantly decreased. The aN2A titin levels were unaffected which was caused by the M-band deficient pN2A titin having the same size. M-band deficient aN2A titin was significantly expressed only in KO animals (Figure 14 B, N2A-M, p. 48). Additional significant differences of the cardiac N2BA and N2B isoforms were determined (Figure 14 A, T1 right, p. 48), including an additional band reflecting the N2B M-band deficient titin (N2B-M) in the TiMexMCK knockout animals. This observation was verified by the quantification of the gel. Total titin (T1) as well as the cardiac N2BA titin were non-significantly altered, while the N2B isoform of cardiac titin was significantly down regulated (Figure 14 C, p. 48). The N2B-M deficient titin was significantly expressed only in the TiMexMCK knockout animals, similar to the quadriceps muscle samples (Figure 14 C, p. 48). This isoform shift was transmitted to the titin degradation products, indicated by a third band (Figure 14 A, T2 left and right, p. 48). The quantification of the T2 degradation products indicated no change of the total amount of titin T2 in the quadriceps but a significant reduction in the left ventricle. The signals of the specific isoforms were normalized to myosin heavy chain (MHC) and a two tailed t-test analysis was used to determine the significances.

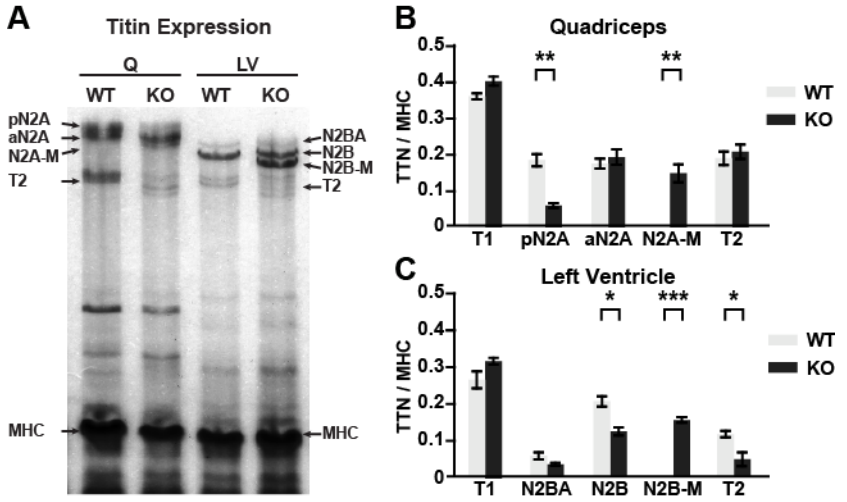

Figure 14: Titin expression in the M-band KO heart and quadriceps. (A) The Coomassie VAGE of wild-type (WT) and knockout (KO) left ventricle (LV) and quadriceps (Q) tissues. The skeletal muscle titin isoform pN2A (3.5 MDa, postnatal) expression was decreased. The expression of aN2A (3.4 MDa, adult) (left) was normal. In addition the KO expressed an M-band deficient aN2A. The KO animals had decreased N2BA (3.3 MDa) but no differences in N2B (3 MDa) cardiac titin (right) and expressed additionally an M-band deficient N2B titin (right). This effect was transferred to the titin degradation products in both tissues (T2 left and right). **(B)** The total skeletal muscle titin (T1) was not significantly changed. The postnatal N2A isoform was significant decreased. The adult N2A titin was unaffected caused by the M-band deficient pN2A isoform having the same size. The M-band deficient aN2A titin (N2A-M) was significantly expressed in the KO animals. The degradation of titin was unaffected. **(C)** The quantification analysis of the cardiac samples determined no differences in total cardiac titin (T1). The N2BA titin was not significantly changed whereas the N2B isoform was significantly decreased. M-band deficient N2B titin (N2B-M) was significantly expressed in the KO animals. The degradation of cardiac titin (T2) was significantly affected (Mean with SEM, significances calculated by a two tailed T-test, $p < 0.05$ *, $p < 0.01$ **, $p < 0.001$ ***).

In order to uncover differences in the stability of titin we compared the T1 to T2 ratios (Figure 15 A and B, left, p. 49). Additionally we calculated the ratios of the skeletal muscle specific titin N2A isoforms (Figure 15 A, right, p. 49) as well as the cardiac titin isoforms N2BA and N2B (Figure 15 B, right, p. 49). No significant changes in the degradation of titin were determined in the quadriceps (T1 to T2). The overall ratio of pN2A to aN2A was unaffected. The separation of the pN2A and the M-band deficient pN2A titin indicated a significant decrease of pN2A ($p < 0.01$) and simultaneously a significantly increased expression of the pN2A-M ($p < 0.01$). Additionally aN2A was decreased ($p < 0.05$) and aN2A-M increased ($p < 0.01$) (Figure 15 A, p. 49). Furthermore the M-band deficiency led to a significantly decreased degradation of titin in the heart (T1 to T2). Similar to the quadriceps muscle the overall ratio of N2BA to N2B was unaffected. Including the M-band deficient N2BA-M and N2B-M into the analysis we determined a significant decrease of functional N2BA ($p < 0.01$) and N2B titin ($p < 0.001$) and simultaneously a significantly increased expression of N2BA-M and

N2B-M ($p < 0.001$) titin (Figure 15 B, p. 49). These results indicated an unaffected titin expression in the M-band KO and significantly demonstrated the expression of M-deficient skeletal and cardiac titin isoforms.

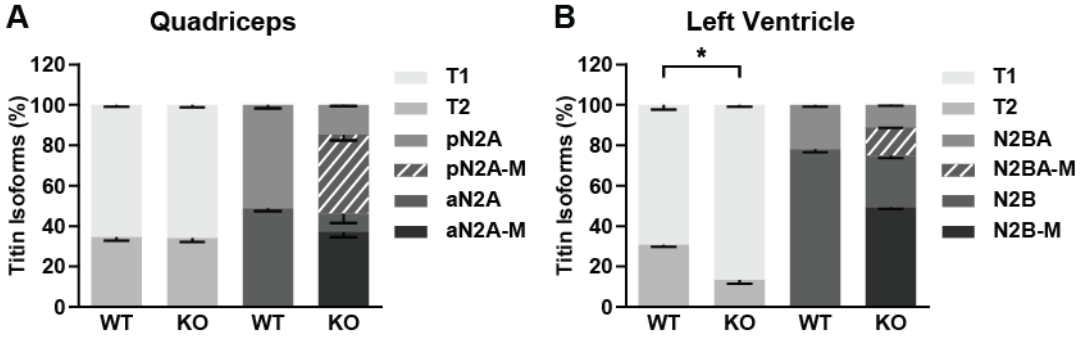

Figure 15: Titin and its isoform ratio in the M-band KO heart and quadriceps.(A) The skeletal titin to titin degradation ratio (T1:T2) (left) was not significantly changed but were shifted to the overexpression of M-band deficient pN2A (postnatal) and aN2A (adult) titin. **(B)** M-band deficiency led to a significantly affected titin degradation in the heart as well as to the overexpression of M-deficient cardiac N2BA and N2B titin (Mean with SEM, significances calculated by a two tailed T-test, $p < 0.05$ *).

5.3 Comparative phenotyping of the Ex2 and the M-band knockout

5.3.1 Skeletal muscle phenotypes

5.3.1.1 Skeletal muscle morphology of the Ex2 and the M-band knockout

The E2 knockout developed a severe progressive muscle weakness, which affected posture and gait.

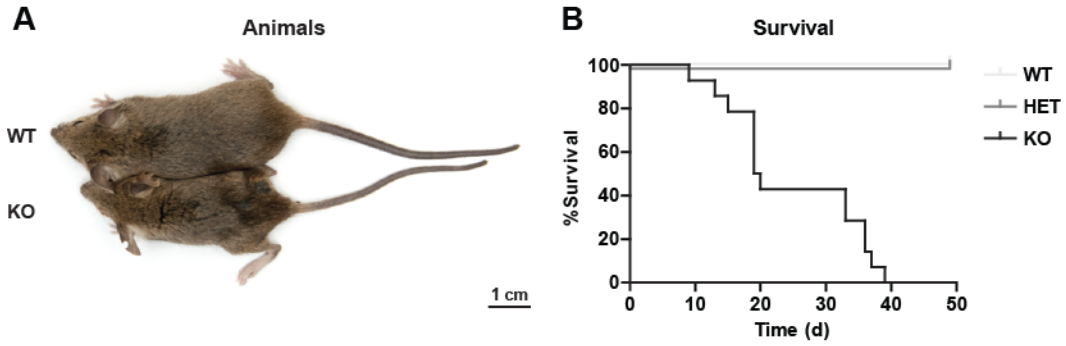

Figure 16: Appearance and survival of the Ex2 KO mice. (A) The 5 weeks old Ex2 knockout mouse (KO, bottom) was smaller and weaker than its unaffected wild-type littermate (WT, top) and developed a bent spine and paresis in the lower extremities. **(B)** Compared to the WT and heterozygous (HET) the Ex2 KO animals significantly died before an age of 40 days (percent with SE, Log-rank (Mantel Cox) Test: $p < 0.0001$, Log-rank Test for trend: $p < 0.0001$; WT, HET, KO $n = 14$).

This resulted in a bent spine, paresis in the lower extremities and ptosis of the eyelids (Figure 16 A, p. 49). As the severity of the phenotype increased, Ex2 KO mice died before an age of 40 days. Half of the complete titin deficient animals died before an age of 20 days (Figure 16 B, p. 49). The weights of wild-type (n = 6), heterozygous (n = 6) and titin null (n = 3) littermates were determined every 7 days over a time range of 5 weeks with a strong decrease of body weight for the knockout animals from week two. This decreased weight stagnated significantly between the 3rd and the 5th week. The weight and the development of the heterozygous animals were normal and similar to the wild-type animals (Figure 17 A, p. 50).

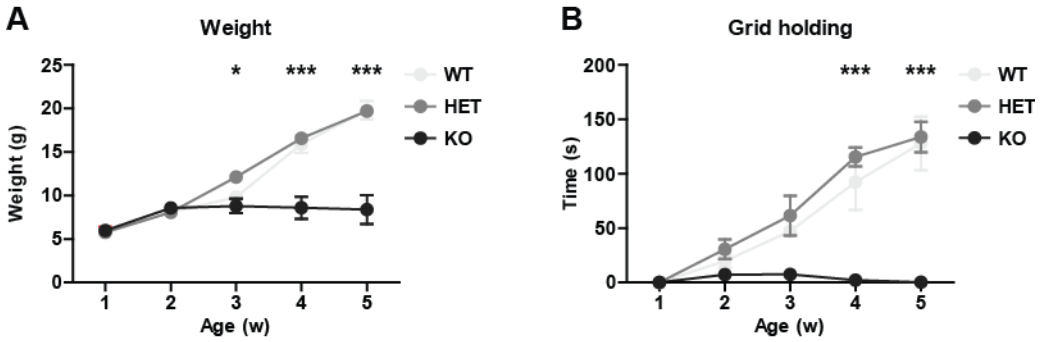

Figure 17: Decreased weight and strength endurance in titin null mice. (A) Compared to the wild-type (WT, n = 6) and heterozygous (HET, n = 6) the Ex2 KO littermates (KO, n = 3) significantly stopped growing after the second week and stayed at a weight of less than 10g. The WT and HET animals had a normal gain of weight. **(B)** The strength endurance of the Ex2 KO mice was significantly reduced, starting at the first week of age. The WT and HET littermate males developed normal (mean with SEM, Two-way ANOVA analysis with Bonferroni posttest $p < 0.05$ *, $p < 0.001$ ***, time points 4 and 5 = KO vs. WT, time point 3 = KO vs. HET).

To evaluate skeletal muscle function of the Ex2 KO animals we measured the strength endurance using a four limb wire grid holding test. This experiment measures the capability of the mice to hold their own body weight. Six wild-type (WT), heterozygous (HET) and titin null (KO) animals were measured every 7 days over a time range of 5 weeks. Strength endurance was already reduced after the 1st week, significant from the 4th week of age (Figure 17 B, p. 50). Force development of the HET animals was not compromised. The loss of body weight and the loss of strength endurance suggested skeletal muscle atrophy which was verified by skeletal muscles weights of the lower extremities (Figure 18, p. 51).

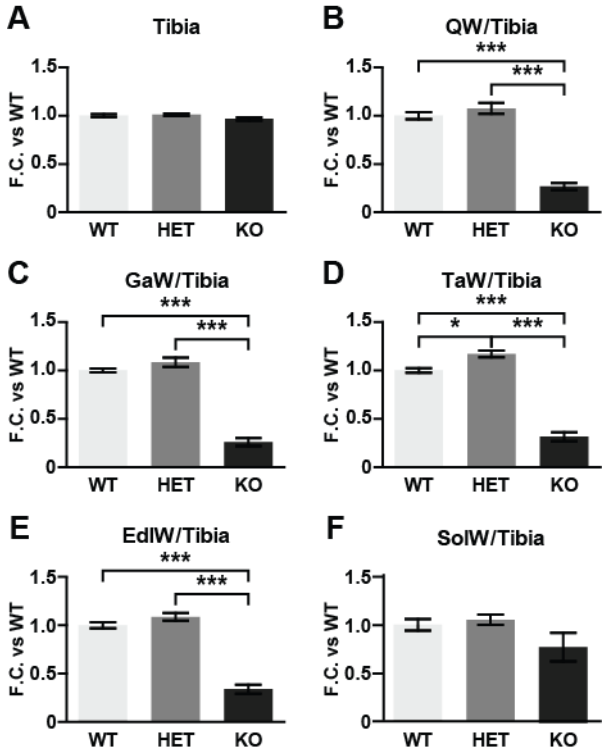

Figure 18: Skeletal muscle atrophy of the Ex2 knockout. (A) The tibia length of wild-type (WT), heterozygous (HET) and their knockout littermates (KO) was equal. **(B-F)** The Quadriceps weights of the Ex2 KO mice were significantly decreased **(B)**, Gastrocnemius **(C)**, Tibialis anterior **(D)** and Extensor digitorum longus **(E)** but not in Soleus muscle **(F)** (n = 6, mean with SEM, significances determined by One-way ANOVA with Bartlets test for equal variances and Bonferroni's multiple comparison tests, $p < 0.05$ *, $p < 0.001$ ***).

The KO animals developed major differences in body weight compared to the WT and HET animals (Figure 17 A, p. 50). Hence we determined the tibia length of Ex2 wild-type (WT), heterozygous (HET) and knockout (KO) animals (n = 6) for normalization. By comparing the KO, the HET and WT animals no significant differences in the length of the tibia were determined (Figure 18 A, p. 51). The ratio of the skeletal muscle weight to tibia length ratio suggested a significant and global decrease of skeletal muscle mass, reflected by significant skeletal muscle atrophy in quadriceps (Q), gastrocnemius (Ga), tibialis anterior (Ta), and extensor digitorum longus (Edl) muscles (Figure 18 B to E, p. 51). The weight of soleus (Sol) muscle was not changed (Figure 18 F, p. 51). The 5 weeks old M-band knockout mice had a severe progressive muscle weakness similar to the Ex2 knockout. The M-band deficient mice were paralyzed and highly constricted in their posture and gait. Additionally the knockouts developed a bent spine and paresis of the lower extremities. Furthermore the KO animals had an acute ptosis of the eyelids (Figure 19 A, p. 52). This phenotype was present from 15 days of age (Figure 19 B, p. 52).

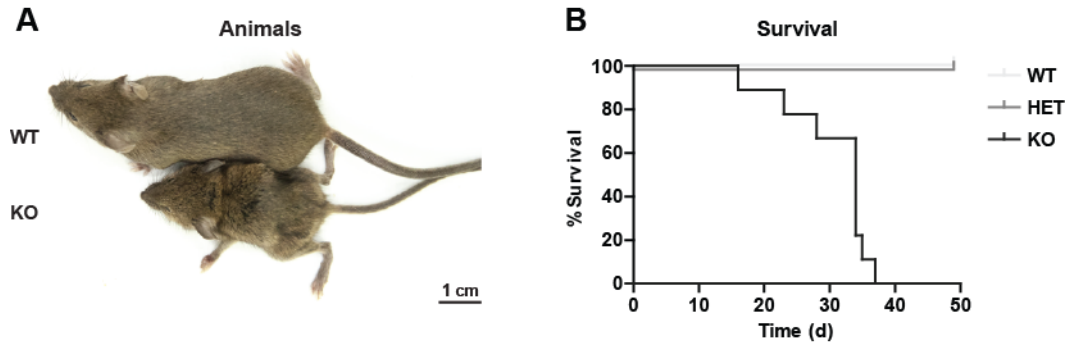

Figure 19: Appearance and survival of the M-band knockout mice. (A) The M-band knockout mouse (KO, bottom) developed severe paresis in the lower extremities and a strongly contorted spine. The KO animal was smaller and weaker than its unaffected wild-type littermate (WT, top). **(B)** The survival of the M-band KO animals was significantly decreased. The animals died before an age of 40 days. The control WT and HET animals developed normal (n = 9, percent with SE, Log-rank (Mantel-Cox) Test: $p < 0.0001$, Log-rank Test for trend: $p < 0.0001$).

The weight of M-band wild-type (WT), heterozygous (HET) and knockout (KO) littermate males (6 per group) were determined every 7 days over time range of 5 weeks. The M-band deficient mice were decreased in body weight starting at the second week which became significant at the third week. Moreover the animals failed to thrive and stay at a level of 5-10 g of body weight (Figure 20 A, p. 52). Similar to the Ex2 KO animals we expected a correlation of the loss of body weight and a skeletal muscle atrophy significantly decreasing strength endurance and force development. To evaluate skeletal muscle function of the M-band KO animals we measured the strength endurance using a four limb wire grid holding test. This experiment measures the capability of the mice to hold their own body weight. Six wild-type (WT), heterozygous (HET) and titin null (KO) animals were measured every 7 days over a time range of 5 weeks.

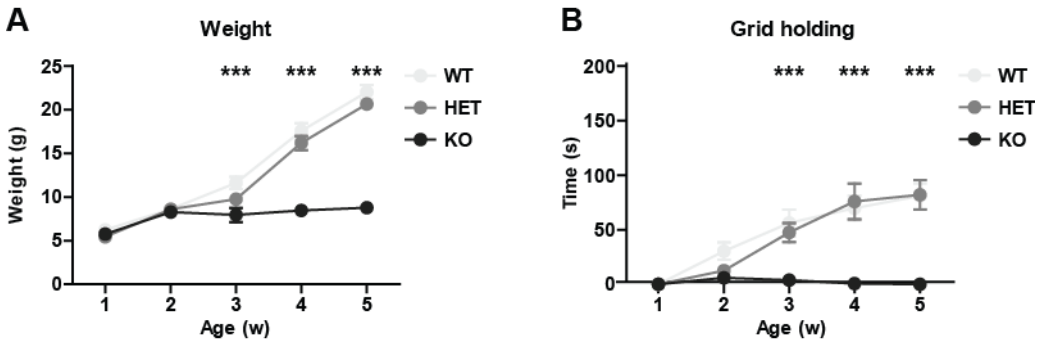

Figure 20: Decreased weight and strength endurance of the M-band knockout. (A) The M-band KO mice had a significantly decreased gain of weight compared to the wild-type (WT) and heterozygous (HET) littermate males. **(B)** The WT and HET animals developed normal with no abnormalities, while the KO mice significantly failed to develop strength endurance (n = 6, mean with SEM, Two-way RM ANOVA analysis with Bonferroni posttest $p < 0.001$ ***, time points 3, 4 and 5 = KO vs. WT, same significance for KO vs. HET at the time points 4 and 5; Data was checked for outlier by Grubbs outlier test)

Strength endurance was already reduced after the 1st week, significant from the 3rd week of age. The WT and HET animals developed normal muscle forces (Figure 20 B, p. 52). Adjacent we dissected the animals after finishing the weight and grid holding experiments. We collected and measured the weight of the quadriceps (Q), the gastrocnemius (Ga), the soleus (Sol), the tibialis anterior (Ta) and the extensor digitorum longus. Huge differences of the body weight of wild-type (WT), heterozygous (HET) and knockout (KO) animals (n = 6, Figure 20 A, p. 52) compelled us to use the tibia length for normalization. We determined no significant differences in the tibia length (Figure 21 A, p. 53). The analysis of the skeletal muscle weights of the M-band WT, HET and KO animals indicated significantly a skeletal muscular atrophy in the knockout, affecting all analyzed muscles. The weights of all measured muscles of the KO animals were up to 75% lighter compared to the WT or the HET animals (Figure 21 B and E, p. 53). In contrast to the Ex2 deficient strain the weight of soleus muscle in the M-band knockout was significantly decreased (Figure 21 F, p. 53).

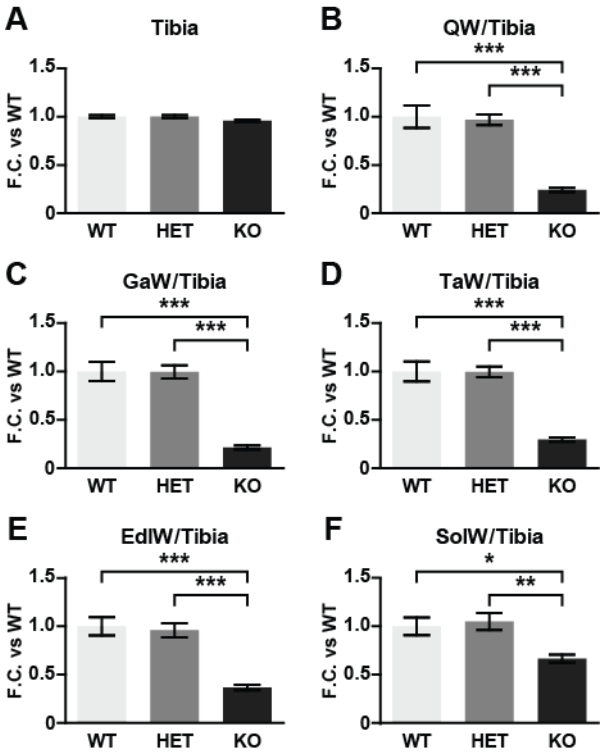

Figure 21: Skeletal muscle atrophy of the M-band knockout. (A) Wild-type (WT), heterozygous (HET) and knockout littermates (KO) held no significant differences in tibia length. The M-band KO mice had significantly decreased muscle weights in Quadriceps **(B)**, Gastrocnemius **(C)**, Tibialis anterior **(D)**, Extensor digitorum longus **(E)** and Soleus muscle **(F)** (n = 6, mean with SEM, significances determined by One-way ANOVA with Bartlets test for equal variances and Bonferroni's multiple comparison tests, $p < 0.05$ *, $p < 0.01$ **, $p < 0.001$ ***).

Morphological differences of the complete titin deficient and the M-band deficient mouse models were analyzed by comparing our collected survival, weight and grid holding data. Because of the complete loss of titin we expected a stronger effect and a more severe phenotype in the Ex2 knockout. The survival, weight or strength endurance of both strains was significantly different (Figure 22 A-B, p. 54).

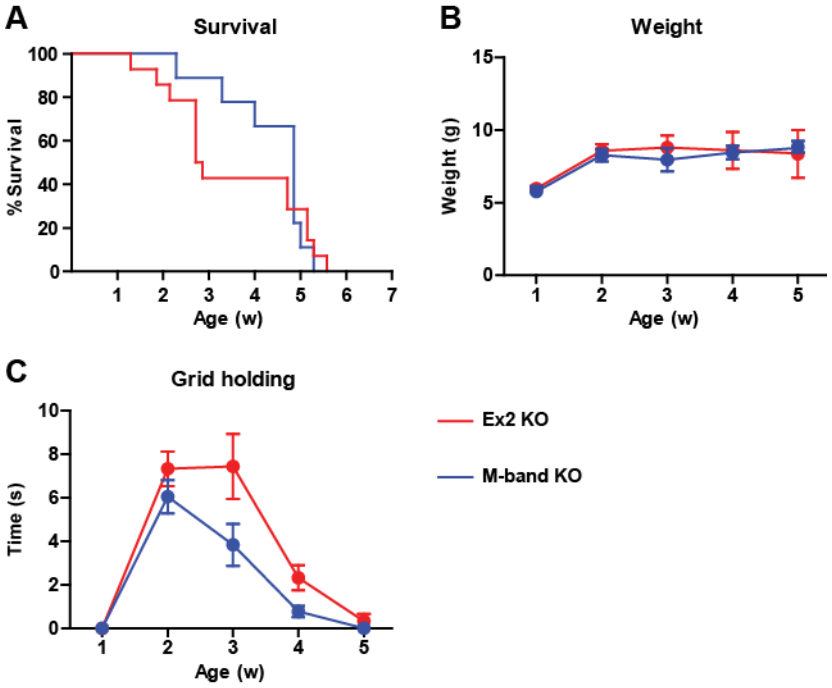

Figure 22: Comparison of the Ex2- and the M-band knockout. (A) Both knockouts led to early death by six weeks of age. There was no significant difference in survival between genotypes (Ex2 KO n = 14, M-band KO n = 9, Log-rank (Mantel-Cox) Test, Gehan-Breslow-Wilcoxon posttest), **(B)** in weight or **(C)** in strength endurance (Ex2 KO n = 3, M-band KO n = 6, mean with SEM; T-test (Mann Whitney Test)).

5.3.1.2 Skeletal muscle histology of the Ex2 and the M-band knockout

The severe skeletal muscle atrophy was verified by the dissection and the extraction of the quadriceps muscles of 5 weeks old Ex2 wild-type (WT) and knockout (KO) animals (n = 3). Compared to the Ex2 WT the KO held an increased cell number and an unorganized structure along the myofibers (Figure 23 A, longitudinal, p. 55). Additionally the loss of titin led to smaller cells with centralized nuclei (Figure 23, p. 55).

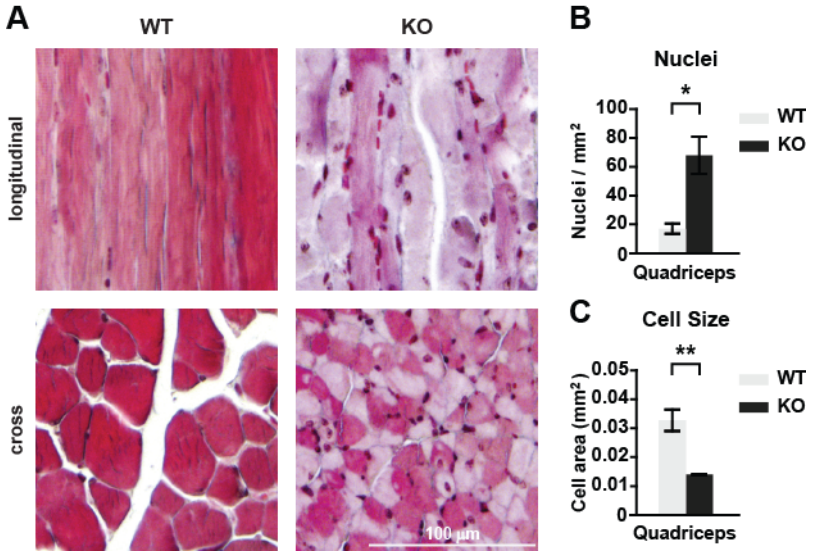

Figure 23: Skeletal muscle pathology in the Ex2 knockout. (A) The longitudinal and cross sections of the Ex2 KO quadriceps indicated an unorganized structure and smaller cells with centralized nuclei compared to the WT. **(B)** Quantification of the number of nuclei for the WT and KO mice. The number of nuclei in the KO animals was significantly increased. **(C)** The cell size of the KO animals were significantly decreased compared to the WT ($n = 3$, mean with SEM, significances calculated by two tailed T-test, $p < 0.05$ *, $p < 0.01$ **).

To evaluate the structural basis of the skeletal muscle atrophy we performed electron microscopy of quadriceps muscle tissue from 3-weeks-old male wild-type (WT), heterozygous (HET) and Ex2 knockout (KO) animals ($n = 1$) (Figure 24, p. 55). The sarcomeres of WT and HET quadriceps muscles were well organized with a normal Z-disc, I-band, A-band and M-band structure (Figure 24, p. 55). In KO animal myofibrils disassembled and looked compressed with a macerated Z-discs. The disruption of the sarcomere proceeded from the Z-disc to the M-band (Figure 24, p. 55).

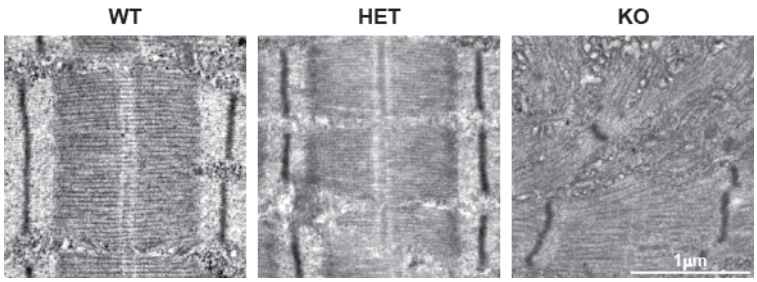

Figure 24: Disassembly of the sarcomere in the Ex2 knockout. Electron microscopy of the quadriceps of 3 weeks old wild-type (WT, left), heterozygous (HET, middle) and Ex2 knockout (KO, right) mice. The sarcomeres of the WT and HET animals were well organized and Z-disc, I-band, A-band and M-band structure was properly maintained. In KO mice, sarcomeric structures were partially disrupted (right). The tissue was characterized by completely disrupted sarcomeres next to some potential functional sarcomeres.

The severe skeletal muscle atrophy of the M-band knockout was verified by microscopic analysis similar to the experiments of the Ex2 deficient strain. Similar to the Ex2

knockout the M-band deficient mice indicated an unorganized structure along the myofibers (Figure 25 A, longitudinal, p. 56). Additionally cells of the KO-quadriceps were smaller with centralized nuclei (Figure 25 A, cross, p. 56). The increased number of nuclei and the decreased cell size were verified by quantification (Figure 25 B and C, p. 56).

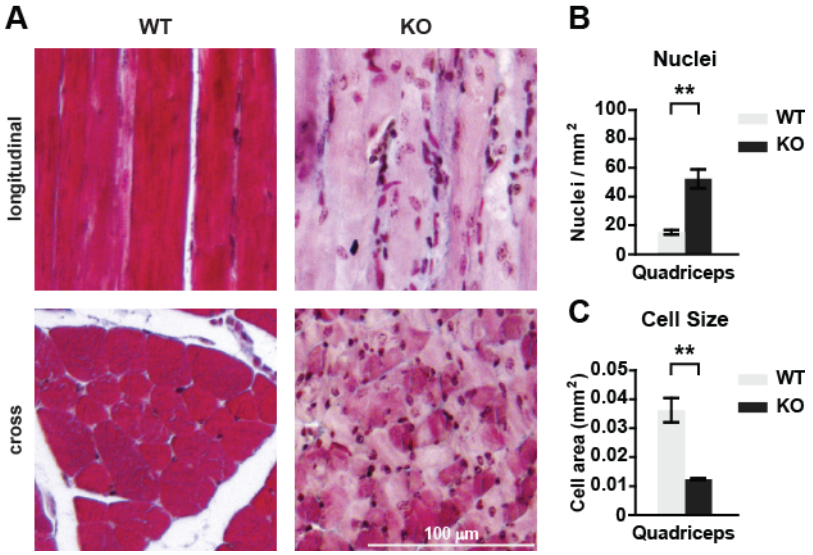

Figure 25: Skeletal muscle disruption of the M-band knockout. (A) The longitudinal and cross sections of 5 weeks old M-band knockout (KO) animals indicated an unorganized structure with smaller cells and centralized nuclei compared to the wild-type (WT) animals. **(B)** The number of nuclei in the M-band KO animals was significantly increased, compared to the WT animals. **(C)** The cell size of the M-band KO animals were significantly decreased compared to the WT (n = 3, Mean with SEM, significances calculated by two tailed T-test, $p < 0.01$ **).

In order to investigate the skeletal muscle atrophy of the M-band deficient animals we performed electron microscopy experiments similar to the analysis of the titin null mice (Figure 26, p. 57). The sarcomeres of WT and HET quadriceps muscles were well organized with a normal Z-disc, I-band, A-band and M-band structure, similar to the Ex2 deficient strain (Figure 26, left and middle, p. 57). This structure was disrupted in the M-band knockout animals. The affected myofibrils were compressed sarcomeres and weak M-band structures. The disruption of the sarcomere proceeded from the M-band to the Z-disc (Figure 26, right, p. 57).

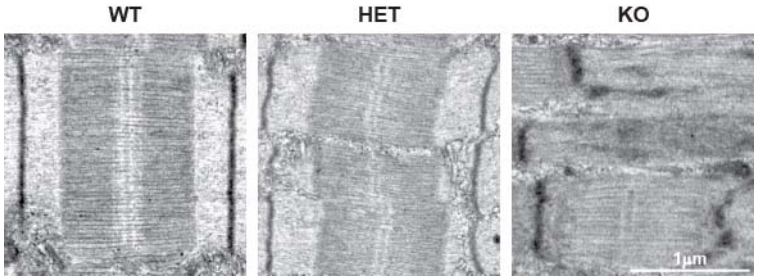

Figure 26: Disassembling of the sarcomere in the M-band knockout. The Z-disc, I-band, A-band and M-band structure of 3 weeks old wild-type (WT, left) and heterozygous (HET, middle) mice were unaffected compared to the knockout animals (KO, right). The quadriceps muscles were normal developed and held no disruption or disarrangement. Contrary the M-band structures of the M-band KO (right) were diffuse. The Z-discs remained normal until the sarcomere started disassembling at the M-band.

5.3.2 Cardiac phenotypes

Expression of the CRE recombinase under control of the creatin kinase promotor started at day E13 in striated muscle. In both mouse models, we therefore expected a developmental cardiac phenotype.

5.3.2.1 The morphology of the complete titin deficient heart (TiEx2MCK)

To evaluate the morphology of cardiac muscle, we dissected the hearts of 5-week-old wild-type (WT), heterozygous (HET) and knockout (KO) animals. Compared to the WT, hearts from Ex2 KO animals were enlarged with weak ventricles and enlarged atria. Especially the enlarged atria indicated a cardiac insufficiency (Figure 27 A, p. 58). We validated our findings in 6 WT, HET and titin null (KO) animals. The hearts were removed, and weighted, together and with atria, right and left ventricle separately. Because of the differences in body weight (Figure 17 A, p. 50) and the unchanged tibia length (Figure 18 A, p. 51) we used the tibia length for normalization of the heart weight. The hearts of the WT, the HET and KO were not significantly different (Figure 27 B, p. 58). In order to analyze which heart compartments are specifically affected we determined the compartment weight to heart weight ratio (HW). The Ex2 KO animals developed a significantly increased weight of the atria (ATW) which could be a secondary effect of the heart insufficiency (Figure 27 C, p. 58). Furthermore there was no difference in weight of the right ventricle (RVW; Figure 27 D, p. 58), but the data indicated a significantly increased weight of the left ventricle (LVW) (Figure 27 E, p. 58). This suggested the development of a dilated cardiomyopathy in the complete titin deficient animals.

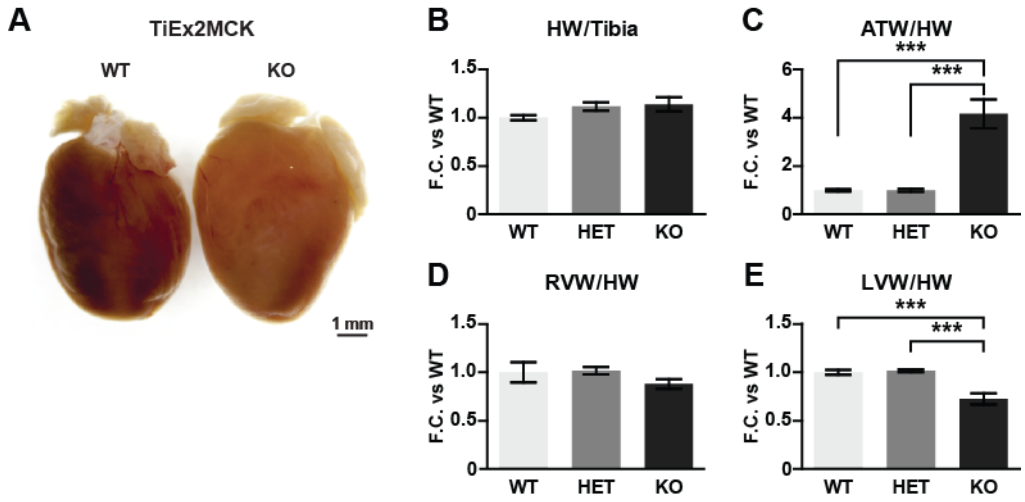

Figure 27: Dilated cardiomyopathy of the Ex2 KO heart. (A) The 5 weeks old Ex2 knockout (KO) heart was enlarged with increased atria and ventricles compared to the wild-type (WT). **(B)** The heart weight of wild-type (WT), heterozygous (HET) and complete titin deficient (KO) hearts were not significantly different. **(C)** The KO hearts developed significant enlarged atria in contrast to the WT and HET organs. **(D and E)** The right ventricle (RV) of the knockout heart was unaffected in weight, while the left ventricle (LV) weight was significantly decreased in comparison to the WT and HET hearts (n = 6, mean with SEM, significances determined by One-way ANOVA with Bartlets test for equal variances and Bonferroni's multiple comparison tests, $p < 0.001$ ***).

5.3.2.2 Histology of the complete titin deficient heart

To investigate genotype dependent cardiac morphology we dissected 5 weeks old Ex2 wild-type (WT) and knockout (KO) animals (n = 3) and extracted the hearts. The longitudinal sections of the WT and KO hearts confirmed the enlarged atria in the titin null animals. Furthermore we determined thinner walls of the ventricles which especially increased the lumen of left ventricle (Figure 28 A, top, p. 59). The higher magnification (20 x) of the septum (black arrow and square) indicated an unorganized structure of the cardiomyocytes in the knockout heart. The cells were smaller and held centralized nuclei (Figure 28 A, down, p. 59). Additionally we quantified the number of nuclei and the cell sizes. Compared to the WT, a significantly increased number of nuclei as well as a significantly decreased size of the cardiomyocytes could be determined in the Ex2 KO mice (Figure 28 B and C, p. 59).

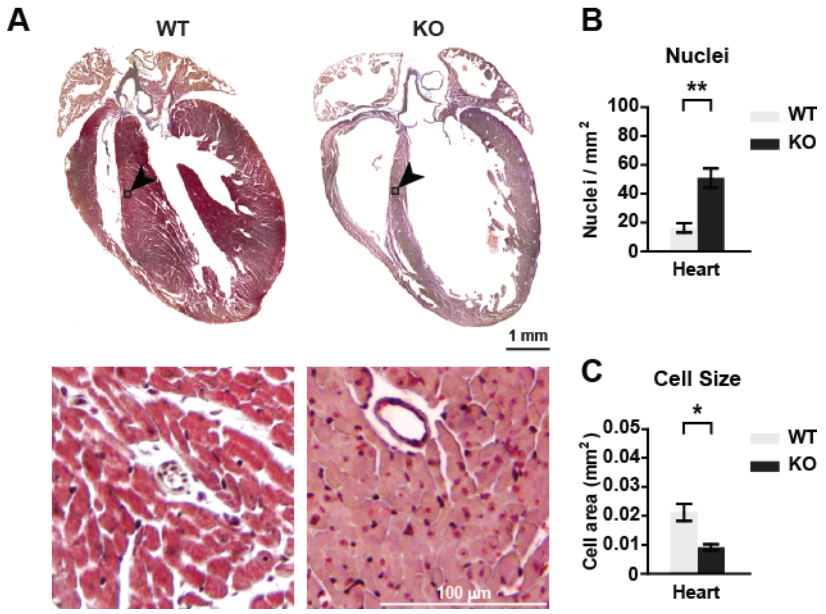

Figure 28: Impaired postnatal development of complete titin deficient heart. (A, top) The 5 weeks old Ex2 knockout (KO) animals developed enlarged hearts with increased atria compared to the wild-type (WT). The walls of the left ventricles were thinner indicating an increased lumen. **(A, down)** The number of nuclei was increased and the size of the cardiomyocytes was decreased in the KO mice (20x magnifications; areas marked by the black arrow and square). **(B)** The number of the nuclei was significantly increased in the knockout heart. **(C)** The cell size was significantly increased in the Ex2 knockout ($n = 3$, mean with SEM, significances determined by T-test, $p < 0.05$ *, $p < 0.01$ **).

The sarcomeric structure of the cardiomyocytes was investigated by electron microscopy (Figure 29, p. 60). Therefor the hearts of 3 weeks old Ex2 wild-type (WT) heterozygous (HET) and knockout (KO) animals were dissected. Continuously the left (LV) and the right ventricles (RV) were separated. The sarcomeres of the WT and HET animals developed normal and held a well-organized Z-disc, I-band, A-band and M-band structure (Figure 29, left and middle, p. 60). The differences in the length of the sarcomeres of the left and the right ventricle were caused by the perfusion of the hearts. The sarcomeric structure of the left and in the right ventricle was disarranged in the Ex2 KO animals. Similar to the quadriceps muscle, completely disrupted myofibrils and some close to disarrangement were observed. These sarcomeres appeared compressed with abnormalities in the I-band, A-band and M-band. The induction of the disruption of two adjacent sarcomeres started at the Z-disc and was followed by the M-band. This process additionally affected following Z-disc and continued until the myofibril was completely damaged (Figure 29, right, p. 60).

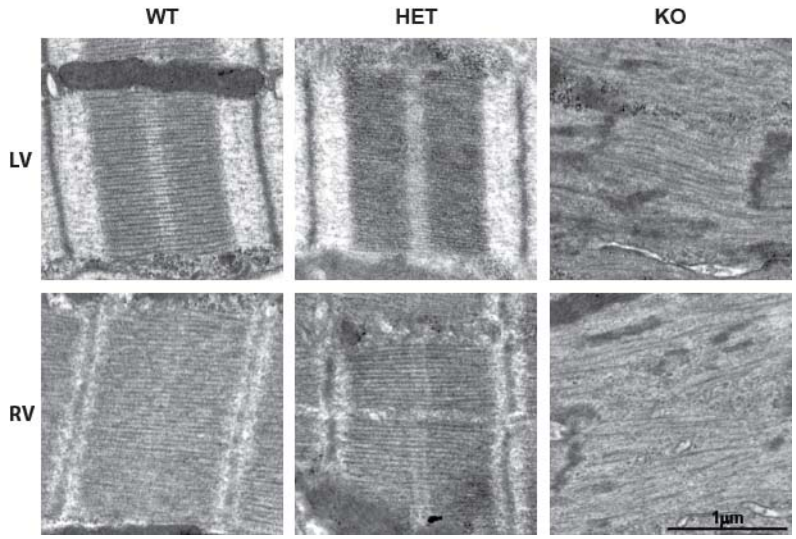

Figure 29: Disruption of the cardiac sarcomeres in Ex2 knockout mice. The electron microscopy of the left (LV, top) and the right ventricle (RV, bottom) of 3 weeks old wild-type (WT, left), heterozygous (HET, middle) and knockout (KO, right) mice held a well-organized sarcomere with a proper Z-disc, I-band, A-band and M-band formation in the WT and HET hearts. The I-band of the non-stretched right ventricle appeared smaller (artefact of perfusion). This sarcomeric structure was completely disrupted in the KO ventricles.

5.3.2.3 The morphology of the M-band deficient heart (TiMexMCK)

The morphological differences of the M-band deficient heart were investigated by experiments equal to the analysis of the Ex2 deficient strain. Therefor we dissected 6 wild-type (WT), heterozygous (HET) and M-band knockout (KO) hearts. In difference to the Ex2 knockout the M-band deficient animals developed a cardiac atrophy. The M-band KO hearts were smaller and weaker with enlarged atria (Figure 30 A, p. 61). Additionally we determined the weight of the hearts, the weight of the compartments of the hearts as well as the tibia length. The heart weight/tibia length ratio of the KO animals indicated a significantly decreased weight of the heart (HW) in comparison to the WT and HET animals (Figure 30 B, p. 61). Similar to the titin null mouse model we analyzed the specific compartments of the hearts and determined the tissue weight to heart weight ratio. The M-band knockout animals had significantly increased atria, indicating a heart insufficiency (Figure 30 C, p. 61). Furthermore no significant differences were determined for the weight of the right ventricle (RVW) and the left ventricle (LVW) suggesting a global cardiac atrophy (Figure 30 D and E, p. 61).

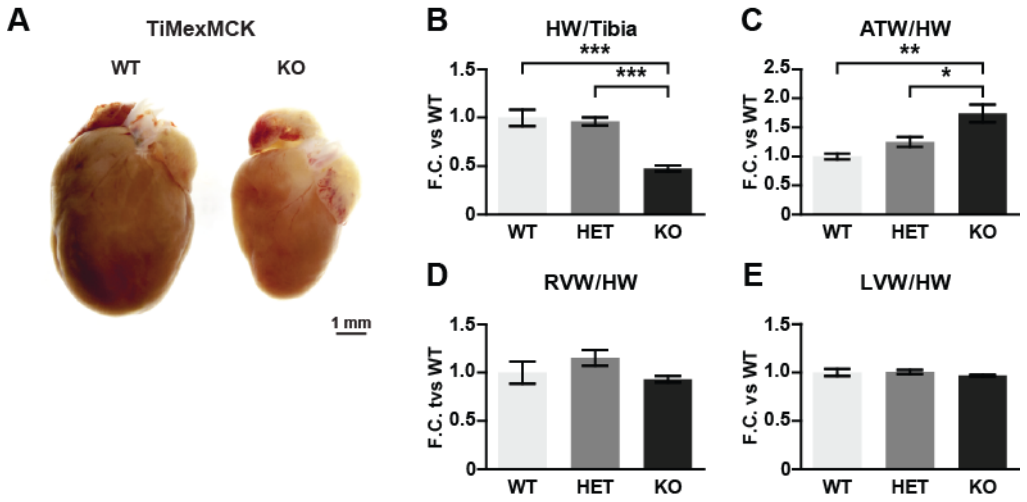

Figure 30: Cardiac atrophy in the M-band deficient mice. (A) The hearts of 5 weeks old M-band knockout (KO) mice were atrophic with enlarged atria compared to the wild-type (WT). **(B)** The weight of the KO hearts was significantly decreased compared to the WT and heterozygous (HET) animals. **(C)** The KO animals developed a significantly increased weight of the atria. **(D and E)** There was no significant change in the weight of the right (RV) and left ventricles (LV) of WT, HET and KO hearts indicating a global cardiac atrophy (n = 6, mean with SEM, significances determined by One-way ANOVA with Bartlets test for equal variances and Bonferroni's multiple comparison tests, $p < 0.05$ *, $p < 0.01$ **, $p < 0.001$ ***).

5.3.2.4 Histology of the M-band deficient heart

In order to analyze the cardiac morphology we dissected the hearts of 5 weeks old M-band wild-type (WT) and knockout (KO) animals (n = 3). The longitudinal sections of the WT and KO hearts confirmed the enlarged atria of the M-band deficient mice. Additionally the KO animals developed a smaller left (LV) and right ventricle (RV) (Figure 31 A, top, p. 62). The higher magnification (20x) of the septum (black arrow and square) determined an unorganized structure of the cardiomyocytes in the knockout heart. The cells were smaller and held centralized nuclei (Figure 31 A, down, p. 62). The quantification determined a significantly increased number of nuclei in the M-band KO (Figure 31 B, p. 62). Additionally the size of the cardiomyocytes was significantly decreased (Figure 31 C, p. 62).

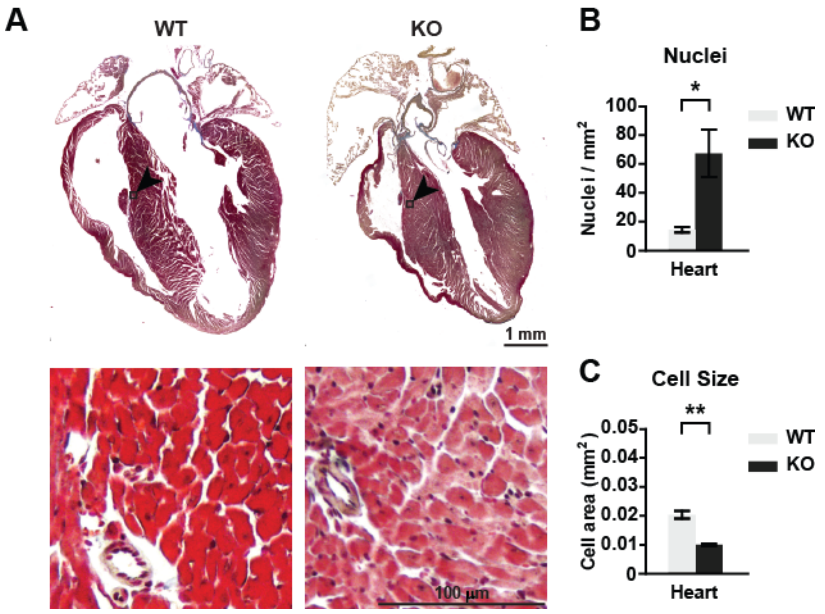

Figure 31: Impaired development of M-band knockout cardiomyocytes. (A, top) The hearts of 5 weeks old M-band deficient (KO) animals developed cardiac atrophy with enlarged atria compared to the wild-type (WT) hearts. **(A, down)** The number of nuclei was increased and the size of the cardiomyocytes was decreased in the KO mice (20x magnifications; areas marked by the black arrow and square). **(B and C)** Both the number of nuclei and the size of the cardiomyocytes were significantly changed (n = 3, mean with SEM, significances determined by T-test, $p < 0.05$ *, $p < 0.01$ **).

Electron microscopy was used to visualize the sarcomeric structure of M-band deficient cardiomyocytes (Figure 32, p. 63). Therefor the hearts of 3 weeks old M-band wild-type (WT) heterozygous (HET) and knockout (KO) animals were dissected. The left (LV) and the right ventricle (RV) were separated and send for electron microscopy (Magnification 8900x). Differences in stretch for the left and right ventricle were caused by the perfusion of the hearts. The sarcomeres of the WT and HET animals were normal with a well-organized Z-disc, I-band, A-band and M-band structure (Figure 32, left and middle, p. 63). The deletion of the MEx1 and 2, present in the M-band KO animals, led to a sarcomeric disarrangement of the left and the right ventricle similar to the quadriceps muscle (Figure 26, p. 57). The myofibrils were completely damaged or close to disarrangement. Affected sarcomeres were compressed with weak M-band structures which burst during progression. The disruption of the sarcomere proceeded from the M-band to the Z-disc (Figure 32, right, p. 63).

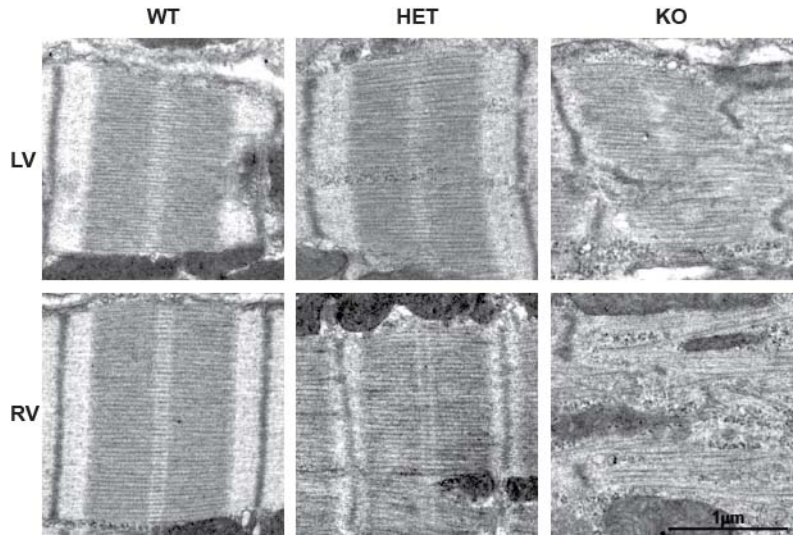

Figure 32: Sarcomeric disruption in M-band knockout cardiomyocytes. The electron microscopy of the left (LV, top) and the right ventricle (RV, bottom) of 3 weeks old wild-type (WT, left), heterozygous (HET, middle) and knockout (KO, right) mice held a well-organized sarcomere with a proper Z-disc, I-band, A-band and M-band formation in the WT and HET hearts. The I-band of the non-stretched right ventricle appeared smaller (artefact of perfusion). This sarcomeric structure was completely damaged in the KO ventricles.

5.3.3 Analysis of the Ex2 and M-band knockout transcriptome

5.3.3.1 Comparison of the skeletal muscle transcriptome

5.3.3.1.1 Analysis of atrophy and hypertrophy markers in the Ex2 knockout

Quantitative real time polymerase chain reaction (RT-qPCR) was performed for the verification of the skeletal muscle atrophy abundant in the titin null animals. The transcription levels of the atrophy/hypertrophy marker RAC-alpha serine/threonine-protein kinase 1 (AKT1), ankyrin repeat domain-containing protein 23 (DARP), tumor necrosis factor alpha (TNF-α), F-box only protein 32 (Atrogin1) and E3 ubiquitin-protein ligase TRIM63 (MURF1) were analyzed to determine the atrophic transcription level (Table 5, Table 13, Table 14, p. 22, 32 and 32). The transcription of AKT1 and DARP not changed in the Ex2 KO mice, whereas the transcription of TNF-α was significantly down regulated (Figure 33 A, p. 64). Furthermore we determined a significant upregulation of atrogin1 as well as an upregulation of MURF1 (Figure 33 B, p. 64). The upregulation of atrogin 1 and MURF1 as well as the simultaneous downregulation of TNF-α indicated the skeletal muscle atrophy of the complete titin deficient animals.

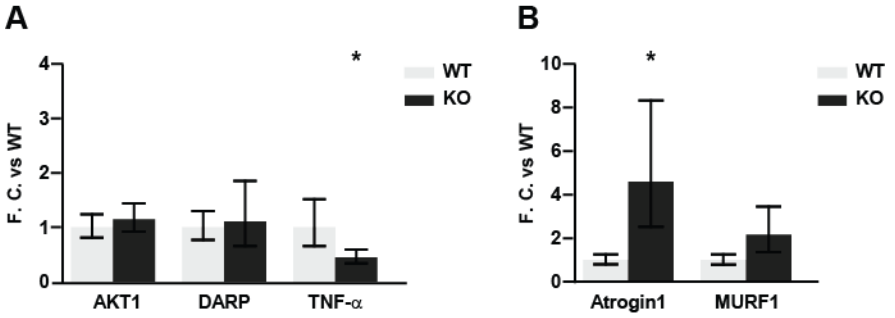

Figure 33: Activated atrophy/hypertrophy transcription in the Ex2 knockout. (A) RT-qPCR of wild-type (WT) and knockout (KO) gastrocnemius RNA. The transcription level of AKT1 and DARP was not changed, whereas TNF-α was significantly downregulated. **(B)** The mRNA level of atrogin1 and MURF1 was upregulated but only atrogin1 was significantly deregulated in quadriceps tissue (n = 5, mean with +/- error, T-test without posttest, $p < 0.05$ *).

5.3.3.1.2 Analysis of atrophy and hypertrophy markers in the M-band knockout

The M-band deficient mice developed skeletal muscle atrophy similar to the titin Ex2 knockout animals. In order to analyze the atrophy we run RT-qPCR on wild-type (WT) and knockout (KO) gastrocnemius muscles RNA samples using the same primer and probes used for the titin null strain. The transcription of all markers were not changed in the M-band KO mice, but we determined light upregulation of AKT1 and TNF-α and a nearly downregulation of DARP by half (Figure 34 A, p. 64). Atrogin 1 and MURF1 were additionally upregulated but not significantly changed (Figure 34 B, p. 64). This upregulation of atrogin 1 and MURF1 indicated the skeletal muscle atrophy of the M-band deficient mice. The downregulation of DARP interfered with the observed skeletal muscle atrophy.

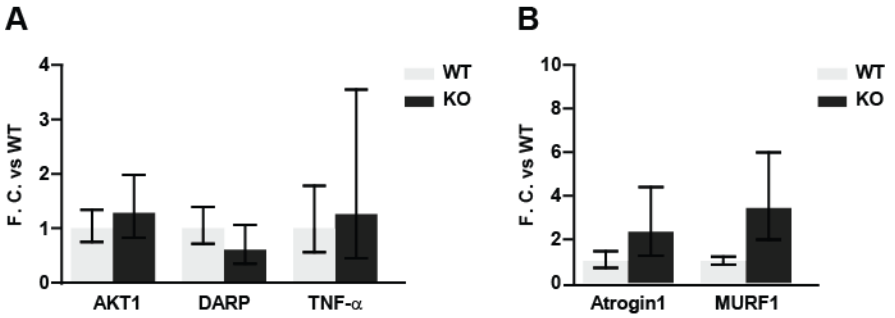

Figure 34: Impaired atrophy/hypertrophy transcription in the M-band knockout. (A) RT-qPCR of wild-type (WT) and knockout (KO) gastrocnemius RNA. The AKT1, DARP and TNF-α transcription was not changed. **(B)** Atrogin1 and MURF1 were more than 2 fold upregulated, but not significant (n = 5, mean +/- error, t-test without posttest).

5.3.3.2 Comparison of the cardiac muscle transcriptome

5.3.3.2.1 Analysis of atrophy and hypertrophy markers in the Ex2 knockout

Morphological changes of the heart characteristically lead to a deregulated transcription of the natriuretic peptide A (ANP), the β–myosin heavy chain (βMHC), the ankyrin repeat domain-containing protein 1 (CARP), the brain natriuretic peptide (BNP) and the sarcoplasmic/endoplasmic reticulum calcium ATPase 2 (SERCA2). In order to analyze potential deregulations of the cardiac transcriptome of the complete titin deficient mice we performed a quantitative real time polymerase chain reaction (RT-qPCR) for the genes of these proteins. We determined a significant upregulation of ANP, βMHC and CARP (Figure 35 A, p. 65) in the knockout animals. Furthermore we determined a significant increase of the BNP RNA. SERCA2 was also upregulated but not significant (Figure 35 B, p. 65).

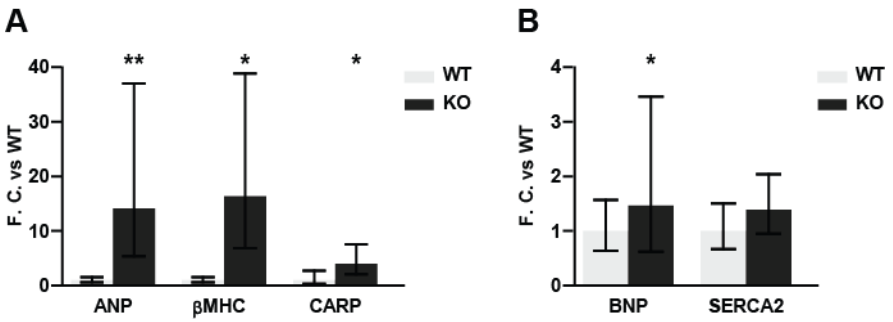

Figure 35: Deregulation of cardiac atrophy/hypertrophy marker in the Ex2 KO. (A) The RT-qPCR analysis of wild-type (WT) and knockout (KO) left ventricular RNA held a significantly upregulated transcription of ANP, βMHC and CARP. **(B)** BNP and SERCA2 RNA levels were upregulated in Ex2 KO animals, but only BNP was significant (n = 5, mean with +/- error, T-test without posttest, $p < 0.05$ *, $p < 0.01$ **).

5.3.3.2.2 Analysis of atrophy and hypertrophy markers for the M-band knockout

The Ex2 KO mouse model developed a dilated cardiomyopathy instead of the cardiac atrophy observed in the M-band KO. We expected differences in the transcription of the natriuretic peptide A (ANP), the β–myosin heavy chain (βMHC), the ankyrin repeat domain-containing protein 1 (CARP), the brain natriuretic peptide (BNP) and the sarcoplasmic/endoplasmic reticulum calcium ATPase 2 (SERCA2). Therefore were analyzed the M-band KO model by RT-qPCR parallel to the experiments done for the Ex2 KO strain. The ANP and βMHC transcription was significantly upregulated similar to the Ex2 KO. CARP (Figure 36 A, p. 66) and BNP (Figure 36 B, p. 66) were

additionally upregulated but not significant. The sarcoplasmic/endoplasmic reticulum calcium ATPase 2 (SERCA2) was downregulated which was different to the transcription of SERCA2 in the Ex2 KO (Figure 36 B, p. 66).

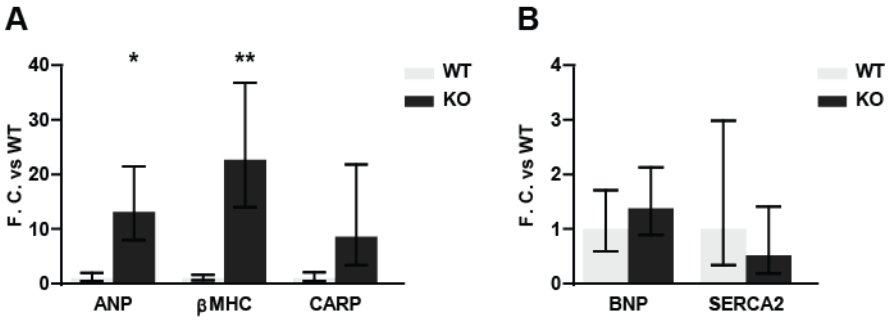

Figure 36: Deregulation of cardiac atrophy/hypertrophy marker in the M-band KO. (A) The RT-qPCR analysis of wild-type (WT) and knockout (KO) left ventricular RNA held a significant upregulated transcription of ANP and βMHC. CARP was upregulated but not significant. **(B)** The BNP transcription was lightly increased. SERCA2 was downregulated but not significant. (n = 5, mean with +/- error, T-test without posttest, $p < 0.05$ *, $p < 0.01$ **).

5.4 Analysis of the Ex2 and M-band knockout proteome

5.4.1.1 Comparison of the skeletal muscle proteome

5.4.1.1.1 qMS analysis of the skeletal muscle proteome

Quantitative mass spectrometry was used to analyze the changes of the skeletal muscle proteome. We dissected the quadriceps muscles of Ex2 as well as M-band wild-type and knockout animals. 895 upregulated and 925 downregulated proteins were determined in the titin null mice. For the M-band KO we determined 440 upregulated and 1695 downregulated proteins compared to the wild-type animals. Furthermore we identified 269 equally upregulated and 681 equally downregulated proteins in both strains (Figure 37 A and B, p. 67). To investigate the differences of protein expression which are caused by the absence of titin in the sarcomere we compared the Ex2 KO to the M-band KO and identified 452 counter-regulated proteins (Figure 37 C, p. 67).

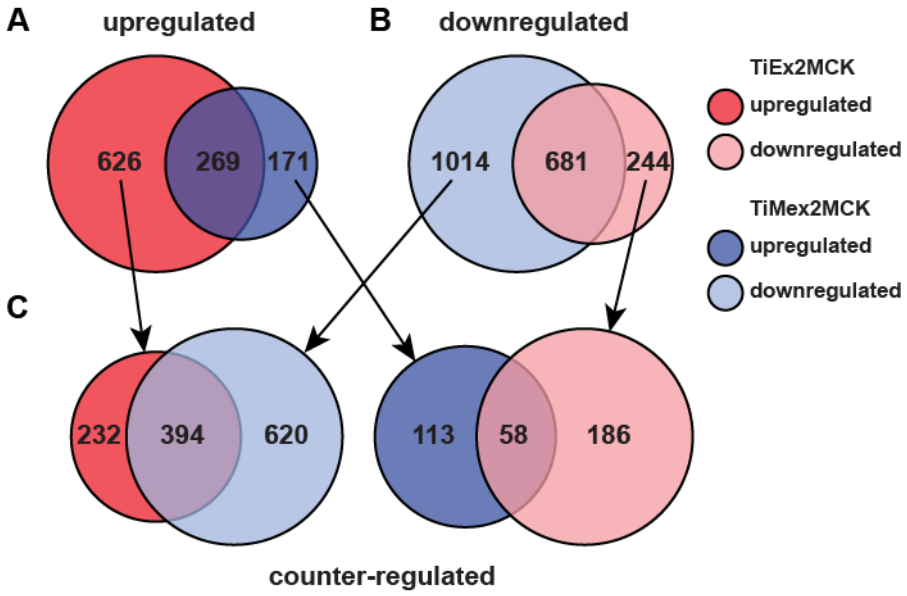

Figure 37: Quantitative mass spectrometry analysis of the quadriceps muscle. (A and B) The number of up and downregulated proteins in the TiEx2MCK KO mice was similar (895 up to 925 down). There were more downregulated than upregulated proteins in the TiMexMCK KO mice (440 up to 1695 down). 269 equally upregulated and 681 equally downregulated proteins were found by the comparison of the upregulated and downregulated proteins in the complete titin (TiEx2MCK) and M-band deficient (TiMexMCK) mice. **(C)** Analysis of counter-regulation. The comparison of the unequal upregulated proteins of the TiEx2MCK KO to the unequal downregulated proteins of the TiMexMCK KO as well as the inverted comparison (black arrows) indicated 452 counter-regulated proteins.

5.4.1.1.2 Gene ontology of the differential skeletal muscle proteome

The titin null and the M-band deficient animals developed skeletal muscle atrophy but the M-band KO differed to the Ex2 KO in the expression of a truncated titin which still consist of the Z-disc, the I-band and the A-band. Thus the M-band deficient titin provided multiple binding sites for sarcomeric structural and signaling proteins. The 452 counter-regulated proteins identified could be explained by the absence or availability of titin binding sites. In order to investigate the function and the location of the counter-regulated proteins we performed a gene ontology analysis for the biological function, the cellular component and the molecular function using the Cytoscape 3.2.0 software. We could link the counter-regulated proteins to the catabolism and the organization of the contractile fiber as well as to the translational factory of the cell (Figure 38, p. 68).

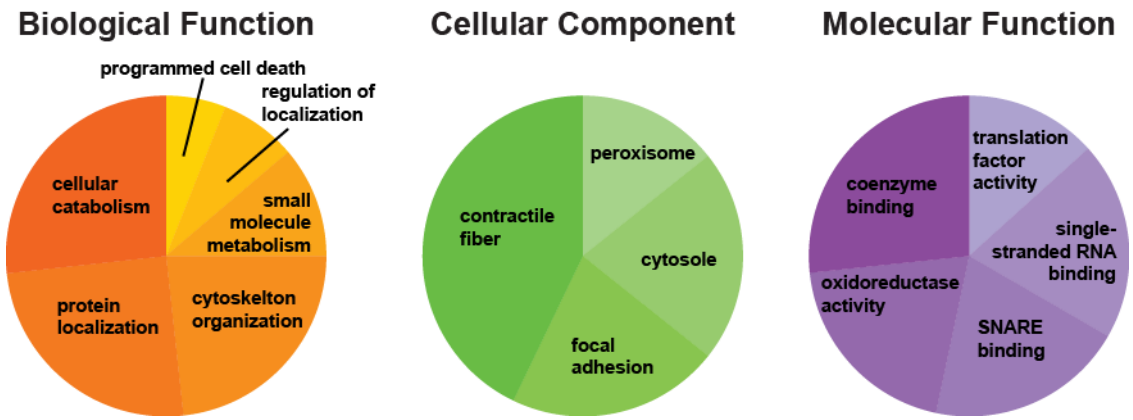

Figure 38: Function of the counter-regulated skeletal muscle proteins. The 452 counter-regulated proteins determined in the skeletal muscle were involved in the catabolism and the organization of the contractile fiber as well as the translational factory of the cell.

5.4.1.2 Comparison of the cardiac muscle Ex2 and M-band proteome

5.4.1.2.1 Quantitative mass spectrometry analysis of the cardiac proteome

The cardiac muscle proteome was investigated by quantitative mass spectrometry. Therefore we dissected the hearts of Ex2 as well as M-band wild-type and knockout animals. We determined 852 upregulated and 1766 downregulated proteins in the titin null mice. 403 upregulated and 1967 downregulated proteins were detected in the M-band deficient animals. Furthermore 250 proteins were equally upregulated and 1405 proteins were equally downregulated in both strains (Figure 39 A and B, p. 69). The differences in the ratios of up and downregulated proteins and the number of downregulated proteins as well as the 2 fold increased number of upregulated proteins in the Ex2 KO indicated an increased activation of translation in the complete titin deficient hearts. In order to identify potentially counter-regulated proteins we compared the 602 upregulated proteins of the Ex2 KO with the 562 downregulated proteins of the M-band KO as well as the 361 downregulated proteins of the Ex2 KO (TiEx2MCK) with the 153 upregulated proteins of the M-band KO (TiMexMCK). 400 counter-regulated proteins were determined (Figure 39 C, p. 69).

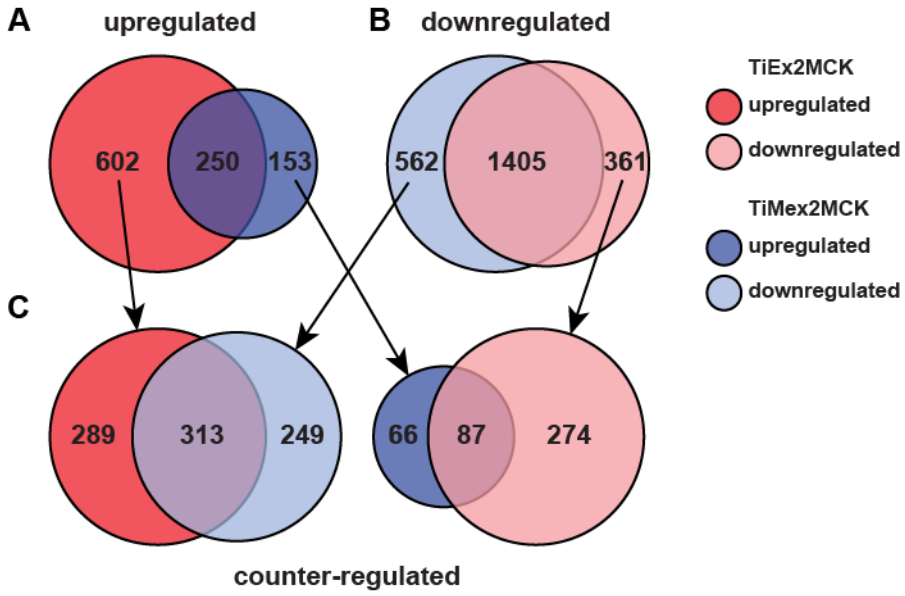

Figure 39: Quantitative mass spectrometry analysis of the heart. (A) There were more downregulated than upregulated proteins in both KO mouse models, whereas the differences were more distinct in the M-band deficient mice (TiEx2MCK: 852 up to 1766 down; TiMexMCK: 403 up to 1967 down). 250 equally upregulated and 1405 equally downregulated proteins were found by the comparison of the upregulated and downregulated proteins in the complete titin (TiEx2MCK) and M-band deficient (TiMexMCK) mice. **(B)** Analysis for counter-regulation. The comparison of the unequal upregulated proteins of the TiEx2MCK KO to the unequal downregulated proteins of the TiMexMCK KO as well as the inverted comparison (black arrows) indicated 400 counter-regulated proteins.

5.4.1.2.2 Gene ontology of the cardiac muscle proteome

The titin deficiency led to the development of dilated cardiomyopathy whereas the M-band deficient animals developed cardiac atrophy. Both strains differed in the expression of a truncated titin which still consist of the Z-disc, the I-band and the A-band. Thus the M-band deficient titin provided multiple binding sites for structural and signaling proteins important for cardiac development and function. The 400 counter-regulated proteins identified could be associated with the absence or availability of these binding sites. In order to investigate the function of these counter-regulated proteins we performed a gene ontology analysis for the biological function, the location and the molecular function using Cytoscape 3.2.0. All three ontologies indicated an influence of the proteins to cardiac muscle contraction and development. Additionally the proteins were associated with the metabolism, the excitability and the transcription of the cardiomyocytes (Figure 40, p. 70).

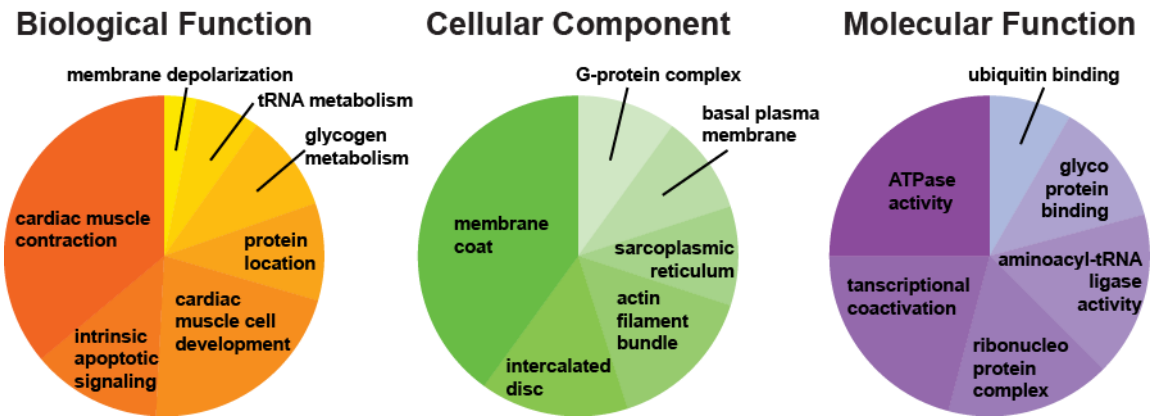

Figure 40: Function of the counter-regulated cardiac proteins. The 400 counter-regulated proteins determined in the heart were involved in the contraction, the development, the metabolism, the excitability and the transcription in the cardiomyocytes.

5.4.1.2.3 Western blot analysis of the cardiac muscle proteome

The different cardiac phenotype in of Z-disc vs. M-band titin knockouts prompted us to focus the molecular analysis on the heart. We verified the results of the transcriptome and proteome analysis by Western Blot (Figure 41, p. 71). The left ventricle of titin null (TiEx2MCK) as well as M-band deficient (TiMexMCK) wild-type (WT) and knockout (KO) hearts were dissected and prepared for SDS-PAGE. The respective antibodies against the Z-disc and I-band binding proteins CryAB (Crystalline, Alpha B), T-CAP (titin cap protein), CARP (Cardiac Ankyrin Repeat Protein), DARP (Diabetes Related Ankyrin Repeat Protein), FHL1 (Four And A Half LIM Domains 1) and FHL2 (Four And A Half LIM Domains 2) as well as GAPDH (Glyceraldehyde-3-Phosphate Dehydrogenase) as loading control were used (Table 6). CryAB was significantly downregulated in the Ex2 KO but not in the M-band KO. T-CAP was significantly upregulated in both knockout models but stronger in the complete titin deficient knockout mice. CARP was significantly downregulated in the complete titin knockout but only slightly upregulated in the M-band KO. In contrast diabetes related ankyrin repeat protein DARP was significantly upregulated in the M-band KO, but unchanged in the titin null mice. FHL1 was significantly upregulated in both mouse models. The deregulation of FHL1 was stronger in the M-band deficient than in the titin null mice. Interestingly the regulation of FHL2 was opposite to FHL1: FHL2 was upregulated in the Ex2 KO mice and downregulated in the M-band KO animals (Figure 41, p. 71).

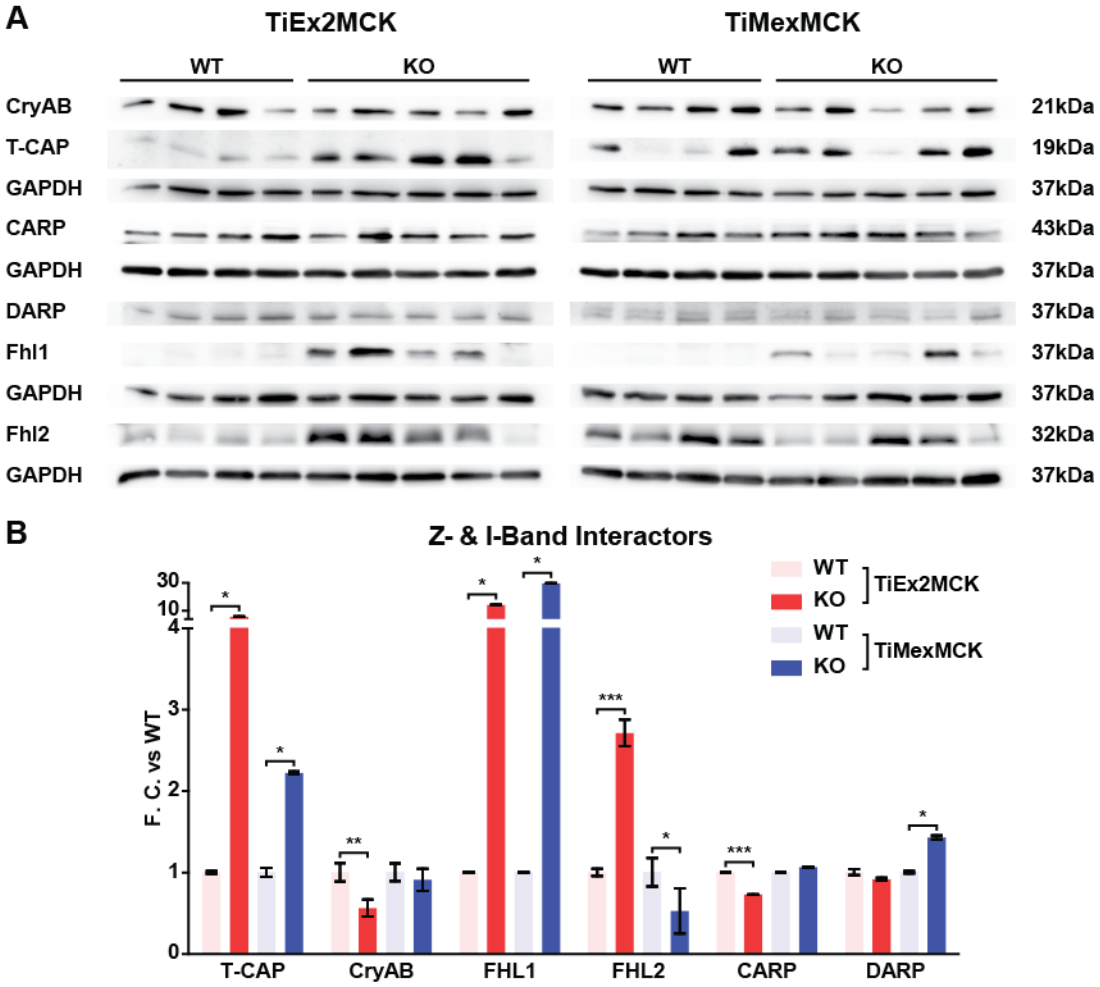

Figure 41: Altered expression of titin's Z-disc and I-band binding partners. (A) The Western Blot analysis of the Ex2 (left) and M-band (right) WT and KO animals. The expressions of CryAB, T-CAP, CARP, DARP, FHL1 and FHL2 were different compared to the wild-type. **(B)** In the titin null (TiEx2MCK, red) and M-band deficient (TiMexMCK, blue) animals T-CAP and FHL1 were significantly upregulated. CryAB and CARP were significantly decreased in the Ex2 KO animals. The expression of DARP was increased in the M-band KO animals. FHL2 expression was significantly increased in the Ex2 KO and significantly downregulated in the M-band KO animals (WT n = 4, KO n = 5, mean with SEM, T-test $p < 0.05$ *; $p < 0.01$ **; $p < 0.001$ ***).

In addition to the Z-disc and I-band binding partner of titin we analyzed the A-band and M-band titin interactors MYOM1 (Myomesin 1), NBR1 (Neighbor of BRCA1 Gene 1), MURF1 (E3 Ubiquitin-Protein Ligase TRIM63), MURF2 (Muscle-Specific RING Finger Protein 2 TRIM55) and p62 (Sequestosome 1) as summarized in (Figure 42 A, p. 72; Table 6, p. 23). We used the same samples as in Figure 41 (p. 71). In both knockout models myomesin1 was significantly downregulated - stronger in the titin Ex2 KO, which also significantly downregulation cardiac NBR1expression. NBR1 was not deregulated in the M-band deficient animals. The muscle-specific RING finger protein 2 MURF2 was slightly upregulated in the Ex2 KO and slightly downregulated in the M-band KO (not significant). MURF1 - another RING finger protein - was

significantly upregulated in the titin null and the M-band titin deficient animals. Inexpertly the M-band specific interactor p62 was significantly upregulated only in the Ex2 KO, whereas the p62 levels were normal in the M-band KO (Figure 42, p. 72).

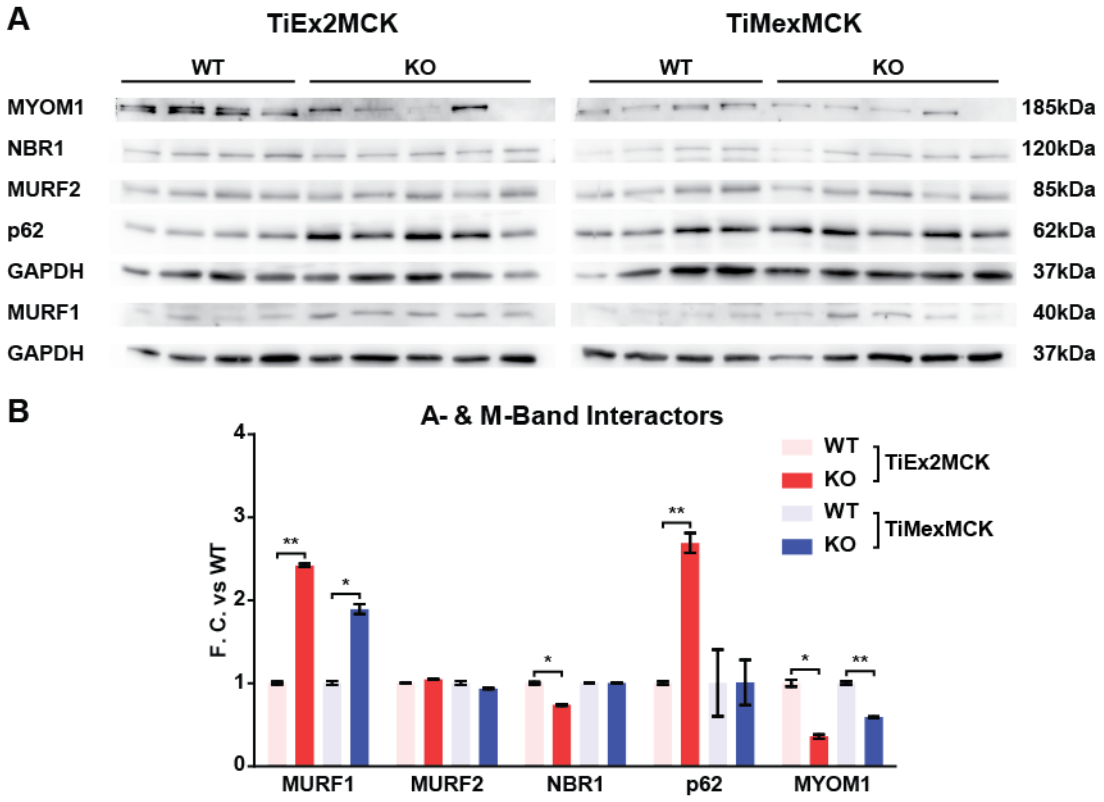

Figure 42: Impaired expression of titin's A-band and M-band binding proteins. (A) The expression of MYOM1, NBR1, p62 and MURF1 was different in the Ex2 (left) and M-band (right) WT and KO animals, but was no change in the expression of MURF2. **(B)** Quantification of the Western Blots. The MURF1 level was significantly increased and the MYOM1 level was a significantly decreased in both KO animals. NBR1 was significantly downregulated and p62 was significantly upregulated in the Ex2 KO (TiEx2MCK, red). The expression of MURF2 was not changes in both KO animals (WT n = 4, KO n = 5, mean with SEM, T-test $p < 0.05$ *; $p < 0.01$ **).

Based on the different cardiac phenotypes between titin knockouts, we expected a deregulation of transcription factors regulated by titin interacting proteins. We probed blots of the same samples as described for Figure 41 (p. 71) with the antibodies directed against NFκB1 (Nuclear Factor of Kappa Light Polypeptide Gene Enhancer in B-Cells), NFκB2 (Nuclear Factor of Kappa Light Polypeptide Gene Enhancer in B-Cells 2), CREB1 (CAMP Responsive Element Binding Protein 1) and TBP (TATA Box Binding Protein) (Figure 43 A, p. 73; Table 6, p. 23). The expression of NFκB1 and its isoforms was differentially regulated between the titin knockouts. The native p105 and the processed NFκB1 p84 were significantly upregulated in both knockouts, while NFκB1 p63 was significantly downregulated. Upregulation of p70 was only detected in

the Ex2 KO and upregulation of NFκB1 p50 and downregulation of NFκB2 only in the M-band KO. The Transcription factor TBP was significantly upregulated in both animal models, whereas CREB1 was significantly upregulated only in the complete titin deficient mice (Figure 43, p. 73).

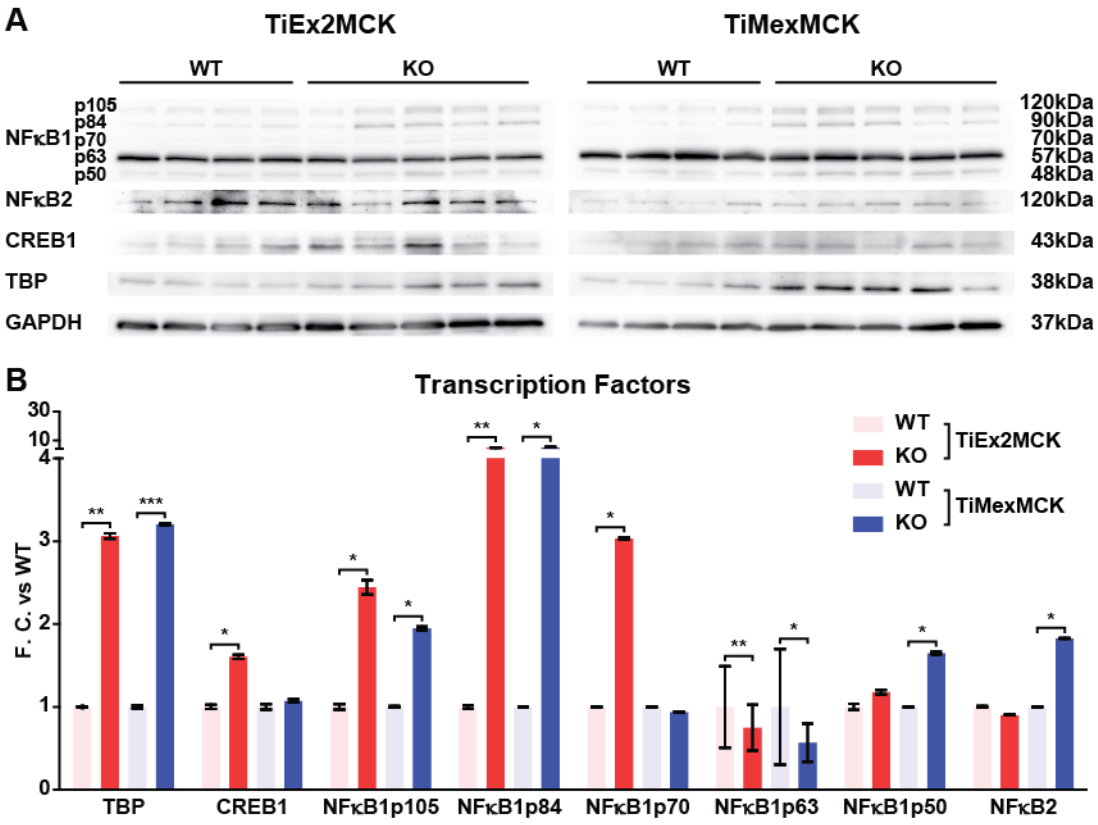

Figure 43: Deregulation of transcription factors. (A) The expression of NFκB1 and its isoforms, NFκB2, CREB1 and TBP was different in the Ex2 (left) and M-band (right) WT and KO animals. **(B)** Quantification of the Western Blots. TBP and the NFκB1 isoforms p105 and p84 were significantly upregulated in both strains. Simultaneously the NFκB1 p63 was significantly decreased in both knockout animal models. The transcription factor CREB1 and NFκB1 p70 were significantly increased only in the Ex2 KO animals (TiEx2MCK, red). The active isoform of NFκB1 p50 and the active isoform of NFκB2 were significantly upregulated in the M-band KO animals (TiMexMCK, blue) (WT n = 4, KO n = 5, mean with SEM, T-test $p < 0.05$ *; $p < 0.01$ **; $p < 0.001$ ***).

In order to investigate titin dependent signaling pathways we analyzed kinases interacting with titin and titin binding signaling proteins. Furthermore we were interested in ubiquitin ligases which are known to be associated with atrophy or hypertrophy signaling. The blots were probed with the antibodies directed against CAMK2 (Calcium/Calmodulin-Dependent Protein Kinase II α, β, γ and δ), MAPK3 (Mitogen-Activated Protein Kinase 3; ERK1), MAPK1 (Mitogen-Activated Protein Kinase 1; ERK2) and TRAF6 (TNF Receptor-Associated Factor 6) (Figure 44 A, p. 74; Table 6, p. 23).

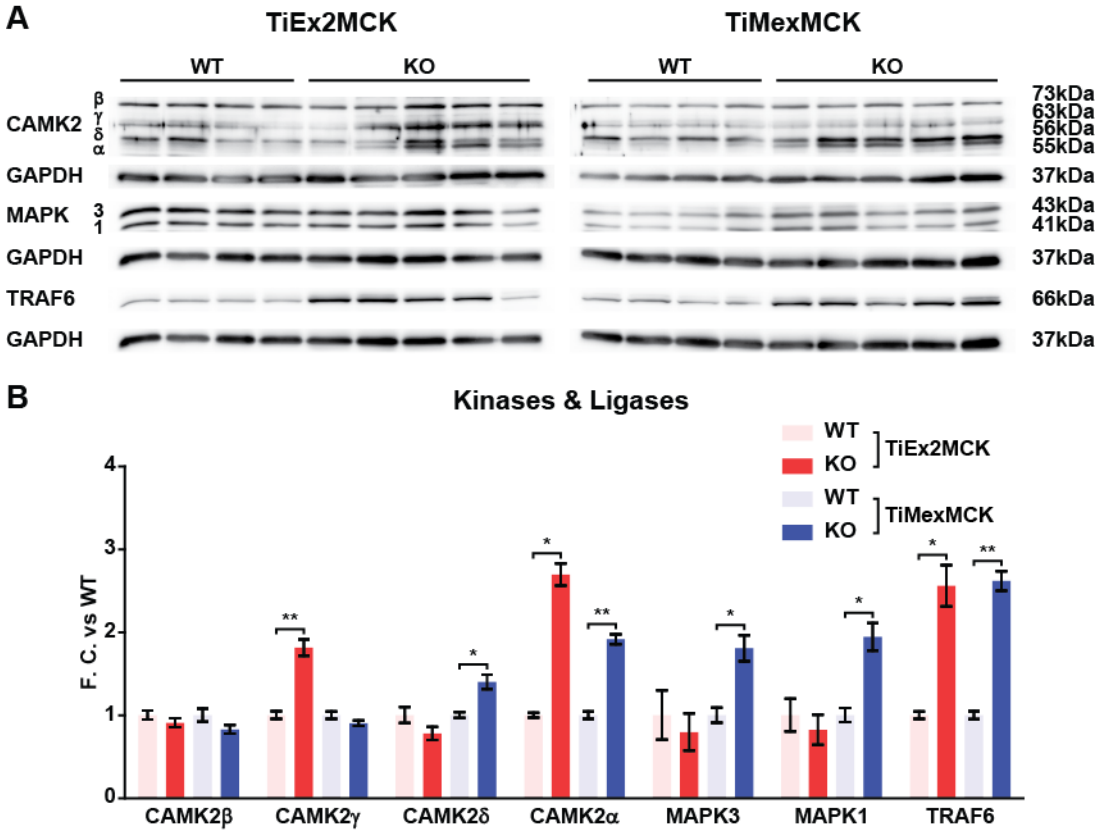

Figure 44: Deregulated expression of important kinases and ligases. (A) The Western Blot analysis of the Ex2 (left) and M-band (right) WT and KO animals held differences in the expression of the sub units γ, δ and α of the CAMK2, the MAPK3 and 1 as well as TRAF6. (B) Quantification of the Western Blots. The four units of the CAMK2 were different expressed. The α unit was significantly upregulated in both KO animal models. The expression of the γ unit was significantly increased only in the Ex2 KO animals (TiEx2MCK, red) similar to the δ unit which significantly increased only in the M-band KO animals (TiMexMCK, blue). CAMK2β was not changed in both KO animal models. The MAPK3 and 1 were significantly increased in the M-band KO. The E3 ubiquitin ligase TRAF6 was significantly increased in both animal models (WT n = 4, KO n = 5, mean with SEM, T-test $p < 0.05$ *; $p < 0.01$ **; $p < 0.001$ ***).

We found no deregulation of CamK2β in either animal model. The CAMK2γ was significantly upregulated in the Ex2 KO and slightly downregulated in the M-band KO. The α unit of the CAMK2 was significantly upregulated in both knockouts, but stronger in the complete titin knockout. Furthermore the MAPK3 and 1 were significantly upregulated in the M-band deficient mice. The E3 ubiquitin ligase TRAF6 was significantly upregulated in both knockout strains (Figure 44, p. 74). The different expressions of the titin I-band binding proteins FHL2, CARP and DARP as well as the different expression levels of the titin M-band binding proteins NBR1 and p62 in the Ex2 and M-band KO animals could be associated with the activation and/or deactivation of atrophy and hypertrophy inducing pathways. The different expression of the transcription factors CREB1, NFκB1 and 2 as well as the deregulations of the CAMK2 and MAPK1 and 3 supported this hypothesis.

6 Discussion

6.1 Genetic approaches towards understanding titin biology

The human titin gene contains 363 exons; the second contains the start site for all titin isoforms (Bang et al., 2001). We deleted this exon using the cre lox system with the CRE recombinase expressed from day E13 under control of the MCKcre promoter (Figure 5, p. 40). The correct genotype was confirmed by PCR (Figure 6, p. 41). The Ex2 KO mouse model was compared with the M-band deficient animal model published in 2003 (Figure 11, p. 45). Here the 1st and 2nd of 6 M-band exons which encode for a serine/threonine kinase like domain are conditionally deleted using the same cre-lox approach (Labeit et al., 1992, Kolmerer et al., 1996, Gotthardt et al., 2003, Willis et al., 2007). The genotype of the M-band deficient animal model additionally was confirmed by PCR (Figure 12, p, 46). Both animal models produced offspring at the expected mendelian ratios and heterozygotes did not have an obvious phenotype (Gotthardt et al., 2003; Weinert et al., 2006). Both models were validated on the RNA and protein levels and showed the expected deletion of the holoprotein for the Exon 2 knockout vs. a truncation in the M-band of the MEx1 and -2 knockout (Figure 8,Figure 9,Figure 13 andFigure 14, p. 43, 47 and 48).

Titin is essential for the development and the function of striated muscles. The loss of titin during embryogenesis leads to embryonic lethality (Gotthardt et al., 2003; Weinert et al., 2006). Therefore both KO models were generated to express titin normally through mid-gestation until the MCK-CRE recombinase is active in striated muscle from day E13 with gradual elimination of titin in through the first weeks of life. The residual titin is sufficient for survival but incompatible with life after 5 weeks. Both the long postnatal (pN2A; 3.5 MDa) and a short adult (aN2A; 3.4 MDa) skeletal muscle titin isoforms were significantly decreased in the Ex2 KO compared to the wild-type animals (Figure 9 A and B, p. 43). The cardiac titin isoforms N2BA and N2B were significantly decreased in the left ventricular tissue (Figure 9 A and C, p. 43) indicating a global reduction of functional titin in striated muscle tissue.

In the M-band mutant, only the smaller skeletal and cardiac titin molecules were expressed corresponding to the M-band deficient titin (Figure 14 A, p. 48; Gotthardt et al., 2003; Peng et al., 2007). This leads to a normal titin to titin degradation ratio (T1:T2) in skeletal muscle suggesting a normal degradation of skeletal titin (Figure 14 B, p. 48). We found a significantly decreased level of the degradation products (T2) of cardiac titin (Figure 14 C, p. 48). This could either be explained by a reduced proteolysis of titin in cardiomyocytes as an attempt to maintain protein function or as an artefact of preparation. The inactivation of the matrix metalloproteinase 2 which normally contributes to titin degradation in myocardial ischemia/reperfusion injury could be a reason for the decreased titin degradation (Ali et al., 2010). The protein levels of pN2A were significantly reduced whereas the expression of the aN2A (3.4 MDa) titin were unchanged. This could be explained by the same size of M-band deficient pN2A titin and aN2A (~3.4 MDa). In addition we documented an exclusive band, which reflects a M-band deficient aN2A isoform (Gotthardt et al., 2003; Peng et al., 2007). All analysis of titin expression correspond to the published data (Gotthardt et al., 2003; Peng et al., 2007) indicating that there was no change resulting from 10 years of maintaining the strain.

The skeletal T1 to T2 and the pN2A to aN2A ratios are not changed in the Ex2 KO, suggesting globally decreased expression of titin in the skeletal muscle. The cardiac titin N2BA to N2B ratio is unchanged but we see a significantly decreased T2 titin levels similar to the M-band deficient mice. These observations correspond to the results of the analysis of the M-band KO hearts and support the explanation of the repressed titin proteolysis in cardiomyocytes (Figure 10, p. 44). An artefact of preparation is highly unlikely because of the denaturing conditions of the sample buffer. Experiments were confirmed with two independent experiments. In summary, the complete titin deficiency leads to decreased titin protein levels in striated muscle. M-band deficiency does not affect the amount of titin but leads to an increased level of truncated titin in striated muscle. Both do not affect the degradation of titin in skeletal muscles. Surprisingly titin degradation in the heart is decreased which was predicted to be increased during myocardial ischemia/reperfusion injury. This suggests disturbed proteolysis in hearts from both genotypes, which could be an attempt to maintain titin protein levels and muscle wasting.

6.2 Titin deletions lead to skeletal and cardiac abnormalities

The unsurpassed dimension of the titin molecule (3.7 MDa) as well as its indispensability for sarcomere assembly complicate the analysis of its structural and signaling functions (McElhinny et al., 2000). In order to investigate and to understand the mechanisms assumed by the functional domains of titin different research groups generated domain specific knockout models. The M-band KO titin molecule is able to integrate into the Z-disc but fails to integrate into the M-band (Gotthardt et al., 2003; Peng et al., 2006). Thus the sarcomeres disassemble which leads constitutively to embryonic lethality and conditionally to skeletal muscle atrophy and cardiac atrophy finally leading to a decreased survival (Gotthardt et al., 2003; Peng et al., 2006; Weinert et al., 2006). These investigations and the predicted kinase like domain of the M-band led to the assumption that the M-band domain could be the most important domain for the sarcomeric integrity as well as titin atrophy and hypertrophy signaling (Mayans et al., 1998). The skeletal muscle specific N2A deficient mouse model lacks 83 amino acids from the N2A domain important for calpain-3 (CAPN3) binding. These mice develop similarities to the human limb-girdle muscular dystrophy type 2A (LGMD2A) which is associated with a severe muscular atrophy (Garvey et al., 2002). Titin N2B deficiency is dispensable for cardiac development and systolic properties but is important to integrate trophic and elastic functions of the heart. Furthermore the N2B domain reduces the hysteresis and increases the passive myofibrillar stiffness and thereby the diastolic and systolic efficiency of the heart. The animals survive but develop a cardiac atrophy phenotype with decreased FHL2 levels (Granzier et al., 2009; Nedrud et al., 2011; Radke et al., 2007). All these models explain only the functions of one specific titin domain but do not examine potential cooperative functions. In this study we generated a complete titin deficient mouse model (TiMexMCK) which was compared to the M-band deficient mouse. Both titin deficiencies lead to a sarcomeric disruption. The residual titin molecules have to assume the passive stiffness functions leading to an increased force and stretch on the molecules. The M-band deficient titin stabilizes the sarcomere from the Z-disc to the A-band inducing a distinct M-band and ablating a Z-disc or I-band mediated signaling. Complete titin deficiency induces the potential mediated signaling of all titin domains. The Ex2 KO should be answering the questions if the M-band is the main domain important for muscle development or if there are cooperative function with other titin domains. Both animal models develop skeletal muscle atrophy (5.3.1.1, p. 49). The development of the skeletal

muscle weakness in both knockout models could relate to the loss of the N2A domain in titin null animals on the one hand and on the other hand by the low stretch dependent activity of the N2A domain in the M-band deficient mice. Both can potentially lead to a decreased binding and activation of CAPN3 inducing skeletal muscle atrophy (Garvey et al., 2002). Complete titin deficiency lead to a dilated cardiomyopathy with increased FHL2 levels (Figure 27 andFigure 41, p. 58 and 71). M-band deficiency leads to cardiac atrophy with decreased FHL2 levels (Figure 30 andFigure 41, p. 61 and 71). Both results can be associated with the investigations of the N2B KO and support the cooperative functions of titins domains (Granzier et al., 2009; Nedrud et al., 2011; Radke et al., 2007). The cardiac development of the M-band KO corresponds to the cardiac atrophy and decreased FHL2 levels of the N2B KO. This relates to the ablation of the stretched induced N2B mediated signaling by the sarcomeric unintegrated M-band deficient titin. Complete titin deficiency leads to an increased stretch of the N2B domain which increases the possibility of FHL2 binding and activation, inducing its expression. Increased levels of FHL2 are associated with hypertrophy signaling (Johannessen et al., 2006; Lange et al., 2002; McGrath et al., 2006; Müller et al., 2000). The titin deficiency in both KO models leads to an distinct M-band mediated atrophy inducing signaling for example by MURF1 (Arya et al., 2004; Centner et al., 2001; Lange et al., 2006; Perera et al., 2010; Pizon et al., 2002). The induced FHL2 mediated hypertrophy signaling of the N2B domain and the simultaneously MURF1 mediated M-band signaling could explain the development of the dilated cardiomyopathy in the Ex2 KO mice. This assumption is supported by titin PEVK KO model. The PEVK domain is the critical site of PKCα's involvement in passive myocardial stiffness. A deletion of this domain induce diastolic dysfunction combined with cardiac hypertrophy initiated by the upregulation of FHL proteins as cause to an increased stretch of the N2B domain (Granzier et al., 2009; Hudson et al., 2010). In summary, the similar skeletal muscle development in both KO strains suggests a dominant M-band mediated signaling which induces skeletal atrophy. The differential cardiac development of both KO models suggests a cooperative function of the I-band and M-band titin, which could be predominantly resumed by the titin N2B and M-band domain.

6.2.1 Sarcomeric disassembly results in skeletal muscular atrophy

Titin is an important component of the sarcomeric structure and important for fundamental tasks in skeletal and cardiac muscle contraction and relaxation (Hein and Schaper, 2002; Monroy et al., 2012; Nishikawa et al., 2012). Mutations of/in the N2A, PEVK or M-band domains are associated with skeletal muscular myopathies like TDM or HMERF (Buck et al., 2014; Garvey et al., 2002; Gotthardt et al., 2003; Peng et al., 2006). We compared our titin null animal model with the M-band deficient knockout and expected a stronger phenotype in the complete titin knockout caused by the additional deletion of the Z-disc, I-band and A-band domain of titin. We see a compatible phenotypical development, characterized by a severe progressive muscle weakness paired with confinements of the posture and gait in both animal models. The knockout mice develop a bent spine, paresis in the lower extremities and ptosis of the eyelids (Figure 16 A andFigure 19 A, p. 49 and 52) usually appearing after 15 days and proceeding until death with less than 40 days (Figure 16 B andFigure 19 B, p. 49 and 52). Heterozygous mice of both strains develop normal and survive suggesting the rescue of the phenotype by a non-mutated titin allele (Minamisawa et al., 1999; Musa et al., 2006). Both knockouts have a significantly decreased weight (Figure 17 A andFigure 20 A, p. 50 and 52), a significant reduction of strength endurance (Figure 17 B and Figure B, p. 50 and 52) and significant decreased in tibia length to muscle weight ratios of several skeletal muscles (Figure 18 andFigure 21, p. 51 and 53) compared to the WT and HET animals. These results suggest severe skeletal muscle atrophy affecting the global musculoskeletal system which potentially causes the decreased survival in both animal models (Figure 22, p. 54). The phenotype of both KO strains corresponds to the phenotype of patients with TMD or HMERF. TMD is characterized by muscle weakness as well as atrophy and is associated with mutations of the M-band exons (MEx5 and MEx6). Amino acid substitutions in MEx6 found in TMD patients affect the binding affinity of the protease calpain-3 (CAPN3) which significantly controls the protein degradation of sarcomeric proteins (Van den Bergh et al., 2003; Hackman et al., 2002; Huang and Forsberg, 1998; Pollazzon et al., 2010). The loss of the titins M-band in both KO models could lead to the loss of the CAPN3 interaction and therefore to an interruption of the activity of CAPN3. This potentially leads to an increased degradation of sarcomeric proteins. Furthermore, the development of both KO models corresponds to frame shift mutations of MEx5 which lead to a premature stop in

the M-band titin in human. These truncated titin molecules are associated with a more severe phenotype and earlier onset of the TMD (Hackman et al., 2008). Both KO phenotypes can be compared to HMERF, which is associated with distal, proximal and respiratory muscle weaknesses causing gait disturbances and respiratory problems in human (Ohlsson et al., 2012; Pfeffer et al., 2014a). Mutations in the A-band to M-band junction of titin lead to an interrupted binding of myosin and myosin binding protein C (Izumi et al., 2013; Ohlsson et al., 2012; Palmio et al., 2014; Pfeffer et al., 2014b; Toro et al., 2013; Vasli et al., 2012). This interaction is important for the assembly and the stability of the sarcomere (Freiburg and Gautel, 1996; Furst et al., 1992). Other mutations found in patients with DCM affect the binding of T-CAP as well as α-actinin at the Z-disc and influences the sarcomeric integrity and thereby the stability of striated muscles (Itoh-Satoh et al., 2002). The titin deficiency of the Ex2 KO mice leads to the loss of the titin to T-CAP and α-actinin interaction, which destabilizes the sarcomeric structure. Thus, the severe skeletal muscle weakness of both KO models relates to the loss of important titin interactions leading to sarcomeric disassembly.

The morphological background of both knockout models was verified by a histological approach. Therefore we analyzed longitudinal and cross sections of the quadriceps. Gotthardt as well as Peng and colleagues described a severe disarrangement of the skeletal muscle including a decreased fiber diameter as well as an increased number of nuclei and additionally multiple centralized nuclei for the M-band KO (Gotthardt et al., 2003; Peng et al., 2006). There are no differences in quadriceps morphology between genotypes as determined by trichrome staining. The structure of myofibers is disorganized, the size of myocytes is significantly decreased, the number of nuclei is significantly increased and there are centralized nuclei (Figure 23 andFigure 25, p. 55 and 56). This indicates a similar underlying cause for the skeletal myocyte morphology in the Ex2 and M-band knockout (Gotthardt et al., 2003; Peng et al., 2006). The centralization of the nuclei suggests a centronuclear myopathy in both KO models which is caused by the disintegration of titin into the sarcomere (Ceyhan-Birsoy et al., 2013). M-band knockout mice indicate sarcomeres in various stages of disassembly (Figure 26, right, p. 57). The M-band deficiency might interrupt the binding for structural, regulatory, and contractile proteins such as myomesin 1, 2 and 3 (M-proteins), obscurin or the tumor suppressor protein bridging integrator protein 1 (BIN1) (Figure 4, p. 10). Myomesin 1 cross-bridges titin's M-band with the thick filament

system by interacting with the heavy chain of myosin (Nave et al., 1989; Obermann et al., 1996, 1997). Furthermore, the affected interaction to obscurin interferes the stability of the sarcomeric M-band (Fukuzawa et al., 2008; Witt et al., 2006; Young et al., 2001). The binding of BIN1 to M-band titin is important for the assembling of mature sarcomeres. Therefore, the M-band deficiency could interrupt the coordination of the skeletal muscle cell differentiation (Fernando et al., 2009). These changes could explain the initiated disruption of the sarcomere at the M-band instead of the Z-disc where titin is properly integrated. The later affection of the Z-disc could be a result of the progressive disarrangement of the A-band and the I-band. The myofibrils of the Ex2 knockout animals were completely disrupted and some were close to decay. Those sarcomeres are compressed with weak Z-discs followed by the affection of the residual structures. The disruption of the sarcomere starts with the depletion of the Z-disc of two adjacent sarcomeres followed by the realignment of the other sarcomeric structures (Figure 24, right, p. 55). The primary affection of the Z-disc explains the importance of titin for the assembly and the maintenance of the sarcomeric structure. Complete titin deficiency could interfere the interaction to T-CAP which promotes titins proper integration into the Z-disc (Gregorio et al., 1998; Zou et al., 2006). The interrupted T-CAP binding could also affect the interaction of T-CAP to the muscle LIM protein (MLP) which stabilizes the system of the contractile apparatus and the sarcolemma (Flick and Konieczny, 2000). Complete titin deficiency could additionally interrupt the binding of sANK1 which is another Z-disc binding protein. Both sANK and T-CAP mediate the organization between the Z-disc and the surrounding SR (Kontrogianni-Konstantopoulos and Bloch, 2003). α-actinin binds distal of titin's Z-repeats and in an interdomain sequence of Z-disc titin (Labeit et al., 2006; Young et al., 1998). The interaction of α-actinin and Z-disc titin is essential for the assembly and the maintenance of the Z-disc and cross-links titin to the thin filament system. The missing interaction of titin and α-actinin could explain the progressive affection of the thin filament (Ohtsuka et al., 1997; Peckham et al., 1997; Sorimachi et al., 1997; Young et al., 1998). The Z-disc domain of titin is important the for obscurin (~720-900 kDa) and nebulin (600-900 kDa) binding (Bang et al., 2001; Labeit et al., 2006; Young et al., 2001). Nebulin is known to regulate the length of the actin filaments and the interaction of titin and nebulin suggest specifying the width of the Z-disc in striated muscles. The interaction of titin and obscurin indicates a significant function of titin in signal transduction. (Witt et al., 2006;

Young et al., 2001). Complete titin deficiency leads to an interruption of these bindings which could initiate the disassembly of the sarcomere starting at the Z-disc. The residual titin molecules of the sarcomere are not able to compensate the reduced amount of titin which leads to the sarcomeric compression and to the progressive disarrangement of the residual sarcomeric structures in the Ex2 KO mice. The ultrastructure of the wild-type and the heterozygous animals mice of both strains are normal indicating a post-transcriptional compensatory effect induced by one unaffected titin allele (Figure 24 andFigure 26, left and middle, p. 55 and 57) (Minamisawa et al., 1999; Musa et al., 2006). In summary, the disruption of the sarcomere neither by complete titin nor by M-band deficiency could be the reason for the skeletal muscle atrophy. Both lead to the interruption of important structural complexes of the sarcomeres which finally leads to damage of the myofibrils. Furthermore, both titin deficiencies interfere with myofibrillogenesis, which leads to apoptosis of the myocytes as a basis for skeletal muscle atrophy. Our results suggest that similar mechanisms underly the skeletal muscle atrophy.

6.2.1.1 Titin dependent deregulation of atrophy/ hypertrophy associated genes

In both titin deficient models sarcomeres are disrupted. The Ex2 KO does not express titin whereas the M-band KO expresses a truncated titin molecule consisting of the Z-disc, the I-band and the A-band. Thus we expect different transcriptomic deregulations of proteins associated with skeletal muscle atrophy and hypertrophy. Therefore we analyzed the transcription levels of DARP (Ankyrin Repeat Domain 23) and MURF1 (E3 ubiquitin-protein ligase TRIM63) as well as for other markers like AKT1 (RAC-alpha serine/threonine-protein kinase), TNF-α (tumor necrosis factor alpha) and Atrogin1 (F-box only protein 32) (Figure 33 andFigure 34, p. 64 and 64). The Transcription levels of AKT1 are slightly but not significant upregulated in both knockouts (Figure 33 A andFigure 34 A, p. 64 and 64). These results suggest an activation of hypertrophy signaling and repression of atrophy by downregulation of Atrogin1 and MURF1 (Glass, 2003, 2005). AKT1 overexpression was found in patients with chronic obstructive pulmonary disease with muscle atrophy where its increased levels were discussed as an attempt to restore muscle mass (Doucet et al., 2007). The slight increased transcription of AKT1 in both KO models and the simultaneously increased transcription

of the atrophy marker Atrogin1 (significant for Ex2 KO) and MURF1 in both knockout models potentially support this hypothesis (Figure 33 B andFigure 34 B, p. 64 and 64). MURF1 functions as an E3 ubiquitin ligase which binds together with MURF2 to the M-band as well as together with the MURF3 to the Z-disc domain of titin. These interactions link the contractile system to the regulation of protein synthesis and degradation. Furthermore, MURF1 is able to inhibit hypertrophy, for example by interaction with the receptor for activated protein kinase C (RACK1) which blocks the translocation of PKCε to focal adhesions. The increased transcription of MURF1 correlates to the upregulated MURF1 levels found in human skeletal muscle atrophy (Arya et al., 2004; McElhinny et al., 2004; Tskhovrebova and Trinick, 2003; Witt et al., 2005). Therefore both titin deficiencies lead to an upregulation of MURF1 and atrogin1 transcription which explains the skeletal muscle atrophy in both animal models. Interestingly the TNF-α transcription was converse regulated. Transcription of this cytokine was decreased in the Ex2 knockout and downregulated in the M-band knockout (Figure 33 A andFigure 34 A, p. 64 and 64). TNF-α mediates atrophy and activates the transcription activity of NFκB which initiate the expression of Atrogin1 and MURF1 (Glass, 2003, 2005; Jackman and Kandarian, 2004). The significantly decreased transcription of TNF-α as well as the slight increased transcription of AKT1 in the titin null mice could suggest an attempt to repress the atrophy initiated by atrogin1 and MURF1. The increased transcription of TNF-α in the M-band deficient mice supports the development of skeletal muscle atrophy by the activated transcription of atrogin1 and MURF1. DARP is slightly increased in the Ex2 KO but decreased in the M-band KO (both not significant; Figure 33 A andFigure 34 A, p. 64 and 64). DARP, CARP and ANKRD2 are members of the muscle ankyrin repeat proteins (MARP) and interact with N2A titin and act as stress dependent regulators of muscle protein expression. Furthermore, DARP is nuclear transcription co-factor which deactivates the activity of the MAPK3 and 1 important for the NFAT hypertrophy pathway (Jeyaseelan et al., 1997; Miller et al., 2003; Song et al., 2012). The increased transcription of DARP in the Ex2 KO indicates an inactivation of the MAPK3 and 1 which could reduce the transcription activity of the calcineurin-NFAT circuit leading to atrophy. The decreased transcription of DARP in the M-band KO indicates a reduced inhibition of MAPK3 and 1 which could enhance the transcription activity of the calcineurin-NFAT circuit (Doucet et al., 2007). This hypertrophic response could be an attempt to repress the atrophy caused

by the M-band deficiency. The investigation of the atrophy and hypertrophy associated markers suggest an activation and response of different pathways associated with atrophy or hypertrophy, which could be dependent of the availability of specific titin binding sites. The M-band deficient animals still expressed the Z-disc, the I-band and the A-band titin and therefore multiple binding sites which were completely absent in the complete titin deficient strain (Gotthardt et al., 2003). The differences in the SEM values could be caused by the high variances in the affection of the KO animals. This additionally has an effect on the calculation of significances especially for the M-band deficient strain. These variances in disease relate to the advanced and different stages of the muscle disease in the KO animals. The high mortality in both strains supports this hypothesis and suggests different stages of affection at the time point of 35 days where the samples were collected.

6.2.1.2 Titin dependent deregulation of sarcomeric proteins

It was shown that the transcriptome and the proteome can be different (Griffin et al., 2002). Therefore we performed a quantitative mass spectrometry approach (qMS) of the same samples used for transcriptomics (Paul et al., 2011; Trinkle-Mulcahy et al., 2008). The results displayed in Figure 37 (p. 67) indicate a causal affection of the development and the organization of the contractile fiber as well as the transcriptional factory of the cell (Figure 38, p. 68). Interestingly the determined proteins are mostly upregulated in the Ex2 knockouts and simultaneously downregulated in the M-band knockouts. This observation could be explained by the loss of the titin expression which leads to a force overload and therefore to an increased stretch of the remaining natural titin molecules. Thus the titin N2A, PEVK and M-band domains could provide more binding sites for signaling proteins which leads to an increased activation of the transcription and expression of sarcomeric proteins. The truncated M-band deficient titin expressed in the M-band KO mice is not able to be stretched because of the failing integration into the M-band. Therefore the M-band deficient titin binds fewer proteins than the force overloaded residual titin molecules. This could lead to an ablation of the transcription and expression of sarcomeric proteins in the M-band KO. Furthermore the absence of Z-disc, I-band and A-band titin in the Ex2 KO could interrupt complexes important for the sarcomeric structure. Thus titin dependent structural proteins are over expressed in the Ex2 knockouts and simultaneously downregulated in the M-band knockout. One of these

proteins is caveolin-3 which drives caveolae formation and is a component of the dystrophin-glycoprotein complex (DGC), linking cytoplasmic actin to the membrane and the extracellular matrix of striated muscle. Patients lacking caveolin-3 develop muscular dystrophy and mice develop a severe cardiomyopathy (McNally et al., 1998; Park et al., 2002). Furthermore caveolin-3 interacts with dysferlin which reveal the same converse expression between our knockout models. Dysferlin, calveolin and mitsugumin 53 are members of a membrane repair mechanism. Titin deficiency could lead to an interruption of this complex which is associated with muscular dystrophies (Bansal et al., 2003). Desmin is an essential component of the Z-disc as well as the intercalated disc and is reverse regulated in addition. It interacts with nebulin and plectin as well as modulates the actin filament lengths and organization. Desmin deficiency causes skeletal and cardiac myopathies. The upregulation of Desmin in the Ex2 KO models indicates a disruption of the Z-disc and actin filament organization which is associated with atrophy (Conover et al., 2009; Goldfarb and Dalakas, 2009; Shah et al., 2001). The reverse deregulated nuclear lamina proteins lamin A/C are proteins fundamental in sustaining the structural integrity and mechanical stability of the nuclear envelope. Lamins are involved in chromatin organization, DNA repair, transcriptional regulation, intracellular signaling pathways, cell cycle checkpoints and development. Mutations of lamin A/C are associated with different diseases including muscular dystrophies and dilated cardiomyopathy. The deregulation of lamin A/C suggest functional changes which are associated with skeletal muscle atrophy (Arimura et al., 2005; Mounkes et al., 2005). Apart from the structural proteins we determine several deregulated kinases. Most interestingly we investigate a converse expression of the exercise activated p38 MAP kinase (upregulated in Ex2 KO; qMS data, not verified) as well as the MAPK1 and 3 which are involved in atrophy and hypertrophy signaling. The p38 MAPK triggers the skeletal muscle atrophy by activation of the TNF-α pathway as well as the initiation of atrogin1 and MURF1 expression. MAPK1 and 3 are known to reduce the expression of atrogin1 and MURF1 and therefore the ubiquitin dependent protease pathway. The overexpression of the p38 MAPK in the Ex2 KO corresponds to the increased transcription of MURF1 and atrogin1 explaining the development of the skeletal muscle atrophy. The increased expression of MAPK3 and 1 instead indicate an activation of hypertrophy pathways which could be a response to the proceeding atrophy. The decreased protein levels of all 3 kinases in the M-band deficient animals indicate an attempt to repress the atrophy similar to the EX2 KO but in a converse direction (Kim et

al., 2009; Kramer and Goodyear, 2007). The upregulation of structural proteins and atrophy/ hypertrophy associated kinases in the Ex2 knockout animals indicate the severe derangements of the sarcomere. This is caused by the missing titin molecule affecting on the one hand the structural integrity of the Z-disc, the thick and the thin filament and on the other hand the interaction of titin with proteins important for signal transduction. The downregulation in the M-band knockout relates to the integration of the M-band deficient titin into the Z-disc and the possible interaction of titin with the actin filament as well as the existence of several binding sites important for signaling (Gotthardt et al., 2003). This hypothesis is supported by the detection of multiple M-band associated proteins, deregulated in the same direction. Smtnl1 (Smoothelin-Like 1), Obscn (Obscurin) and MYOM3 (Myomesin 3) (qMS data, not verified by western blot) are upregulated in both KO models. Smtnl1 is important for the regulation of contractile properties of both striated and smooth muscles, promoting the relaxant actions of PKA/PKG (Wooldridge et al., 2008). Obscurin binds to the last Ig domain of titin and additionally interacts with myomesin as well as obscurin like 1 protein forming a complex necessary for myofibril organization. Both titin deficiencies could interrupt this complex which is linked to limb-girdle muscular dystrophy 2J or tibial muscular dystrophy (Fukuzawa et al., 2008; Kontrogianni-Konstantopoulos et al., 2004; Pernigo et al., 2010). The upregulation of MYOM3 as well as the simultaneously downregulation of MYOM1 and MYOM2 (Myomesin 1 and 2) in both knockouts could be associated with the disruption of the M-band. All three proteins interact with titin and obscurin, cross-linking the myosin filament to the M-band. MYOM1 is expressed in all skeletal muscles whereas MYOM2 expression is localized to fast skeletal muscle fibers and cardiomyocytes. MYOM3 is highly upregulated in in slow muscle fibers type IIA as well as developmental myocytes. Moymesin deficient mice develop muscle weakness and progressive sarcomere disassembly similar to the Ex2 and the M-band KO (Auerbach et al., 1999; Fukuzawa et al., 2008; Schoenauer et al., 2005, 2008; van der Ven and Fürst, 1997; van der Ven et al., 1996). Additionally the expression of CKM (Muscle-type Creatine Kinase) is decreased in both knockouts (qMS data). The CKM interacts with the myomesin proteins and resumes an important role in cellular energy metabolism at the M-band by replenishing ATP from phosphocreatine (Hornemann et al., 2003). Both titin deficiencies lead to deregulations of CKM and myomesin indicating an interrupted energy metabolism. The increased expression of Smtnl1, Obscn MYOM3 and the simultaneously downregulation of MYOM1 and 2 in both KO models correlates with the observed sarcomeric disruption

and suggest the muscle attempted to rearrange the sarcomere. The decreased CKM level reflects a reduced ATPase activity at the M-band indicating a decreased contraction activity which is additionally reflected by the overexpression of the contraction regulating protein Smtnl1 (Hornemann et al., 2003). In summary, the different regulation of structural and metabolic sarcomeric proteins suggest a different induction of the sarcomeric disassembly but finally leads to a global skeletal muscular atrophy in both knockout models. Titin deficiency seems to affect much more proteins and associated pathways as observed for the M-band deficient mice which correspond to our hypothesis of an increased affection in the Ex2 KO. Finally, both titin mutations influence the correct function of titin in the sarcomere leading to the disruption of all structural and contractile filaments and therefore to skeletal muscle atrophy. For a better separation of the differences it would be beneficial to analyze earlier stages for example animals with an age of 15 to 21 days.

6.2.2 Disruption of the sarcomere structure affects cardiac development

The expression of the MCKcre DNA recombinase is controlled by the muscle creatin kinase promotor active only in striated muscle. Thus we expected morphological changes of the hearts in addition to the observed affection of the skeletal muscles. Therefore the hearts of the titin null and the M-band deficient animal models were investigated by a comparative approach. Cardiac titin is characterized by the additional expression of the elastic N2B domain which is not expressed in the skeletal muscle (Watanabe et al., 2002). In adaption to the development of the heart the large (~3.6-3.8 MDa) embryonic/neonatal N2BA titin undergoes several steps of alternative splicing. This process ensures the stability and passive stiffness of the heart (Neagoe et al., 2003; Prado et al., 2005). The expression of titin's exon 49 and the simultaneous repression of the exons 51-218 generates the relatively small (~2.97 MDa) cardiac N2B titin (Bang et al., 2001; Freiburg et al., 2000). Therefore the perinatal ratio of N2BA and N2B changes dramatically by replacing the long N2BA titin by the shorter N2B isoform (Greaser et al., 2005; Lahmers et al., 2004; Opitz et al., 2004). Mutations of cardiac titin affect the contractile function and the myocardial stiffness and lead to the development of cardiomyopathies (Linke, 2008). For example the deletion of titin's I-band/A-band junction which is associated with diastolic dysfunctions and heart failure (Granzier et al., 2014). Mutations or the deletion of the elastic N2B domain are predicted to initiate cardiomyopathy in human and

provoke cardiac atrophy in mice (Borbély et al., 2009; Nedrud et al., 2011; Radke et al., 2007). Mutations of the PEVK domain induces cardiac hypertrophy and diastolic dysfunction caused by an increased stiffness of the cardiac sarcomere (Granzier et al., 2009; Hudson et al., 2010). Furthermore truncations, especially at the M-band domain of titin are known to be responsible for centronuclear myopathies (CNM) with hypotonia and dilated cardiomyopathy in humans (Carmignac et al., 2007; Ceyhan-Birsoy et al., 2013; Herman et al., 2012; Wang et al., 1998). M-band deficient mice, generated by Gotthardt and colleagues develop skeletal muscle atrophy and cardiac atrophy in addition (Gotthardt et al., 2003; Lange et al., 2006). This striated muscle development could be caused by the disruption of the sarcomere and/or be the affection of M-band associated signaling pathways. The M-band deficient titin still integrates into the Z-disc and interacts with the thin and thick filament but fail to integrate into the M-band leading to skeletal muscle atrophy (Figure 21, p. 53) as well as to cardiac atrophy (Figure 30 A, p. 61) (Gotthardt et al., 2003). The titin null mice are disable to express titin leading to skeletal muscle atrophy (Figure 18, p. 51) and enlarged hearts in addition (Figure 27 A, p. 58). This observation conflicts with the cardiac atrophy described by Gotthardt and colleagues (Figure 30 A, p. 61; Gotthardt et al., 2003). The enlarged hearts of the Ex2 knockout could be explained by the deletion of the PEVK domain. Mutations of this elastic spring element are known to induce the development of enlarged hearts and cardiac hypertrophy (Granzier et al., 2009; Hudson et al., 2010). Both knockout hearts have enlarged atria (Figure 27 C andFigure 30 C, p. 58 and 61). These enlarged atria could be a site effect caused by the dysfunction of the ventricles and the consequential overload of the atria (Pan et al., 2009). An additional explanation could be the increased FHL1 expression level observed in the left ventricle which could be additionally increased in the atria (Figure 41 B, p. 71). FHL1 regulates the expression of the cardiac K^+ channel KCNA5 which is important for the function and the development of the atria. A deregulation of this interaction is associated with arrhythmias and atrial fibrillation (Dobrev and Wettwer, 2008; Yang et al., 2008). To specify the cardiac morphologies of both knockouts we analyzed the heart-weight (HW) to body-weight (BW) ratio (Figure 27 B andFigure 30 B, p. 58 and 61). Surprisingly the heart weight of the Ex2 knockouts is not significantly different compared to the WT and HET animals. These results suggest a dilated cardiomyopathy instead of a cardiac hypertrophy as reason of the enlarged heart. Furthermore we see a decreased left ventricle weight (LVW) and no differences in the right ventricle weight (RVW) compared to the heart weight (HW)

(Figure 27 D and E, p. 58). These observations suggest the development of a left ventricular dilated cardiomyopathy in the complete titin deficient mice. This hypothesis is supported by mutations found in DCM patients which affect the Z-disc-I-band transition zone or the A-band of titin and lead to a truncated titin molecule (Gerull et al., 2002, 2006; Wu et al., 2002). Compared to the wild-type, the HW-BW ratios of the M-band knockout are significantly decreased whereas the RVW and LVW to HW ratios are not changed which suggests a global cardiac atrophy (Figure 30 B, D and E, p. 61). This cardiac development corresponds to the published M-band KO data (Gotthardt et al., 2003). The normal cardiac of the HET animals in both strains could be explained by a post-transcriptional compensatory rescue by the remaining healthy titin allele (Figure 27 andFigure 30, p. 58 and 61; Minamisawa et al., 1999; Musa et al., 2006). In order to analyze the morphological background of both knockout models we performed a histological approach. Therefore we analyzed longitudinal and trichromatic stained sections of wild-type and knockout hearts. This experiment corresponds to the observed cardiac differences of both KO strains (Figure 28 andFigure 31 A top, p. 59 and 62). Furthermore we confirm a decreased ventricular size in the M-band KO (Gotthardt et al., 2003). The cell size is significantly reduced and the number of nuclei is significantly increased in both KO mice. The nuclei are centralized (Figure 28 andFigure 31 A down, B and C, p. 59 and 62), which suggests a cardiac core myopathy in hearts of both strains (Chauveau et al., 2014). The ultrastructure of the WT and HET mice is not affected, indicating a rescue of the sarcomeric structure by one unaffected titin allele (Figure 29 andFigure 32, left and middle) (Minamisawa et al., 1999; Musa et al., 2006). The sarcomeric structures of the LV and RV in both knockout models correspond to the ultrastructure of the skeletal muscle (Figure 29 andFigure 32, right, p. 60 and 63). These results suggest the abnormal cardiac development by the disruption of the cardiac sarcomere in both knockout models. An explanation for the different cardiac development could be a differential activation of atrophy or hypertrophy mediating pathways. The stronger encroachment of the residual titin molecules could cause to more interactions of titin to structural and sarcomeric signaling proteins. M-band deficiency potentially stabilizes the Z-disc, I-band and A-band region of the sarcomere which is not the case in complete titin deficiency. The stabilization could lead to signals of non-stretched titin ablating the signals of the overstretched titin present in complete titin deficiency. Thus only the M-band domain of the residual titin molecules are stronger activated and lead to an increased atrophy

mediating M-band signaling in the M-band KO (Gotthardt et al., 2003). In the Ex2 KO instead all domains of titin could be over activated by stretch which could lead to a simultaneously atrophy and hypertrophy mediating signaling and finally to dilated cardiomyopathy.

6.2.2.1 Titin dependent deregulation of cardiac atrophy/ hypertrophy markers

The hearts of the Ex2 and the M-band knockout animals develop differences in the cardiac morphology. Therefore we expected a different transcriptional deregulation of atrophy and DCM associated factors like the natriuretic peptide A (ANP), β-myosin heavy chain (βMHC), ankyrin repeat domain-containing protein 1 (CARP), brain natriuretic peptide (BNP) and sarcoplasmic/endoplasmic reticulum calcium ATPase 2 (SERCA2) (Arimura et al., 2009; Bubikat et al., 2005; Clerico and Iervasi, 1995; Duboscq-Bidot et al., 2009; Hayashi et al., 2004a; Miller et al., 2003; Periasamy et al., 1999; Pikkarainen et al., 2003). Both knockout models have a significantly increased transcription of ANP and βMHC as well as an increased transcription of CARP and BNP (significant in Ex2 KO). The transcription levels of SERCA2 are converse regulated (Figure 35 andFigure 36, p. 65 and 66). The increased transcription of ANP in both knockout models (Figure 35 andFigure 36 A, p. 65 and 66) indicates an activation of hypertrophic pathways in the heart. Increased ANP levels induce the expression of the MAPK phosphatase-1 (MKP-1) which inhibits the activation of the MAP kinases. These kinases regulate the expression of vasoactive peptides like angiotensin II (ANGII) and endothelin-1 (ET-1) which induces cardiomyocyte hypertrophy (Hayashi et al., 2004a). The increased transcription of ANP in the Ex2 KO explains the enlarged size of the titin null hearts whereas the increased transcription in the M-band deficient hearts could be an attempt to repress the cardiac atrophy. There are two motor proteins myosin heavy chain α and β expressed in mammalian heart. It has been investigated that failing hearts increase the expression of βMHC while αMHC is highly downregulated. This observation relates to the higher ATPase activity and the resulting contractile velocity of myosin consisting of more αMHC than βMHC. Therefore the upregulation of βMHC in both animal models indicate a cardiomyopathy associated with pressure overload as well as cardiac diastolic and systolic dysfunction (Allen and Leinwand, 2001). CARP is together with DARP and ANKRD2 a member of the muscle ankyrin repeat proteins (MARP)

interacting with titin. Both are nuclear transcription co-factors which negatively regulate cardiac gene expression by inactivation of the hypertrophy inducing MAPK1 and 3 (Miller et al., 2003). The increased transcription of CARP in the Ex2 KO suggests a stretch overload in the titin molecule and could be an attempt to repress the cardiac enlargement. This hypothesis is supported by the increased transcription of ANP. The increased transcription of CARP in the M-band KO explained the development of cardiac atrophy (Figure 35 andFigure 36 A, p. 65 and 66). BNP stimulates the expression of the cGMP kinases PKA and PKG. These kinases are able to phosphorylate the N2B domain of titin which decreases the passive tension. The upregulation of BNP in the M-band deficient mice (Figure 36 B, p. 66) indicate a repression of cardiac atrophy. The upregulation in the titin null mice (Figure 35 B, p. 65) explains the dilation of the left ventricle by an over activity of PKA and PKG leading to a hyper-phosphorylation of the N2B domain which increases the passive stiffness and is associated with dilated cardiomyopathy (Bishu et al., 2011). The sarcoplasmic/endoplasmic reticulum calcium ATPase 2 (SERCA2) pumps Ca^{2+} out of the cytosol back into the sarcoplasmic reticulum thereby contributing to the low diastolic Ca^{2+} levels required for relaxation and replenishing Ca^{2+} stores needed for the next contraction. Overexpression of SERCA2 leads to concentric hypertrophy, diastolic dysfunction and increased ventricular stiffness (Ji et al., 2000; Periasamy et al., 1999; Vangheluwe et al., 2006). The upregulation of SERCA2 in the Ex2 knockout hearts suggest a potential deregulation of the cardiac contraction system and explain the increased size of the hearts (Figure 35 B, p. 65). The downregulation in the M-band knockout indicate a potential deregulation of the cardiac contraction system similar to the Ex2 KO and explains the cardiac atrophy in addition (Figure 36 B, p. 66). In summary, the transcription activity of both KO models is affected by titin deficiency. Furthermore the differences in the transcription suggest the evidence of the simultaneously activation of atrophy and hypertrophy associated pathways. The exact prediction is influenced by the huge differences in the SEM values which could be caused by the high transcriptional variances in the KO animals. This additionally affects the calculation of significance. The transcriptional variances relate to the advanced and different stages of the muscle disease in the KO animals. The high mortality in both strains supports this hypothesis and suggests different stages of affection at the time point of 35 days where the samples were collected. A further explanation could be the quality and the different sample number of the independent experiments.

6.2.2.2 Titin regulates atrophy and hypertrophy associated pathways

The results of the analysis of the cardiac transcriptome indicate evidence of a different regulation of the cardiac proteome in both KO models. The transcriptomic data should be supported by quantitative mass spectrometry (qMS) approach (Paul et al., 2011; Trinkle-Mulcahy et al., 2008). The results displayed in Figure 39 (p. 69) suggest a potentially converse regulation of atrophy and hypertrophy associated pathways. The number of deregulated proteins indicates an increased downregulation in both knockout models whereas 2 fold more proteins were upregulated in the Ex2 knockout mice compared to the M-band deficient animals. The comparative analysis of the transcriptomic and the proteomic data significantly support the transcriptomic upregulation of ANP, βMHC and SERCA2 (Figure 35 andFigure 36, p. 65 and 66). For the determination of the affected converse regulated pathways as well as for the analysis of the function of the counter-regulated proteins we performed a gene ontology analysis for biological function, the molecular function as well as the cellular component (Figure 40, p. 70). All three ontologies indicate an influenced development, organization and contraction of the cardiac muscle as well as differences in the activation of the cardiac transcription (Figure 40 p. 70). These findings correspond to the observed morphological cardiac changes of both KO models.

In order to investigate the potential affected pathways we selected the titin interacting proteins as well as its known atrophy and hypertrophy associated binding partner for Western Blot analysis (Figure 41,Figure 42,Figure 43 andFigure 44, p. 71, 72, 73 and 74). The small 19 kDa titin cap protein (T-CAP) is significantly but differently increased in both knockout models (Figure 41, p. 71). Both knockout models fail to generate a functional sarcomere neither by the loss of titin expression nor by the M-band deficient titin. This sarcomeric disassembly induces the release of T-CAP which is important to integrate titin into the Z-disc (Gregorio et al., 1998). The lower T-CAP level in the M-band knockout mice could be explained by the partially integration of the M-band deficient titin into the Z-disc. T-CAP interacts with muscle-LIM-protein (MLP), alpha-actinin-2, calsarcin and the potassium channel β-subunit (MinK) building a complex important for Z-disc mediated hypertrophy signaling by activation of calcineurin-NFAT signaling pathway. The interruption of this complex indicated by the deregulation of T-CAP in both KO models is associated with idiopathic dilated and hypertrophic cardiomyopathy (Gregorio et al., 1998; Hayashi et al., 2004b; Hershberger

et al., 2008). Additionally T-CAP binds to ankyrin repeat domain 2 (ANKRD2), myostatin, protein kinase D (PKD) and murine double minute 2 (MDM2). MDM2 binding leads to the ubiquitin-independent degradation of T-CAP which is associated with cardiac hypertrophy (Tian et al., 2006). The increased expression of T-CAP in both animal models suggests a disordered interaction of T-CAP and its binding partners which lead to an increased activation of hypertrophy signaling. The stronger expression of T-CAP in the Ex2 knockout mice could explain the dilated cardiomyopathy. The lower levels in the M-band knockout animals could be explained by the stabilizing function of the M-band deficient titin and suggest an ablated induction of hypertrophy signaling. Myomesin 1 (MYOM1) was significantly decreased in both knockout strains which could be associated with a disrupted titin interaction. MYOM1, 2 and 3 interact with titin and obscurin, cross-linking the myosin filament to the M-band and an interrupted interaction is associated with muscle weakness and atrophy (Auerbach et al., 1999; Fukuzawa et al., 2008; Schoenauer et al., 2005, 2008; van der Ven and Fürst, 1997; van der Ven et al., 1996). In summary, the similar deregulation of T-CAP as Z-disc binding partner and MYOM1 as M-band binding partner indicate a simultaneously activation and inhibition of hypertrophy and atrophy signaling in both animal models. The different cardiac development cannot be explained by these sarcomeric structural and regulating proteins.

6.2.2.2.1 Cardiac atrophy in the M-band knockout

The cardiac atrophy of the M-band deficient animals could be explained by the enhanced activity of the E3 ubiquitin ligase MURF1 which mediates ubiquitin ligated proteolysis. MURF1 is significantly overexpressed in M-band deficiency (Figure 42 A and B, blue, p. 72). MURF1 and MURF2 are able to bind to the M-band and both are known to induce atrophy and simultaneously inhibit hypertrophy. MURF1 inactivates the PKCε hypertrophy signaling by interaction with the receptor for activated protein kinase C (RACK1) blocking the binding of PKCε and therefore the translocation of PKCε to focal adhesions. The increased MURF1 levels in the M-band KO indicate an increased ubiquitin turn over and activated proteolysis (Arya et al., 2004; Centner et al., 2001; Lange et al., 2006; Perera et al., 2010; Pizon et al., 2002). The expression of MURF1 is controlled by the processed transcription factors NFκB1 and NFκB2. Both are significantly increased in the M-band knockout (Figure 43 A and B, blue, p. 73; Cai et al., 2004; Hunter and Kandarian, 2004; Wu et al., 2014). Furthermore, the increased NFκB1

and 2 expression suggests a transcriptional activation of genes involved in the immune, inflammatory, anti-apoptotic and acute phase response like the vascular endothelial growth factor (VEGF) (Bai et al., 2005; Heusch et al., 1999; Leychenko et al., 2011). The transcriptional activation of NFκB is regulated by interacting IκB inhibitor proteins and controlled by IκB inactivation for example by TGF-β or TRAF6 (Bai et al., 2005; Heusch et al., 1999; Leychenko et al., 2011). M-band deficiency leads to a significant upregulation of the E3 ubiquitin ligase TRAF6 suggesting the ubiquitination and subsequent degradation of IκB. This initiates the transcriptional activation of the NFκB's (Figure 44 A and B, blue, p. 74). The activity of TRAF6 can be suppressed by the four and a half LIM domain protein FHL2 (Bai et al., 2005; Johannessen et al., 2006). FHL2 is significantly downregulated in the M-band KO which supports the activation of TRAF6 and finally the NFκB mediated increased MURF1 expression (Figure 41 A and B, blue, p. 71). The decreased levels of the signaling protein FHL2 could be explained by the interaction of FHL2 with the N2B domain of titin (Purcell et al., 2004). M-band deficient titin still interacts with the thin and thick filaments of the sarcomere but fails to integrate into the M-band (Gotthardt et al., 2003). Thus the M-band deficient titin is not stretched but stabilizes the sarcomere from the Z-disc to the A-band. This could ablate the stretch induced activation and expression of FHL2. The M-band domain of the remaining natural titin is simultaneously exposed and predominantly stretch which leads to activation and upregulation of MURF1. This hypothesis is supported by the unchanged αB-crystalin (CryAB) levels in the M-band KO animals (Figure 41 A and B, blue, p. 71). The chaperon CryAB is a member of the small heat shock proteins (sHSP) preventing extensive structural damage of the sarcomere especially during ischemia. The binding of CryAB to titin protects its domain structures and correlates with myofibril stress. CryAB especially binds to the N2B domain and protects the FHL2 binding site during force overload (Bullard et al., 2004; Golenhofen et al., 2002). M-band deficiency additionally leads to an upregulation of the CAMK2δ and α which explains the increased expression of NFκB (Figure 44 A and B, blue, p. 74). The calcium/calmodulin dependent kinases (CAMK2) activate transcription by phosphorylation of HDAC's class II and MEF2, which activates the NFκB expression after infarction (Anderson, 2009). In summary, the cardiac atrophy of the M-band deficient mice could be explained by the activation and overexpression of the CAMK2δ and α which leads to an overexpression of NFκB. The loss of TRAF6 regulation by FHL2

could mediate the transcriptional activation of NFκB by inactivation of IκB inhibition. This leads to the increased expression of MURF1 associated with cardiac atrophy as well as inhibition of hypertrophy (Arya et al., 2004; Centner et al., 2001; Lange et al., 2006; Perera et al., 2010; Pizon et al., 2002).

6.2.2.2.2 Inhibition of hypertrophy in the M-band knockout heart

M-band deficiency leads to the activation of the atrophy inducing proteins and additionally to the suppression of hypertrophy associated pathways. The downregulation of FHL2 could indicate a suppression of the androgen receptor (AR) mediated transcription. AR is a ligand-inducible transcription factor that belongs to the nuclear receptor superfamily. Upon hormone binding AR is translocated from the cytosol into the nucleus where it binds specific promoter elements (Ikeda et al., 2005). The hypertrophy inducing ligand-activated AR-mediated transcription can be synergistically enhanced by FHL2, CBP/p300 and β-catenin (Fimia et al., 2000; Johannessen et al., 2006; Müller et al., 2000). Although FHL2 recruits the TATA box binding protein (TBP) regulating the β-catenin mediated transcription (Purcell et al., 2004). M-band deficiency leads to increased level of TBP which suggest an activation of AR by β-catenin (Figure 43 A and B, blue, p. 73). Here FHL2 is essential for building and activation of this complex and the decreased levels of FHL2 suggest the ablation of the transcription activity of AR which could lead to a suppression of hypertrophy (Figure 43 A and B, blue, p. 73; Purcell et al., 2004; Fimia et al., 2000; Johannessen et al., 2006; Müller et al., 2000). M-band deficiency additionally leads to increased levels of CAMK2δ which inhibits the calcineurin dependent induction of hypertrophy (Kreusser et al., 2014). The calcium/calmodulin kinases 2 (CAMK2) consist of four isoforms (CAMK2 α, β, γ, δ). CAMK2γ and δ are known to be predominantly expressed in cardiac muscle. The expression of the CAMK2γ and δ is predicted to be activated by pathological induced changes of the Ca^{2+} transient. Increased levels of Ca^{2+} lead to oxidative stress and are known to induce hypertrophy, apoptosis, electric remodeling and sudden death. The M-band deficient mice died before an age of 40 days and developed severe muscle weakness which could be initiated by a pathological changed Ca^{2+} transient. CAMK2δ is able to regulate the Ca^{2+} transient by phosphorylation of Ca^{2+} transport mediating proteins like phospholamban (PLN) and the sarcoplasmic/endoplasmic reticulum calcium ATPase (SERCA). Both proteins regulate the Ca^{2+} uptake into the SR (Diedrichs et al., 2007;

MacLennan and Kranias, 2003). The deregulation of PLN and SERCA3 (qMS data, not validated by WB) support the expression of CAMK2δ caused by an increased intracellular Ca^{2+} gradient. Furthermore, M-band deficiency induce a downregulation of Na^+/K^+ ATPase 1 (MS data, not validated by WB) indicating a change of the Na^+/K^+ transient. A deregulation of the Na^+ transient leads to ventricular tachyarrhythmia and heart failure. Changes in the K^+ transient are additionally indicated by the overexpression of T-CAP in the M-band deficient mice. T-CAP binds the K^+ channel KCNQ1 at the Z-disc and the increased levels of T-CAP could lead to an over activation of this complex which changes the K^+ transient (Neyroud et al., 1999). The significant increased levels of the four and a half LIM domain protein (FHL1) in the M-band KO indicate an increased expression of the cardiac K^+ channel KCNA5 which additionally could influence the K^+ transient (Figure 43 A and B, blue, p. 73; Dobrev and Wettwer, 2008; Yang et al., 2008). The CAMK2δ is able to regulate Na^+ channels by phosphorylation and its increased expression could be an attempt to regulate the Na^+/K^+ transient. Deregulations of Ca^{2+}, Na^+ and K^+ additionally initiate the expression of the protein kinases PKC and PKA as well as calcineurin (Heineke and Molkentin, 2006; Houser and Molkentin, 2008; Lips et al., 2004). Calcineurin is an essential member of the calcineurin-NFAT (activation of the nuclear factor of activated T-cell) circuit associated with cardiac hypertrophic growth (Heineke and Molkentin, 2006). Activated calcineurin dephosphorylates the NFATc proteins (c1 to c4), exposing nuclear localization signals and translocate NFATc into the nucleus (Chang et al., 2004). The NFAT circuit is additionally activated by the mitogen-activated protein kinases 3 and 1 (MAPK3 and 1 / ERK1/2) as well as by the four and a half LIM domain protein FHL1 (Cowling et al., 2008; Heineke and Molkentin, 2006; McGrath et al., 2006). Both kinases and FHL1 are significantly increased in the M-band knockout mice which suggests an attempt to repress the cardiac atrophy by a potentially activation of the NFAT circuit (Figure 41 andFigure 44 and A and B, blue, p. 71 and 74). Furthermore the calcineurin-NFAT signaling pathway can be activated through the T-CAP binding partner muscle-LIM-protein (MLP) which transduces signaling from the Z-disc (Heineke and Molkentin, 2006). The overexpression of T-CAP could in the M-band KO additionally suggest an increased MLP mediated activation of the NFAT circuit. The activation of the calcineurin-NFAT signaling pathway is also NFκB dependent (Liu et al., 2012). The essential NFκB1 p63, a processed isoform of NFκB1, interacts with NFATc1 and

enhances its transcription activity. M-band deficiency leads to significantly decreased levels of NFκB1 p63 suggesting an interruption of the NFκB1 p63 and NFATc1 interaction which is associated with cardiac atrophy (Figure 43 A and B, blue, p. 73; Liu et al., 2012). The slight increased level of CARP and a significant upregulation of DARP in the M-band deficient mice additionally suggest the negatively regulation of the calcineurin-NFAT signaling pathway (Figure 41 A and B, blue, p. 71). The cardiac ankyrin repeat protein (CARP) and the diabetic ankyrin repeat protein (DARP) bind to the N2A domain of I-band titin and are known to be stretch dependent signaling proteins acting as nuclear transcription co-factors which negatively regulate cardiac gene expression by deactivation of the NFAT activating MAPK3 and 1 (Jeyaseelan et al., 1997; Miller et al., 2003; Song et al., 2012). The suppression of MAPK activity by CARP and DARP potentially correspond to the increased MAPK3 and 1 level in the M-band KO, which could be an attempt to repress the atrophy by activation of the NFAT circuit. The atrophic hearts could be furthermore explained by the unchanged expression levels of the proteins neighbor of BRCA1 (NBR1), sequestosome1 (SQSTM1/p62) and the muscle-specific RING finger protein MURF2 in the M-band knockout animals (Figure 42 A and B, blue, p. 72). MURF2 is involved in the primary myogenesis and shuttles between cytosol and nucleus under atrophic conditions. Additionally all three proteins form a complex at the M-band domain of titin which inactivates the transcriptional activity of the serum response factor (SRF). SRF is important for both heart development and postnatal hypertrophic growth (Centner et al., 2001; Lange et al., 2005; Perera et al., 2010; Pizon et al., 2002). M-band deficiency does not affect the expression of NBR1, p62 and MURF2 which indicates a suppression of the SRF mediated hypertrophy signaling. In summary, the cardiac atrophy could be explained by the activation of atrophy pathways described in 6.2.2.2.1 (p. 93) and simultaneously inhibition of hypertrophy pathways. The hypertrophic growth could be negatively regulated by the inhibition of the AR mediated transcription activity. This could be mediated by the decreased FHL2 expression which negatively affects the FHL2, CBP/p300 and β-catenin complex as well as the activation of TBP. Furthermore the hypertrophy associated NFAT circuit could be limited by the decreased levels of NFκB1 p63 which is important for the NFATc activity. M-band deficiency additionally leads to increased CARP and DARP expression which negatively regulate the

MAPK3 and 1 important for NFAT activity. Furthermore the NBR1/p62/MURF2 complex inhibits the transcriptional activity of the hypertrophy associated SRF.

6.2.2.2.3 Initiation of dilated cardiomyopathy in the Ex2 knockout

The development of dilated cardiomyopathy could be initiated by the activation of hypertrophy and atrophy associated pathways simultaneously. The main actors responsible for the development of the dilated cardiomyopathy seem to be the titin N2B interacting proteins FHL1 and 2. Both proteins are significantly increased in the complete titin deficient mice which is associated with hypertrophic growth and dilated cardiomyopathy (Figure 41 A and B, red, p. 71; Johannessen et al., 2006; Lange et al., 2002; McGrath et al., 2006; Müller et al., 2000). The overexpression relates to the loss of titin expression inducing a force overload to the residual titin proteins of the sarcomere. This could lead to an increased stretch of the N2B domain which increased the FHL1 and 2 binding and potentially mediates the increased expression of both four and a half LIM domain proteins. Complete titin deficiency leads to a decreased expression of αB-crystalin (CryAB) (Figure 41 A and B, red, p. 71). CryAB is a member of the small heat shock proteins (sHSP) preventing extensive structural damage especially at the N2B domain where it potentially protects the structure of the FHL1 and 2 binding sites (Bullard et al., 2004; Golenhofen et al., 2002). FHL 1 and 2 interact with each other and both are able to bind the MAPK1 (ERK2) (Johannessen et al., 2006; Sheikh et al., 2008). The FHL1/ERK2 stress signaling complex facilitates hypertrophic growth by enhancing the transcription activity of the calcineurin-NFAT circuit (Heineke and Molkentin, 2006). Complete titin deficiency leads to increased levels of FHL1 which could directly interact to NFATc1. This could mediate the transcriptional activity of the hypertrophy associated calcineurin-NFAT signaling pathway found in patients with hypertrophy or dilated cardiomyopathy (Cowling et al., 2008). Furthermore FHL1 is associated with the disruption of the M-band and the myosin thick filaments by competing with myosin for binding to MyBP-C (Cowling et al., 2008; Johannessen et al., 2006; McGrath et al., 2006; Sheikh et al., 2008). Complete titin deficiency induce the overexpression of T-CAP which could lead to the interruption of the T-CAP-MLP complex (Figure 41 A and B, red, p. 71) (Gregorio et al., 1998; Hayashi et al., 2004b; Hershberger et al., 2008). The subsequently released MLP is another activator of the calcineurin-NFAT signaling pathway (Heineke and Molkentin, 2006). The significantly decreased CARP level in the Ex2 knockout animals additionally indicates the activation of the hypertrophic NFAT signaling pathway

(Figure 41 A and B, red, p. 71). CARP is a stretch dependent titin binding signaling protein which acts as a nuclear transcription co-factor that negatively regulates cardiac gene expression (Jeyaseelan et al., 1997; Miller et al., 2003). Complete titin deficiency leads to reduced levels of CARP which enhances the hypertrophy associated activity of the MAPK1 and 3 as well as the transforming growth factor-β (TGF-β/Smads) signaling pathways (Song et al., 2012). The decreased levels of CARP additionally support the expression and transcriptional activity of the cardiac troponin C and ANP as well as BNP (Figure 35 A, p. 65; Jeyaseelan et al., 1997). Different to the decreased CARP expression the MAPK1 and 3 expressions are not significantly changed which suggest the activation of the NFAT circuit by triggering the dephosphorylation of NFATc1 (Figure 44 A and B, red, p. 74; Jeyaseelan et al., 1997; Miller et al., 2003; Song et al., 2012). Complete titin deficiency leads to significantly increased FHL2 levels indicating competitive interactions of FHL1 and 2 to MAPK1 (Figure 41 A and B, red, p. 71). FHL1/MAPK1 interaction mediates the NFAT activation whereas FHL2/MAPK1 interaction prevents nuclear import or/and stimulates nuclear export of activated MAPK1 which ablate the MAPK1 mediated hypertrophy signaling (Heineke and Molkentin, 2006; Johannessen et al., 2006). Furthermore FHL2 scaffolds several muscle metabolic proteins like the MM-creatine kinase, the adenylate cyclase and the phosphofructokinase to the N2B domain as well as to the M-band. These proteins are known to provide energy during muscle contraction. Thus FHL2 modulates ventricular functions via structural remodeling and/or alternations in energy consumption in response to hypertrophic stimuli (Johannessen et al., 2006; Lange et al., 2002; McGrath et al., 2006; Müller et al., 2000). The increased FHL2 expression additionally suggests the activation of the hypertrophy mediating androgen receptor 1 (AR1) (Johannessen et al., 2006). Furthermore, FHL2 recruits the proline-, glutamic acid-, and leucine-rich protein-1 (PELP1/MNAR) which mediates FHL2 transcription activity as a co-activator by interaction with p300/CBP or as repressor by binding of HDAC2 (Johannessen et al., 2006). Complete titin deficiency induce the significant overexpression of the TATA box binding protein (TBP) which can be bind by FHL2 (Figure 43 A and B, red, p. 73). This complex is suggested to regulate the β-catenin mediated transcription (Purcell et al., 2004). Thus FHL2, CREB binding protein (CBP/p300) and TBP/β-catenin could synergistically enhance ligand-activated AR-mediated transcription, which induces hypertrophy (Fimia et al., 2000; Johannessen et al., 2006; Müller et al., 2000). The significantly increased cAMP responsive element

binding protein 1 (CREB1) is additionally interacts to FHL2 (Figure 43 A and B, red, p. 73). FHL2, CBP and CREB1 form a complex, activating the transcription of cAMP responsive genes like the protein kinases A and C (PKA and PKC) as well as the calcium/calmodulin dependent kinases (CAMK) which could explain significantly increased protein level of the CAMK2α and γ (Figure 44 A and B, red, p. 74; Johannessen et al., 2006). This deregulated expression supports the development of hypertrophic hearts (Anderson, 2009). CAMK2γ and δ contain of similar functional domains which could responsible for similar functions (Anderson, 2009; Hidalgo et al., 2012). Complete titin deficiency leads to increased CAMK2γ levels but do not affect the CAMK2δ expression (Figure 44 A and B, red, p. 74). These increased levels of CAMK2γ could additionally support the functions of CAMK2δ and therefore the phosphorylation of N2B titin analogous to the PKA/PKG which lowers passive tension or the phosphorylation of the PEVK domain like PKCα, what increases passive tension (Anderson, 2009; Hidalgo et al., 2012). The expression of the cAMP responsive genes is activated by pathological induced changes of the Ca^{2+} transient which leads to oxidative stress and finally to hypertrophy, apoptosis, electric remodeling and sudden death. The significant upregulation of phospholamban (PLN) (MS data, not verified by WB) as well as the significantly increased transcription of the sarcoplasmic/endoplasmic reticulum calcium ATPase 2 (SERCA2) in the Ex2 KO suggest a deregulation of the Ca^{2+} uptake into the SR (Figure 35 B, p. 65). The activation of these Ca^{2+} transport mediating proteins is regulated by phosphorylation of cardiac specific CAMK2γ and δ (MacLennan and Kranias, 2003). Furthermore the CAMK2γ and δ regulate Na^{+} channels by phosphorylation and a deregulation leads to ventricular tachyarrhythmia and heart failure (Anderson, 2009; Wagner et al., 2006). Furthermore complete titin deficiency induces a significantly increased expression of the Na^{+}-K^{+}-ATPase α1 (AT1A1) as well as the Na^{+}- channel protein type 5 subunit α (SCN5A) (MS data, not verified by WB) which suggests changes in the Ca^{2+} transport. The significant overexpression of T-CAP in the titin null mice additionally could lead to an over activation of the K^{+} channel KCNQ1 which is a binding partner of T-CAP (Neyroud et al., 1999). These changes of the Ca^{2+}, Na^{+} and K^{+} transients could explain the increased levels of CAMK2γ and δ and potentially indicate an attempt to regulate the changed ion-flux (Heineke and Molkentin, 2006; Houser and Molkentin, 2008; Lips et al., 2004). Furthermore the CAMK2 activate transcription by

phosphorylation of HDACs class II and MEF2 which initiate the NFκB1 as well as the FHL2 expression (Anderson, 2009; Johannessen et al., 2006). The activation of MEF2 could explain the increased expression of FHL2 (Figure 41 A and B, red, p. 71) whereas the activation of HDACs class II suggests the increased expression of non-processed NFκB1 p105 as well as the processed isoforms p84 and p70 (Figure 43 A and B, red, p. 73). A further hypertrophy mediating transcription factor controlled by FHL2 is the serum response factor (SRF). FHL2 inhibits the SRF-dependent transcription in a promoter-specific way by direct binding to SRF. This interaction prevents the recruitment of the SRF coactivator myocardin-related transcription factor A (MRTF-A/MAL) (Johannessen et al., 2006). Additionally the transcriptional activity of the SRF is negatively regulated by a complex of NBR1, SQSTM1 and MURF2 (Centner et al., 2001; Lange et al., 2005; Perera et al., 2010; Pizon et al., 2002). The increased levels of FHL2 in the EX2 KO suggest an inhibition of the SRF activity whereas the significant downregulation of NBR1 and the significant upregulation of SQSM1 indicate an interruption of the NBR1/SQSTM1/MURF2 complex leading to an induction of the SRF transcription activity (Figure 42 A and B, red, p. 72; Centner et al., 2001; Lange et al., 2005; Perera et al., 2010; Pizon et al., 2002). In summary, the complete titin deficiency leads to activation of the hypertrophy associated NFAT circuit by the increased levels FHL1 and the decreased levels of CARP which triggers the dephosphorylation of NFATc1 by the MAPK3 and 1. Furthermore, the increased levels of FHL2 in the Ex2 KO suggest the activation of the hypertrophy associated AR mediated transcription. The activation of AR is supported by the increased expression of TBP and CREB1 which are FHL2 binding partner enhancing the activation of AR. Complete titin deficiency additionally induce the downregulation of NBR1 and simultaneously upregulation of p62 which impairs the function of the NBR1/p62/MURF2 complex important for localization and activity of the SRF.

In addition to the activation of hypertrophy associated pathways the titin null mice overexpress proteins important for atrophy. The muscle-specific RING finger protein MURF1 is significantly increased in the Ex2 knockout animals (Figure 42 A and B, red, p. 72). The overexpression of MURF1 could be explained by the increased force overload and increased stretch of the residual titin molecules. This leads to an increased binding and activation of MURF1. MURF1 is an E3 ubiquitin ligase which binds together with MURF2 to the M-band of titin. Additionally MURF1 interacts

to MURF3 building a complex at the Z-disc titin. These interactions indicate a link of the contractile system to the regulation of protein synthesis and degradation. Therefore increased levels of MURF1 are associated with an upregulation of ubiquitin turnover observed in atrophy. In addition MURF1 is known to interact to the receptor for activated protein kinase C (RACK1) which blocks the translocation of PKCε to focal adhesions which is associated with hypertrophy (Arya et al., 2004; McElhinny et al., 2004; Tskhovrebova and Trinick, 2003; Witt et al., 2005). The ubiquitin ligase activity of MURF1 and the corresponding induction of proteolysis could be enhanced the binding of SQSTM1 (p62) and NBR1. Both proteins mediate the selective autophagy and aggregate formation. The increased expression of SQSTM1 suggests an activated ubiquitin dependent aggregation and degradation of sarcomeric proteins which is associated with atrophy (Figure 42 A and B, red, p. 72). Furthermore SQSTM1 is known to mediate the selective autophagic clearance of non-ubiquitinylated substrates independent of NBR1. The significantly decreased levels of NBR1 in the Ex2 KO could indicate the degradation of non-ubiquitinylated proteins in addition to the MURF1/SQSTM1/NBR1 ubiquitin dependent proteolysis (Figure 42 A and B, red, p. 72) (Kirkin et al., 2009a, 2009b; Watanabe and Tanaka, 2011; Yan et al., 2013). Furthermore the overexpression of SQSTM1 could be associated with the severe sarcomeric disassembly leading to an increased accumulation and protein degradation. The expression of MURF1 is regulated by the transcription factors NFκB1 and 2 (Heusch et al., 1999; Leychenko et al., 2011; Wu et al., 2014). NFκB1 and 2 expressions are regulated by the CAMK2 mediated phosphorylation of HDACs class II (Anderson, 2009; Johannessen et al., 2006). The significantly increased levels of CAMK2γ and α could explain the significant upregulation of the NFκB1 isoforms p105, p84 and p70. The significantly downregulated NFκB1 p63 and unchanged levels of the processed active NFκB1 p50 as well as NFκB2 suggest an interruption of NFκB processing (Figure 43 A and B, red, p. 73). This failing NFκB processing could be explained by low levels of ATP which indicate a pathological deregulation of Ca^{2+}, Na^{+} and K^{+} transient suggested by the overexpression of AT1A1, SCN5A, PLN and SERCA2. However the unchanged levels of the processed NFκB's indicate a potential activation of MURF1 expression (Wu et al., 2014). The transcriptional activity of the NFκB's and therefore the overexpression of MURF1 is regulated by removing the interacting IκB inhibitor proteins (Cai et al., 2004; Hunter and Kandarian, 2004). The TNF receptor-associated factor 6 (TRAF6) is an E3 ubiquitin

protein ligase which induce the ubiquitin dependent phosphorylation and degradation of IκB's (Bai et al., 2005). Complete titin deficiency leads to a significantly increased expression of TRAF6 which suggests a potentially enhanced activation of NFκB transcription activity by ubiquitination of IκB (Figure 44 A and B, red, p. 74). The TRAF6 activity is negatively regulated by the binding of FHL2 and/or SQSTM1 which blocks the processing of IκB by TRAF6 (Bai et al., 2005; Johannessen et al., 2006; Nakamura et al., 2010). The overexpression of FHL2 as well as SQSTM1 in the Ex2 knockout animals could indicate a competitive interaction of FHL2/TRAF6 and SQSTM1/TRAF6 regulating the NFκB activation. In summary, the dilated cardiomyopathy of the Ex2 KO strain could be explained by the simultaneously activation of hypertrophy and atrophy associated pathways. The increased expression of MURF1 and p62 suggest an ubiquitin and proteolysis dependent activation of atrophy pathways. Complete titin deficiency additionally leads to an overexpression of TRAF6 which is important for NFκB activation and finally for MURF1 expression. These atrophy mediating processes are antagonized especially by the increased FHL2 expression.

6.3 Conclusions and perspectives

In summary we compare the Ex2 KO strain with the established M-band deficient inducible knockout in a phenotypic, morphologic, ultrastructural, transcriptomic and proteomic approach (Gotthardt et al., 2003). The experiments indicate a congenerous development of both strains developing similar differences of weight, strength endurance and survival compared to the wild-type. Both the Ex2 knockouts as well as the M-band deficient mice develop a severe progressive muscle weakness paired with confinements of their posture and gait. These muscle weaknesses correspond to the decreased development of muscle force and finally lead to death before an age of 40 days. The Ex2 knockout and the M-band deficient mice suggest multinuclear skeletal muscle atrophy with centralized nuclei as well as unstructured and reduced myofibrils. This muscular transformation is caused by the disruption of the sarcomere initiated by M-band as well as complete titin deficiency. Ultrastructural investigations determine the beginning of the disruption of the sarcomere at the M-Band or at the Z-disc. This diversity results in transcriptomic and proteomic differences but finally mediate skeletal muscle atrophy in both strains. The cardiac development of the Ex2 knockout animals

show a dilated cardiomyopathy (DCM) instead of a cardiac atrophy as developed in the M-band knockout mice (Figure 45, p. 104).

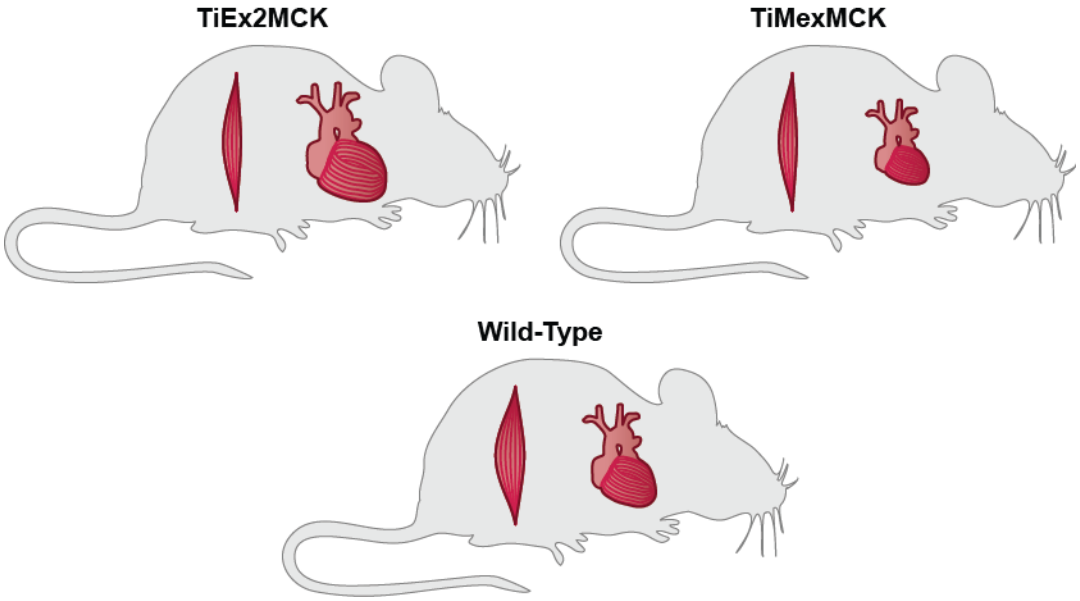

Figure 45: Scheme of Ex2 and M-band KO skeletal and cardiac muscle development. Compared to the wild-type, complete titin deficiency (TiEx2MCK) leads to skeletal muscle atrophy and dilated cardiomyopathy whereas M-band deficiency (TiMexMCK) induces skeletal muscle and cardiac atrophy.

Histological experiments indicate similar multinuclear, unstructured and size-reduced cardiomyocytes. Electron microscopy shows a different induction of the disorganization of the sarcomere. Similar to the skeletal muscle we determine the initiation of sarcomeric disruption at the Z-disc or at the M-band. The comparison of the transcriptome as well as the proteome enable the identification of the potential regulating proteins associated with cardiac atrophy and/or dilated cardiomyopathy. In heart, both titin deficiencies lead to the deregulation of the titin interacting proteins T-CAP, FHL1 and 2, CARP, DARP, MURF1, NBR1 and SQSTM1 as well as other complex building proteins like MAPK1 and 3, TRAF6 and CAMK2. Furthermore we identify deregulations of the transcription factors CREB1, TBP and NFκB1 and 2. The differential expression levels and the possible interactions of titin and these proteins explain the development of the dilated cardiomyopathy in the Ex2 KO as well as cardiac atrophy in the M-band KO. The cardiac atrophy of the M-band deficient mice is caused by the disintegration of titin into the M-band which leads to the disassembly of the sarcomere. In addition this failing titin integration induce a stretch overload of the remaining natural titin and leads to an increased binding and activation of titin interacting signaling proteins like FHL1 and 2, CARP, DARP and MURF1. The M-band deficient titin still integrates into the Z-disc and

stabilizes the sarcomere from the Z-disc to the A-band. In order to the disintegration into the M-band the M-band deficient titin is not stretched which indicates less binding of the named proteins except of MURF1. This reduced binding antagonizes to the increased binding at the residual titin and leads to an attenuation of the titin mediated Z-disc, I-band and A-band signaling. The M-band of the sarcomere is still destabilized which indicate an increased M-band mediated signaling and is suggested by the overexpression of MURF1 in the M-band deficient mice. MURF1 regulates the ubiquitin dependent proteolysis and autophagy which induce the observed cardiac atrophy (Figure 46, top left, p. 107). Furthermore the structural collapse of the sarcomere leads to a deregulated ion transient which explains the overexpression of the atrophy associated transcription factor NFκB1 (Figure 46, top right, p. 107). The transcriptional activation of NFκB1 is known to be regulated by IκB. The overexpressed E3 ubiquitin ligase TRAF6 represses the inhibitory regulation of IκB by ubiquitin dependent proteolysis. FHL2 is known to regulate the activity of TRAF6 by binding. The significantly decreased levels of FHL2 indicate an activation of the transcription activity of NFκB1 by the TRAF6 mediated degradation of IκB (Figure 46, top right, p. 107). Furthermore the decreased FHL2 expression negatively regulates the transcriptional activity of TBP which is important for the activation of the androgen receptor (AR) signaling. The disturbed interaction of both proteins leads to a reduced transcriptional activity of the hypertrophy associated AR pathway (Figure 46, top right, p. 107). The significantly increased levels of DARP and the unchanged expression of CARP additionally indicate a suppression of calcinerin-NFAT hypertrophy signaling. Both proteins are known to decrease the activity of the MAPK1 and 3 which are able to activate the hypertrophy associated calcinerin-NFAT circuit. In addition the overexpression of these MAP kinases in the M-band deficient mice could be an attempt to repress the atrophy (Figure 46, top middle, p. 107). Furthermore MURF2, NBR1 and SQSTM1 (p62) are able to build a complex which negatively regulates the transcription activity of the hypertrophy associated serum response factor (SRF). The regular expression of MURF2, NBR1 and SQSTM1 indicate another M-band mediated signaling which supported the MURF1 induced atrophy by simultaneously suppression of hypertrophy in the M-band KO (Figure 46, top middle, p. 107). Therefore we verify the results of Gotthardt and colleagues and additionally show evidence of the molecular background of the titin M-Band knockout (Figure 46, top, p. 107) (Gotthardt et al., 2003).

The development of the dilated cardiomyopathy in the titin null mice is caused by the loss of titin expression. This leads to severe sarcomeric disassembly similar to the M-band KO. Furthermore the loss of new expressed titin induce a stretch overload of the residual titin which leads to an increased binding and activation of the titin interacting signaling proteins FHL1 and 2, CARP, DARP and MURF1. In difference to the M-band KO the residual titin molecules of the Ex2 KO are not stabilized. This leads to the simultaneously activation of hypertrophy and atrophy associated pathways which causes dilated cardiomyopathy. The MURF1 expression is significantly increased similar to M-band deficiency indicating an activation of atrophy by MURF1 mediated ubiquitin dependent proteolysis and autophagy. In addition the significantly increased expression of SQSTM1 (p62) and the simultaneously significant decreased NBR1 expression support the activation of atrophy associated pathways by mediating the ubiquitin independent proteolysis and autophagy (Figure 46, bottom right, p. 107). Furthermore the deregulations of these proteins suggest an interrupted activity of the MURF2/NBR1/SQSTM1 complex which leads to an increased transcriptional activity of the hypertrophy associated SRF (Figure 46, bottom right, p. 107). The levels of NFκB1 are unchanged which indicate a reduced expression of atrophy initiating proteins. This inhibition of atrophy is supported by the increased levels of FHL2 and SQSTM1. Both proteins deactivate the ubiquitin dependent proteolysis of the NFκB1 inhibitor IκB by binding to TRAF6 (Figure 46, bottom left, p. 107). Furthermore the increased levels of FHL2 positively regulate the hypertrophy associated androgen receptor (AR) by binding and enhancing the transcriptional activity of the overexpressed CREB1 and TBP (Figure 46, bottom left, p. 107). In addition the increased expression of FHL1 suggests an activation of the hypertrophy inducing calcineurin-NFAT circuit by binding and activation of NFATc1 (Figure 46, bottom left, p. 107). Furthermore the activation of the NFAT circuit is supported by the decreased levels of CARP and the unchanged levels of DARP. Both proteins are known to inhibit the activity of the MAPK1 and 3 which activate the NFAT by triggering the dephosphorylation of NFATc1. The simultaneously slight but not significant downregulation of the MAPK1 and 3 could be an attempt to repress the NFAT activity and the hypertrophic growth (Figure 46, bottom middle, p. 107). These results indicate the simultaneously activation and suppression of atrophy as well as hypertrophy associated pathways which lead to the development of dilated cardiomyopathy in the complete titin deficient mice. Furthermore

the investigations indicate evidence of a competitive or cooperative I-band and M-band mediated signaling. Thereby the M-band seem to resume the initiation of atrophy pathways whereas the I-band seem to activate hypertrophic pathways (Figure 46, p. 107). This observation is supported by the investigations of Radke and colleagues, who observed the occurrence of a cardiac atrophy by deletion of the titin N2B domain (Radke et al., 2007).

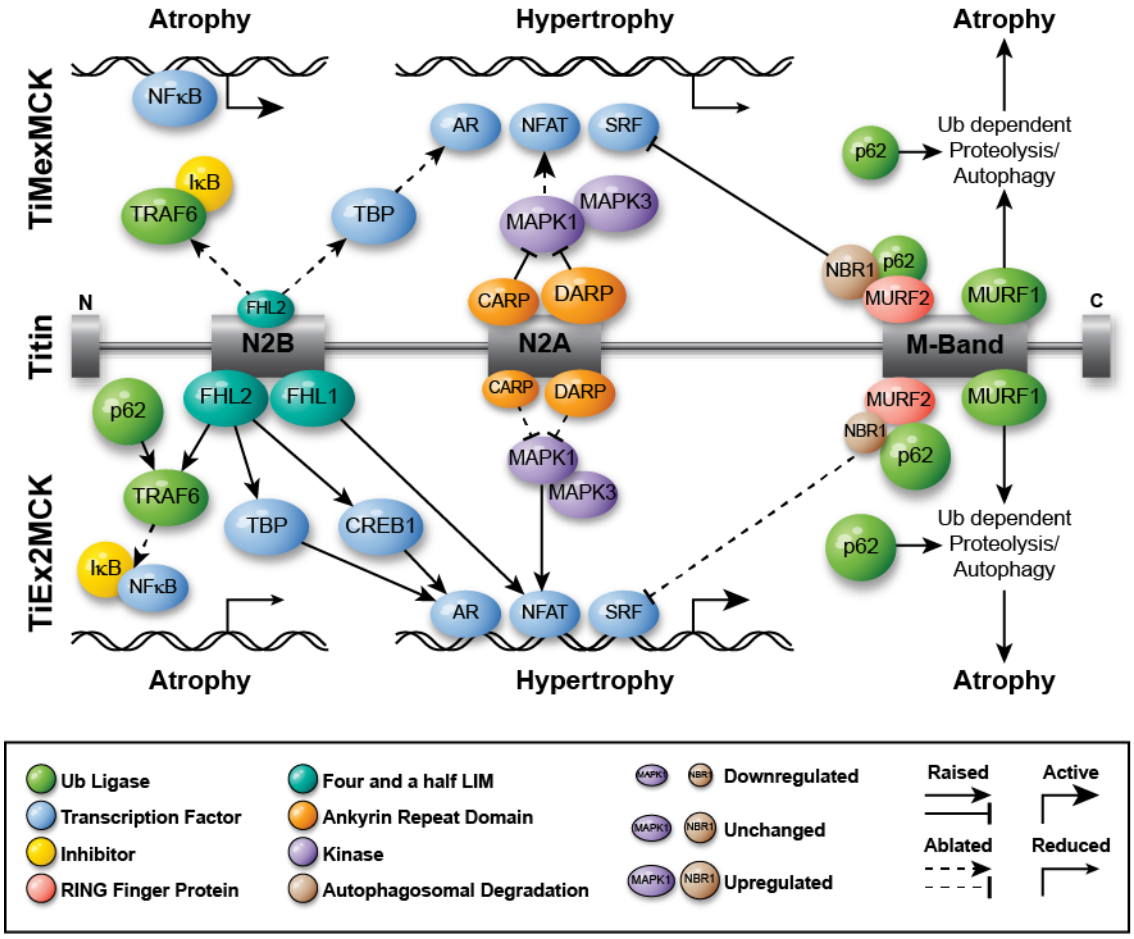

Figure 46: Cardiac titin I-band and M-band signaling. Pathways potentially affected. The proteomics of the M-band knockout mice (TiMexMCK, top) suggested an induction of atrophy signaling and simultaneously inhibition of hypertrophy signaling. The deregulated proteins found in the Ex2 knockout animals (TiEx2MCK, down) indicated the activation of hypertrophy signaling and additionally inhibition of atrophy signaling.

The hypothesis could be perspectival verified on the one hand by the further investigation of the deregulated proteins found in the titin null strain. This study indicates multiple activated pathways which could be influenced by each other and could additionally adulterate the results. Therefore it would be an option to analyze an earlier time point of development where the disruption of the sarcomere and the development is not such advanced like with an age of 35 days. The investigation of 15 days old wild-type,

heterozygous and KO mice indicate no differences in the development of the striated muscles (Figure 7, p. 42) whereas the 35 days old mice develop severe skeletal muscle atrophy and dilated cardiomyopathy (TiEx2MCK) or cardiac atrophy (TiMexMCK; Figure 18,Figure 21,Figure 28 andFigure 31p. 51, 53, 59 and 62). The results of the weight, grid holding and survival experiments suggest an age of less than 21 days for these further analysis (Figure 16,Figure 17,Figure 19 andFigure 20, p. 49, 50, 52 and 52). Furthermore a younger age could by facilitate a fluorescence staining approach which could be used to analyze the localization of the deregulated proteins.

On the other hand the TiEx2MCK strain could be used to generate a Tamoxifen inducible animal model. The according TiEx2MCM animals would develop under normal cardiac conditions until the induction of the CRE-recombinase by Tamoxifen injection. These animals could be compared to the Tamoxifen inducible M-band deficient animal model, described by Peng and colleagues (Peng et al., 2007). Furthermore this animal model facilitates the possibility of functional analysis using an ECG or isolated heart approach.

The TiEx2MCM strain additionally could be used for breeding with other conditional strains containing a titin modification which leads to embryonic or post embryonic lethality. This facilitates a fast investigation of this modification by avoiding a targeting strategy based generation of an inducible KO model. These double heterozygous animals were rescued until the induction of the titin exon 2 deletion by Tamoxifen.

7 Bibliography

Agarkova, I., and Perriard, J.C. (2005). The M-band: an elastic web that crosslinks thick filaments in the center of the sarcomere. Trends Cell Biol.

Ali, Ma., Cho, WJ., Hudson, B., Kassiri, Z., Granzier, H., Schulz, R. (2010). Titin is a target of matrix metalloproteinase-2: implications in myocardial ischemia/reperfusion injury. Circulation 122(20), 2039-47

Allen, D.L., and Leinwand, L.A. (2001). Postnatal myosin heavy chain isoform expression in normal mice and mice null for IIb or IId myosin heavy chains. Dev Biol *229*, 383–395.

Anderson, M.E. (2009). CaMKII and a failing strategy for growth in heart. J. Clin. Invest *119*, 1082–1085.

Arimura, T., Helbling-Leclerc, A., Massart, C., Varnous, S., Niel, F., Lacene, E., Fromes, Y., Toussaint, M., Mura, A.M., Keller, D.I., et al. (2005). Mouse model carrying H222P-Lmna mutation develops muscular dystrophy and dilated cardiomyopathy similar to human striated muscle laminopathies. Hum Mol Genet *14*, 155–169.

Arimura, T., Bos, J.M., Sato, A., Kubo, T., Okamoto, H., Nishi, H., Harada, H., Koga, Y., Moulik, M., Doi, Y.L., et al. (2009). Cardiac ankyrin repeat protein gene (ANKRD1) mutations in hypertrophic cardiomyopathy. J. Am. Coll. Cardiol *54*, 334–342.

Arya, R., Kedar, V., Hwang, J.R., McDonough, H., Li, H.-H., Taylor, J., and Patterson, C. (2004). Muscle ring finger protein-1 inhibits PKC{epsilon} activation and prevents cardiomyocyte hypertrophy. J. Cell Biol *167*, 1147–1159.

Auerbach, D., Bantle, S., Keller, S., Hinderling, V., Leu, M., Ehler, E., and Perriard, J.C. (1999). Different domains of the M-band protein myomesin are involved in myosin binding and M-band targeting. Mol Biol Cell *10*, 1297–1308.

Bai, S., Kitaura, H., Zhao, H., Chen, J., Müller, J.M., Schüle, R., Darnay, B., Novack, D.V., Ross, F.P., and Teitelbaum, S.L. (2005). FHL2 inhibits the activated osteoclast in a TRAF6-dependent manner. J Clin Invest *115*, 2742–2751.

Bang, M.L., Centner, T., Fornoff, F., Geach, A.J., Gotthardt, M., McNabb, M., Witt, C.C., Labeit, D., Gregorio, C.C., Granzier, H., et al. (2001). The complete gene sequence of titin, expression of an unusual approximately 700-kDa titin isoform, and its interaction with obscurin identify a novel Z-line to I-band linking system. Circ Res *89*, 1065–1072.

Bansal, D., Miyake, K., Vogel, S.S., Groh, S., Chen, C.-C., Williamson, R., McNeil, P.L., and Campbell, K.P. (2003). Defective membrane repair in dysferlin-deficient muscular dystrophy. Nature *423*, 168–172.

Bennett, P., Craig, R., Starr, R., and Offer, G. (1986). The ultrastructural location of C-protein, X-protein and H-protein in rabbit muscle. J. Muscle Res. Cell. Motil *7*, 550–567.

Berenji, K., Drazner, M.H., Rothermel, B.A., and Hill, J.A. (2005). Does load-induced ventricular hypertrophy progress to systolic heart failure? Am. J. Physiol. Heart Circ. Physiol. *289*, H8–H16.

Van den Bergh, P.Y.K., Bouquiaux, O., Verellen, C., Marchand, S., Richard, I., Hackman, P., and Udd, B. (2003). Tibial muscular dystrophy in a Belgian family. Ann. Neurol *54*, 248–251.

Bindea, G., Mlecnik, B., Hackl, H., Charoentong, P., Tosolini, M., Kirilovsky, A., Fridman, W.-H., Pagès, F., Trajanoski, Z., and Galon, J. (2009). ClueGO: a Cytoscape plug-in to decipher functionally grouped gene ontology and pathway annotation networks. Bioinformatics *25*, 1091–1093.

Bishu, K., Hamdani, N., Mohammed, S.F., Kruger, M., Ohtani, T., Ogut, O., Brozovich, F.V., Burnett, J.C., Jr, Linke, W.A., and Redfield, M.M. (2011). Sildenafil and B-type natriuretic Peptide acutely phosphorylate titin and improve diastolic distensibility in vivo. Circulation *124*, 2882–2891.

Bogomolovas, J., Gasch, A., Simkovic, F., Rigden, D.J., Labeit, S., and Mayans, O. (2014). Titin kinase is an inactive pseudokinase scaffold that supports MuRF1 recruitment to the sarcomeric M-line. Open Biol *4*.

Borbély, A., Falcao-Pires, I., van Heerebeek, L., Hamdani, N., Edes, I., Gavina, C., Leite-Moreira, A.F., Bronzwaer, J.G.F., Papp, Z., van der Velden, J., et al. (2009). Hypophosphorylation of the Stiff N2B titin isoform raises cardiomyocyte resting tension in failing human myocardium. Circ. Res *104*, 780–786.

Braz, J.C., Bueno, O.F., De Windt, L.J., and Molkentin, J.D. (2002). PKC alpha regulates the hypertrophic growth of cardiomyocytes through extracellular signal-regulated kinase1/2 (ERK1/2). J Cell Biol *156*, 905–919.

Brown, D.D., Davis, A.C., and Conlon, F.L. (2006). Xtn3 is a developmentally expressed cardiac and skeletal muscle-specific novex-3 titin isoform. Gene Expr. Patterns *6*, 913–918.

Bubikat, A., De Windt, L.J., Zetsche, B., Fabritz, L., Sickler, H., Eckardt, D., Godecke, A., Baba, H.A., and Kuhn, M. (2005). Local atrial natriuretic peptide signaling prevents hypertensive cardiac hypertrophy in endothelial nitric-oxide synthase-deficient mice. J Biol Chem *280*, 21594–21599.

Buck, D., Smith, J.E., 3rd, Chung, C.S., Ono, Y., Sorimachi, H., Labeit, S., and Granzier, H.L. (2014). Removal of immunoglobulin-like domains from titin's spring segment alters titin splicing in mouse skeletal muscle and causes myopathy. J. Gen. Physiol. *143*, 215–230.

Bullard, B., Ferguson, C., Minajeva, A., Leake, M.C., Gautel, M., Labeit, D., Ding, L., Labeit, S., Horwitz, J., Leonard, K.R., et al. (2004). Association of the chaperone alphaB-crystallin with titin in heart muscle. J Biol Chem *279*, 7917–7924.

Cai, D., Frantz, J.D., Tawa, N.E., Jr, Melendez, P.A., Oh, B.-C., Lidov, H.G.W., Hasselgren, P.-O., Frontera, W.R., Lee, J., Glass, D.J., et al. (2004). IKKbeta/NF-kappaB activation causes severe muscle wasting in mice. Cell *119*, 285–298.

Caldwell, J.E., Heiss, S.G., Mermall, V., and Cooper, J.A. (1989). Effects of CapZ, an actin capping protein of muscle, on the polymerization of actin. Biochemistry *28*, 8506–8514.

Carlson, C.G., Rutter, J., Bledsoe, C., Singh, R., Hoff, H., Bruemmer, K., Sesti, J., Gatti, F., Berge, J., and McCarthy, L. (2010). A simple protocol for assessing inter-trial and inter-examiner reliability for two noninvasive measures of limb muscle strength. J. Neurosci. Methods *186*, 226–230.

Carmignac, V., Salih, M.A., Quijano-Roy, S., Marchand, S., Al Rayess, M.M., Mukhtar, M.M., Urtizberea, J.A., Labeit, S., Guicheney, P., Leturcq, F., et al. (2007). C-terminal titin deletions cause a novel early-onset myopathy with fatal cardiomyopathy. Ann Neurol *61*, 340–351.

Cazorla, O., Freiburg, A., Helmes, M., Centner, T., McNabb, M., Wu, Y., Trombitas, K., Labeit, S., and Granzier, H.L. (2000). Differential expression of cardiac titin isoforms and modulation of cellular stiffness. Circ Res *86*, 59–67.

Centner, T., Yano, J., Kimura, E., McElhinny, A.S., Pelin, K., Witt, C.C., Bang, M.L., Trombitas, K., Granzier, H., Gregorio, C.C., et al. (2001). Identification of Muscle Specific Ring Finger Proteins as Potential Regulators of the Titin Kinase Domain. J Mol Biol *306*, 717–726.

Ceyhan-Birsoy, O., Agrawal, P.B., Hidalgo, C., Schmitz-Abe, K., Dechene, E.T., Swanson, L.C., Soemedi, R., Vasli, N., Iannaccone, S.T., Shieh, P.B., et al. (2013). Recessive truncating titin gene, TTN, mutations presenting as centronuclear myopathy. Neurology.

Chang, C.P., Neilson, J.R., Bayle, J.H., Gestwicki, J.E., Kuo, A., Stankunas, K., Graef, I.A., and Crabtree, G.R. (2004). A field of myocardial-endocardial NFAT signaling underlies heart valve morphogenesis. Cell *118*, 649–663.

Chauveau, C., Bonnemann, C.G., Julien, C., Kho, A.L., Marks, H., Talim, B., Maury, P., Arne-Bes, M.C., Uro-Coste, E., Alexandrovich, A., et al. (2014). Recessive TTN truncating mutations define novel forms of core myopathy with heart disease. Hum. Mol. Genet. *23*, 980–991.

Clerico, A., and Iervasi, G. (1995). Alterations in metabolic clearance of atrial natriuretic peptides in heart failure: how do they relate to the resistance to atrial natriuretic peptides? J Card Fail *1*, 323–328.

Conover, G.M., Henderson, S.N., and Gregorio, C.C. (2009). A myopathy-linked desmin mutation perturbs striated muscle actin filament architecture. Mol Biol Cell *20*, 834–845.

Cowling, B.S., McGrath, M.J., Nguyen, M.-A., Cottle, D.L., Kee, A.J., Brown, S., Schessl, J., Zou, Y., Joya, J., Bönnemann, C.G., et al. (2008). Identification of FHL1 as a regulator of skeletal muscle mass: implications for human myopathy. J Cell Biol *183*, 1033–1048.

Dabiri, G.A., Turnacioglu, K.K., Sanger, J.M., and Sanger, J.W. (1997). Myofibrillogenesis visualized in living embryonic cardiomyocytes. Proc Natl Acad Sci U S A *94*, 9493–9498.

Diedrichs, H., Hagemeister, J., Chi, M., Boelck, B., Müller-Ehmsen, J., and Schneider, C.A. (2007). Activation of the calcineurin/NFAT signalling cascade starts early in human hypertrophic myocardium. J Int Med Res *35*, 803–818.

Dlugosz, A.A., Antin, P.B., Nachmias, V.T., and Holtzer, H. (1984). The relationship between stress fiber-like structures and nascent myofibrils in cultured cardiac myocytes. J. Cell Biol *99*, 2268–2278.

Dobrev, D., and Wettwer, E. (2008). Four and a half LIM protein 1: a novel chaperone for atrium-specific Kv1.5 channels with a potential role in atrial arrhythmogenesis. Cardiovasc Res *78*, 411–412.

Doucet, M., Russell, A.P., Léger, B., Debigaré, R., Joanisse, D.R., Caron, M.-A., LeBlanc, P., and Maltais, F. (2007). Muscle atrophy and hypertrophy signaling in patients with chronic obstructive pulmonary disease. Am. J. Respir. Crit. Care Med. *176*, 261–269.

Drabikowski, W., and Nowak, E. (1973). Interaction of F-actin with troponin constituents. Biochim. Biophys. Acta *328*, 470–480.

Du, A., Sanger, J.M., Linask, K.K., and Sanger, J.W. (2003). Myofibrillogenesis in the first cardiomyocytes formed from isolated quail precardiac mesoderm. Dev. Biol *257*, 382–394.

Duboscq-Bidot, L., Charron, P., Ruppert, V., Fauchier, L., Richter, A., Tavazzi, L., Arbustini, E., Wichter, T., Maisch, B., Komajda, M., et al. (2009). Mutations in the ANKRD1 gene encoding CARP are responsible for human dilated cardiomyopathy. Eur. Heart J *30*, 2128–2136.

Fernando, P., Sandoz, J.S., Ding, W., de Repentigny, Y., Brunette, S., Kelly, J.F., Kothary, R., and Megeney, L.A. (2009). Bin1 SRC homology 3 domain acts as a scaffold for myofiber sarcomere assembly. J. Biol. Chem *284*, 27674–27686.

Fimia, G.M., De Cesare, D., and Sassone-Corsi, P. (2000). A family of LIM-only transcriptional coactivators: tissue-specific expression and selective activation of CREB and CREM. Mol. Cell. Biol. *20*, 8613–8622.

Flick, M.J., and Konieczny, S.F. (2000). The muscle regulatory and structural protein MLP is a cytoskeletal binding partner of betaI-spectrin. J Cell Sci *113 (Pt 9)*, 1553–1564.

Freiburg, A., and Gautel, M. (1996). A molecular map of the interactions between titin and myosin-binding protein C. Implications for sarcomeric assembly in familial hypertrophic cardiomyopathy. Eur J Biochem *235*, 317–323.

Freiburg, A., Trombitas, K., Hell, W., Cazorla, O., Fougerousse, F., Centner, T., Kolmerer, B., Witt, C., Beckmann, J.S., Gregorio, C.C., et al. (2000). Series of exon-skipping events in the elastic spring region of titin as the structural basis for myofibrillar elastic diversity. Circ Res *86*, 1114–1121.

Fukuzawa, A., Lange, S., Holt, M., Vihola, A., Carmignac, V., Ferreiro, A., Udd, B., and Gautel, M. (2008). Interactions with titin and myomesin target obscurin and obscurin-like 1 to the M-band: implications for hereditary myopathies. J Cell Sci *121*, 1841–1851.

Furst, D.O., Osborn, M., Nave, R., and Weber, K. (1988). The organization of titin filaments in the half-sarcomere revealed by monoclonal antibodies in immunoelectron microscopy: a map of ten nonrepetitive epitopes starting at the Z line extends close to the M line. J Cell Biol *106*, 1563–1572.

Furst, D.O., Vinkemeier, U., and Weber, K. (1992). Mammalian skeletal muscle C-protein: purification from bovine muscle, binding to titin and the characterization of a full-length human cDNA. J Cell Sci *102 (Pt 4)*, 769–778.

Furukawa, T., Ono, Y., Tsuchiya, H., Katayama, Y., Bang, M.L., Labeit, D., Labeit, S., Inagaki, N., and Gregorio, C.C. (2001). Specific Interaction of the Potassium Channel beta-subunit minK with the Sarcomeric Protein T-CAP Suggests a T-tubule-Myofibril Linking System. J Mol Biol *313*, 775–784.

Garvey, S.M., Rajan, C., Lerner, A.P., Frankel, W.N., and Cox, G.A. (2002). The muscular dystrophy with myositis (mdm) mouse mutation disrupts a skeletal muscle-specific domain of titin. Genomics *79*, 146–149.

Gautel, M., Leonard, K., and Labeit, S. (1993). Phosphorylation of KSP motifs in the C-terminal region of titin in differentiating myoblasts. EMBO J *12*, 3827–3834.

Gautel, M., Castiglione, M., Pfuhl, M., Motta, A., and Pastore, A. (1995). A calmodulin-binding sequence in the C-terminus of human cardiac titin kinase. Eur J Biochem *230*, 752–759.

Gautel, M., Goulding, D., Bullard, B., Weber, K., and Fürst, D.O. (1996). The central Z-disk region of titin is assembled from a novel repeat in variable copy numbers. J. Cell. Sci *109 (Pt 11)*, 2747–2754.

Geetha, T., and Wooten, M.W. (2002). Structure and functional properties of the ubiquitin binding protein p62. FEBS Lett *512*, 19–24.

Gerull, B., Gramlich, M., Atherton, J., McNabb, M., Trombitas, K., Sasse-Klaassen, S., Seidman, J.G., Seidman, C., Granzier, H., Labeit, S., et al. (2002). Mutations of TTN, encoding the giant muscle filament titin, cause familial dilated cardiomyopathy. Nat Genet *30*, 201–204.

Gerull, B., Atherton, J., Geupel, A., Sasse-Klaassen, S., Heuser, A., Frenneaux, M., McNabb, M., Granzier, H., Labeit, S., and Thierfelder, L. (2006). Identification of a novel frameshift mutation in the giant muscle filament titin in a large Australian family with dilated cardiomyopathy. J. Mol. Med *84*, 478–483.

Glass, D.J. (2003). Signalling pathways that mediate skeletal muscle hypertrophy and atrophy. Nat Cell Biol *5*, 87–90.

Glass, D.J. (2005). Skeletal muscle hypertrophy and atrophy signaling pathways. Int J Biochem Cell Biol.

Goldfarb, L.G., and Dalakas, M.C. (2009). Tragedy in a heartbeat: malfunctioning desmin causes skeletal and cardiac muscle disease. J. Clin. Invest *119*, 1806–1813.

Golenhofen, N., Arbeiter, A., Koob, R., and Drenckhahn, D. (2002). Ischemia-induced association of the stress protein alpha B-crystallin with I-band portion of cardiac titin. J Mol Cell Cardiol *34*, 309–319.

Gotthardt, M., Hammer, R.E., Hubner, N., Monti, J., Witt, C.C., McNabb, M., Richardson, J.A., Granzier, H., Labeit, S., and Herz, J. (2003). Conditional expression of mutant M-line titins results in cardiomyopathy with altered sarcomere structure. J Biol Chem *278*, 6059–6065.

Granzier, H.L., and Irving, T.C. (1995). Passive tension in cardiac muscle: contribution of collagen, titin, microtubules, and intermediate filaments. Biophys J *68*, 1027–1044.

Granzier, H.L., and Labeit, S. (2006). The giant muscle protein titin is an adjustable molecular spring. Exerc Sport Sci Rev *34*, 50–53.

Granzier, H.L., Radke, M.H., Peng, J., Westermann, D., Nelson, O.L., Rost, K., King, N.M.P., Yu, Q., Tschöpe, C., McNabb, M., et al. (2009). Truncation of titin's elastic PEVK region leads to cardiomyopathy with diastolic dysfunction. Circ. Res *105*, 557–564.

Granzier, H.L., Hutchinson, K.R., Tonino, P., Methawasin, M., Li, F.W., Slater, R.E., Bull, M.M., Saripalli, C., Pappas, C.T., Gregorio, C.C., et al. (2014). Deleting titin's I-band/A-band junction reveals critical roles for titin in biomechanical sensing and cardiac function. Proc. Natl. Acad. Sci. U.S.A. *111*, 14589–14594.

Greaser, M.L., Wang, S.M., Berri, M., Mozdziak, P., and Kumazawa, Y. (2000). Sequence and mechanical implications of titin's PEVK region. Adv. Exp. Med. Biol *481*, 53–63; discussion 64–66, 107–110.

Greaser, M.L., Krzesinski, P.R., Warren, C.M., Kirkpatrick, B., Campbell, K.S., and Moss, R.L. (2005). Developmental changes in rat cardiac titin/connectin: transitions in normal animals and in mutants with a delayed pattern of isoform transition. J Muscle Res Cell Motil *26*, 325–332.

Gregorio, C.C., Trombitás, K., Centner, T., Kolmerer, B., Stier, G., Kunke, K., Suzuki, K., Obermayr, F., Herrmann, B., Granzier, H., et al. (1998). The NH2 terminus of titin spans the Z-disc: its interaction with a novel 19-kD ligand (T-CAP) is required for sarcomeric integrity. J Cell Biol *143*, 1013–1027.

Gregorio, C.C., Granzier, H., Sorimachi, H., and Labeit, S. (1999). Muscle assembly: a titanic achievement? Curr Opin Cell Biol *11*, 18–25.

Gregorio, C.C., Perry, C.N., and McElhinny, A.S. (2005). Functional properties of the titin/connectin-associated proteins, the muscle-specific RING finger proteins (MURFs), in striated muscle. J. Muscle Res. Cell. Motil *26*, 389–400.

Griffin, T.J., Gygi, S.P., Ideker, T., Rist, B., Eng, J., Hood, L., and Aebersold, R. (2002). Complementary profiling of gene expression at the transcriptome and proteome levels in Saccharomyces cerevisiae. Mol. Cell Proteomics *1*, 323–333.

Hackman, P., Vihola, A., Haravuori, H., Marchand, S., Sarparanta, J., De Seze, J., Labeit, S., Witt, C., Peltonen, L., Richard, I., et al. (2002). Tibial muscular dystrophy is a

titinopathy caused by mutations in TTN, the gene encoding the giant skeletal-muscle protein titin. Am J Hum Genet *71*, 492–500.

Hackman, P., Marchand, S., Sarparanta, J., Vihola, A., Pénisson-Besnier, I., Eymard, B., Pardal-Fernández, J.M., Hammouda, E.-H., Richard, I., Illa, I., et al. (2008). Truncating mutations in C-terminal titin may cause more severe tibial muscular dystrophy (TMD). Neuromuscul. Disord *18*, 922–928.

Hayashi, D., Kudoh, S., Shiojima, I., Zou, Y., Harada, K., Shimoyama, M., Imai, Y., Monzen, K., Yamazaki, T., Yazaki, Y., et al. (2004a). Atrial natriuretic peptide inhibits cardiomyocyte hypertrophy through mitogen-activated protein kinase phosphatase-1. Biochem Biophys Res Commun *322*, 310–319.

Hayashi, T., Arimura, T., Itoh-Satoh, M., Ueda, K., Hohda, S., Inagaki, N., Takahashi, M., Hori, H., Yasunami, M., Nishi, H., et al. (2004b). Tcap gene mutations in hypertrophic cardiomyopathy and dilated cardiomyopathy. J. Am. Coll. Cardiol. *44*, 2192–2201.

Hein, S., and Schaper, J. (2002). Weakness of a giant: mutations of the sarcomeric protein titin. Trends Mol Med *8*, 311–313.

Heineke, J., and Molkentin, J.D. (2006). Regulation of cardiac hypertrophy by intracellular signalling pathways. Nat Rev Mol Cell Biol *7*, 589–600.

Herman, D.S., Lam, L., Taylor, M.R.G., Wang, L., Teekakirikul, P., Christodoulou, D., Conner, L., DePalma, S.R., McDonough, B., Sparks, E., et al. (2012). Truncations of titin causing dilated cardiomyopathy. N. Engl. J. Med. *366*, 619–628.

Hershberger, R.E., and Morales, A. (1993). Dilated Cardiomyopathy Overview. In GeneReviews™, R.A. Pagon, M.P. Adam, T.D. Bird, C.R. Dolan, C.-T. Fong, and K. Stephens, eds. (Seattle (WA): University of Washington, Seattle),.

Hershberger, R.E., Parks, S.B., Kushner, J.D., Li, D., Ludwigsen, S., Jakobs, P., Nauman, D., Burgess, D., Partain, J., and Litt, M. (2008). Coding sequence mutations identified in MYH7, TNNT2, SCN5A, CSRP3, LBD3, and TCAP from 313 patients with familial or idiopathic dilated cardiomyopathy. Clin Transl Sci *1*, 21–26.

Heusch, M., Lin, L., Geleziunas, R., and Greene, W.C. (1999). The generation of nfkb2 p52: mechanism and efficiency. Oncogene *18*, 6201–6208.

Hidalgo, C.G., Chung, C.S., Saripalli, C., Methawasin, M., Hutchinson, K.R., Tsaprailis, G., Labeit, S., Mattiazzi, A., and Granzier, H.L. (2012). The multifunctional Ca(2+)/calmodulin-dependent protein kinase II delta (CaMKIIδ) phosphorylates cardiac titin's spring elements. J. Mol. Cell. Cardiol.

Hornemann, T., Kempa, S., Himmel, M., Hayess, K., Furst, D.O., and Wallimann, T. (2003). Muscle-type creatine kinase interacts with central domains of the M-band proteins myomesin and M-protein. J Mol Biol *332*, 877–887.

Houmeida, A., Holt, J., Tskhovrebova, L., and Trinick, J. (1995). Studies of the interaction between titin and myosin. J Cell Biol *131*, 1471–1481.

Houser, S.R., and Molkentin, J.D. (2008). Does contractile Ca2+ control calcineurin-NFAT signaling and pathological hypertrophy in cardiac myocytes? Sci Signal *1*, pe31.

Huang, J., and Forsberg, N.E. (1998). Role of calpain in skeletal-muscle protein degradation. Proc. Natl. Acad. Sci. U.S.A. *95*, 12100–12105.

Hudson, B.D., Hidalgo, C.G., Gotthardt, M., and Granzier, H.L. (2010). Excision of titin's cardiac PEVK spring element abolishes PKCalpha-induced increases in myocardial stiffness. J. Mol. Cell. Cardiol *48*, 972–978.

Hunter, R.B., and Kandarian, S.C. (2004). Disruption of either the Nfkb1 or the Bcl3 gene inhibits skeletal muscle atrophy. J. Clin. Invest. *114*, 1504–1511.

Ikeda, Y., Aihara, K., Sato, T., Akaike, M., Yoshizumi, M., Suzaki, Y., Izawa, Y., Fujimura, M., Hashizume, S., Kato, M., et al. (2005). Androgen receptor gene knockout male mice exhibit impaired cardiac growth and exacerbation of angiotensin II-induced cardiac fibrosis. J Biol Chem *280*, 29661–29666.

Itoh-Satoh, M., Hayashi, T., Nishi, H., Koga, Y., Arimura, T., Koyanagi, T., Takahashi, M., Hohda, S., Ueda, K., Nouchi, T., et al. (2002). Titin mutations as the molecular basis for dilated cardiomyopathy. Biochem Biophys Res Commun *291*, 385–393.

Izumi, R., Niihori, T., Aoki, Y., Suzuki, N., Kato, M., Warita, H., Takahashi, T., Tateyama, M., Nagashima, T., Funayama, R., et al. (2013). Exome sequencing identifies a novel TTN mutation in a family with hereditary myopathy with early respiratory failure. J. Hum. Genet. *58*, 259–266.

Jackman, R.W., and Kandarian, S.C. (2004). The molecular basis of skeletal muscle atrophy. Am J Physiol Cell Physiol *287*, C834–C843.

Jeyaseelan, R., Poizat, C., Baker, R.K., Abdishoo, S., Isterabadi, L.B., Lyons, G.E., and Kedes, L. (1997). A novel cardiac-restricted target for doxorubicin. CARP, a nuclear modulator of gene expression in cardiac progenitor cells and cardiomyocytes. J. Biol. Chem *272*, 22800–22808.

Ji, Y., Lalli, M.J., Babu, G.J., Xu, Y., Kirkpatrick, D.L., Liu, L.H., Chiamvimonvat, N., Walsh, R.A., Shull, G.E., and Periasamy, M. (2000). Disruption of a single copy of the SERCA2 gene results in altered Ca2+ homeostasis and cardiomyocyte function. J Biol Chem *275*, 38073–38080.

Johannessen, M., Moller, S., Hansen, T., Moens, U., and Ghelue, M.V. (2006). The multifunctional roles of the four-and-a-half-LIM only protein FHL2. Cell Mol Life Sci *63*, 268–284.

Kaul, A., Koster, M., Neuhaus, H., and Braun, T. (2000). Myf-5 revisited: loss of early myotome formation does not lead to a rib phenotype in homozygous Myf-5 mutant mice. Cell *102*, 17–19.

Kelly, D.E. (1969). Myofibrillogenesis and Z-band differentiation. Anat. Rec *163*, 403–425.

Kim, J., Won, K.-J., Lee, H.M., Hwang, B.-Y., Bae, Y.-M., Choi, W.S., Song, H., Lim, K.W., Lee, C.-K., and Kim, B. (2009). p38 MAPK Participates in Muscle-Specific RING Finger 1-Mediated Atrophy in Cast-Immobilized Rat Gastrocnemius Muscle. Korean J. Physiol. Pharmacol *13*, 491–496.

Kinbara, K., Sorimachi, H., Ishiura, S., and Suzuki, K. (1997). Muscle-specific calpain, p94, interacts with the extreme C-terminal region of connectin, a unique region flanked by two immunoglobulin C2 motifs. Arch Biochem Biophys *342*, 99–107.

Kirkin, V., Lamark, T., Johansen, T., and Dikic, I. (2009a). NBR1 cooperates with p62 in selective autophagy of ubiquitinated targets. Autophagy *5*, 732–733.

Kirkin, V., Lamark, T., Sou, Y.-S., Bjørkøy, G., Nunn, J.L., Bruun, J.-A., Shvets, E., McEwan, D.G., Clausen, T.H., Wild, P., et al. (2009b). A role for NBR1 in autophagosomal degradation of ubiquitinated substrates. Mol. Cell *33*, 505–516.

Kolmerer, B., Olivieri, N., Witt, C.C., Herrmann, B.G., and Labeit, S. (1996). Genomic organization of M line titin and its tissue-specific expression in two distinct isoforms. J. Mol. Biol *256*, 556–563.

Kontrogianni-Konstantopoulos, A., and Bloch, R.J. (2003). The hydrophilic domain of small ankyrin-1 interacts with the two N-terminal immunoglobulin domains of titin. J. Biol. Chem *278*, 3985–3991.

Kontrogianni-Konstantopoulos, A., Catino, D.H., Strong, J.C., Randall, W.R., and Bloch, R.J. (2004). Obscurin regulates the organization of myosin into A bands. Am J Physiol Cell Physiol *287*, C209–C217.

Kramer, H.F., and Goodyear, L.J. (2007). Exercise, MAPK, and NF-kappaB signaling in skeletal muscle. J. Appl. Physiol. *103*, 388–395.

Kreusser, M.M., Lehmann, L.H., Keranov, S., Hoting, M.-O., Kohlhaas, M., Reil, J.-C., Neumann, K., Schneider, M.D., Hill, J.A., Dobrev, D., et al. (2014). The Cardiac CaMKII Genes δ and γ Contribute Redundantly to Adverse Remodeling but Inhibit Calcineurin-Induced Myocardial Hypertrophy. Circulation.

Labeit, S., Barlow, D.P., Gautel, M., Gibson, T., Holt, J., Hsieh, C.L., Francke, U., Leonard, K., Wardale, J., Whiting, A., et al. (1990). A regular pattern of two types of 100-residue motif in the sequence of titin. Nature *345*, 273–276.

Labeit, S., Gautel, M., Lakey, A., and Trinick, J. (1992). Towards a molecular understanding of titin. EMBO J *11*, 1711–1716.

Labeit, S., Kolmerer, B., and Linke, W.A. (1997). The giant protein titin. Emerging roles in physiology and pathophysiology. Circ Res *80*, 290–294.

Labeit, S., Lahmers, S., Burkart, C., Fong, C., McNabb, M., Witt, S., Witt, C., Labeit, D., and Granzier, H. (2006). Expression of distinct classes of titin isoforms in striated and smooth muscles by alternative splicing, and their conserved interaction with filamins. J Mol Biol *362*, 664–681.

Laemmli, U.K. (1970). Cleavage of structural proteins during the assembly of the head of bacteriophage T4. Nature *227*, 680–685.

Lahmers, S., Wu, Y., Call, D.R., Labeit, S., and Granzier, H. (2004). Developmental control of titin isoform expression and passive stiffness in fetal and neonatal myocardium. Circ. Res *94*, 505–513.

Lange, S., Auerbach, D., McLoughlin, P., Perriard, E., Schäfer, B.W., Perriard, J.-C., and Ehler, E. (2002). Subcellular targeting of metabolic enzymes to titin in heart muscle may be mediated by DRAL/FHL-2. J. Cell. Sci. *115*, 4925–4936.

Lange, S., Xiang, F., Yakovenko, A., Vihola, A., Hackman, P., Rostkova, E., Kristensen, J., Brandmeier, B., Franzen, G., Hedberg, B., et al. (2005). The Kinase Domain of Titin Controls Muscle Gene Expression and Protein Turnover. Science *308*, 1599–1603.

Lange, S., Agarkova, I., Perriard, J.C., and Ehler, E. (2006). The sarcomeric M-band during development and in disease. J Muscle Res Cell Motil 1–5.

Leychenko, A., Konorev, E., Jijiwa, M., and Matter, M.L. (2011). Stretch-induced hypertrophy activates NFkB-mediated VEGF secretion in adult cardiomyocytes. PLoS ONE *6*, e29055.

Linke, W.A. (2008). Sense and stretchability: the role of titin and titin-associated proteins in myocardial stress-sensing and mechanical dysfunction. Cardiovasc. Res *77*, 637–648.

Linke, W.A., Ivemeyer, M., Olivieri, N., Kolmerer, B., Ruegg, J.C., and Labeit, S. (1996). Towards a molecular understanding of the elasticity of titin. J Mol Biol *261*, 62–71.

Linke, W.A., Ivemeyer, M., Labeit, S., Hinssen, H., Ruegg, J.C., and Gautel, M. (1997). Actin-titin interaction in cardiac myofibrils: probing a physiological role. Biophys J *73*, 905–919.

Linke, W.A., Ivemeyer, M., Mundel, P., Stockmeier, M.R., and Kolmerer, B. (1998). Nature of PEVK-titin elasticity in skeletal muscle. Proc Natl Acad Sci U S A *95*, 8052–8057.

Linke, W.A., Rudy, D.E., Centner, T., Gautel, M., Witt, C., Labeit, S., and Gregorio, C.C. (1999). I-band titin in cardiac muscle is a three-element molecular spring and is critical for maintaining thin filament structure. J. Cell Biol. *146*, 631–644.

Lips, D.J., Bueno, O.F., Wilkins, B.J., Purcell, N.H., Kaiser, R.A., Lorenz, J.N., Voisin, L., Saba-El-Leil, M.K., Meloche, S., Pouyssegur, J., et al. (2004). MEK1-ERK2 signaling pathway protects myocardium from ischemic injury in vivo. Circulation *109*, 1938–1941.

Liu, J.P., Schlosser, R., Ma, W.Y., Dong, Z., Feng, H., Liu, L., Huang, X.Q., Liu, Y., and Li, D.W. (2004). Human alphaA- and alphaB-crystallins prevent UVA-induced apoptosis through regulation of PKCalpha, RAF/MEK/ERK and AKT signaling pathways. Exp Eye Res *79*, 393–403.

Liu, Q., Chen, Y., Auger-Messier, M., and Molkentin, J.D. (2012). Interaction between NFκB and NFAT coordinates cardiac hypertrophy and pathological remodeling. Circ. Res. *110*, 1077–1086.

Van der Loop, F.T., van, D., Furst, D.O., Gautel, M., van Eys, G.J., and Ramaekers, F.C. (1996). Integration of titin into the sarcomeres of cultured differentiating human skeletal muscle cells. Eur J Cell Biol *69*, 301–307.

Ma, K., and Wang, K. (2002). Interaction of nebulin SH3 domain with titin PEVK and myopalladin: implications for the signaling and assembly role of titin and nebulin. FEBS Lett *532*, 273–278.

MacLennan, D.H., and Kranias, E.G. (2003). Phospholamban: a crucial regulator of cardiac contractility. Nat Rev Mol Cell Biol *4*, 566–577.

Maruyama, K., and Ebashi, S. (1965). Alpha-actinin, a new structural protein from striated muscle. II. Action on actin. J. Biochem *58*, 13–19.

Maruyama, K., Murakami, F., and Ohashi, K. (1977). Connectin, an elastic protein of muscle. Comparative Biochemistry. J Biochem (Tokyo) *82*, 339–345.

Maruyama, K., Kimura, S., Ohashi, K., and Kuwano, Y. (1981). Connectin, an elastic protein of muscle. Identification of "titin" with connectin. J. Biochem *89*, 701–709.

Matsumoto, Y., Hayashi, T., Inagaki, N., Takahashi, M., Hiroi, S., Nakamura, T., Arimura, T., Nakamura, K., Ashizawa, N., Yasunami, M., et al. (2005). Functional analysis of titin/connectin N2-B mutations found in cardiomyopathy. J Muscle Res Cell Motil *26*, 367–374.

Mayans, O., van der Ven, P.F., Wilm, M., Mues, A., Young, P., Fürst, D.O., Wilmanns, M., and Gautel, M. (1998). Structural basis for activation of the titin kinase domain during myofibrillogenesis. Nature *395*, 863–869.

McElhinney, D.B., Geiger, E., Blinder, J., Benson, D.W., and Goldmuntz, E. (2003). NKX2.5 mutations in patients with congenital heart disease. J Am Coll Cardiol *42*, 1650–1655.

McElhinny, A.S., Labeit, S., and Gregorio, C.C. (2000). Probing the functional roles of titin ligands in cardiac myofibril assembly and maintenance. Adv Exp Med Biol *481*, 67–86.

McElhinny, A.S., Kakinuma, K., Sorimachi, H., Labeit, S., and Gregorio, C.C. (2002). Muscle-specific RING finger-1 interacts with titin to regulate sarcomeric M-line and thick filament structure and may have nuclear functions via its interaction with glucocorticoid modulatory element binding protein-1. J Cell Biol *157*, 125–136.

McElhinny, A.S., Perry, C.N., Witt, C.C., Labeit, S., and Gregorio, C.C. (2004). Muscle-specific RING finger-2 (MURF-2) is important for microtubule, intermediate filament and sarcomeric M-line maintenance in striated muscle development. J Cell Sci *Pt*.

McGrath, M.J., Cottle, D.L., Nguyen, M.-A., Dyson, J.M., Coghill, I.D., Robinson, P.A., Holdsworth, M., Cowling, B.S., Hardeman, E.C., Mitchell, C.A., et al. (2006). Four and a

half LIM protein 1 binds myosin-binding protein C and regulates myosin filament formation and sarcomere assembly. J Biol Chem *281*, 7666–7683.

McNally, E.M., de Sa, M., Duggan, D.J., Bonnemann, C.G., Lisanti, M.P., Lidov, H.G.W., Vainzof, M., Passos-Bueno, M.R., Hoffman, E.P., Zatz, M., et al. (1998). Caveolin-3 in muscular dystrophy. Hum Mol Genet *7*, 871–877.

Miller, M.K., Bang, M.L., Witt, C.C., Labeit, D., Trombitas, C., Watanabe, K., Granzier, H., McElhinny, A.S., Gregorio, C.C., and Labeit, S. (2003). The Muscle Ankyrin Repeat Proteins: CARP, ankrd2/Arpp and DARP as a Family of Titin Filament-based Stress Response Molecules. J Mol Biol *333*, 951–964.

Minamisawa, S., Gu, Y., Ross, J.J., Chien, K.R., and Chen, J. (1999). A post-transcriptional compensatory pathway in heterozygous ventricular myosin light chain 2-deficient mice results in lack of gene dosage effect during normal cardiac growth or hypertrophy. J Biol Chem *274*, 10066–10070.

Monroy, J.A., Powers, K.L., Gilmore, L.A., Uyeno, T.A., Lindstedt, S.L., and Nishikawa, K.C. (2012). What Is the Role of Titin in Active Muscle? Exerc Sport Sci Rev *40*, 73–78.

Mounkes, L.C., Kozlov, S.V., Rottman, J.N., and Stewart, C.L. (2005). Expression of an LMNA-N195K variant of A-type lamins results in cardiac conduction defects and death in mice. Hum Mol Genet *14*, 2167–2180.

Mues, A., van der Ven, P.F., Young, P., Fürst, D.O., and Gautel, M. (1998). Two immunoglobulin-like domains of the Z-disc portion of titin interact in a conformation-dependent way with telethonin. FEBS Lett *428*, 111–114.

Müller, J.M., Isele, U., Metzger, E., Rempel, A., Moser, M., Pscherer, A., Breyer, T., Holubarsch, C., Buettner, R., and Schüle, R. (2000). FHL2, a novel tissue-specific coactivator of the androgen receptor. EMBO J. *19*, 359–369.

Muller-Seitz, M., Kaupmann, K., Labeit, S., and Jockusch, H. (1993). Chromosomal localization of the mouse titin gene and its relation to “muscular dystrophy with myositis” and nebulin genes on chromosome 2. Genomics *18*, 559–561.

Musa, H., Meek, S., Gautel, M., Peddie, D., Smith, A.J.H., and Peckham, M. (2006). Targeted homozygous deletion of M-band titin in cardiomyocytes prevents sarcomere formation. J. Cell. Sci. *119*, 4322–4331.

Nagueh, S.F., Shah, G., Wu, Y., Torre-Amione, G., King, N.M.P., Lahmers, S., Witt, C.C., Becker, K., Labeit, S., and Granzier, H.L. (2004). Altered titin expression, myocardial stiffness, and left ventricular function in patients with dilated cardiomyopathy. Circulation *110*, 155–162.

Nakamura, K., Kimple, A.J., Siderovski, D.P., and Johnson, G.L. (2010). PB1 domain interaction of p62/sequestosome 1 and MEKK3 regulates NF-kappaB activation. J. Biol. Chem. *285*, 2077–2089.

Nave, R., Furst, D.O., and Weber, K. (1989). Visualization of the polarity of isolated titin molecules: a single globular head on a long thin rod as the M band anchoring domain? J Cell Biol *109*, 2177–2187.

Neagoe, C., Opitz, C.A., Makarenko, I., and Linke, W.A. (2003). Gigantic variety: expression patterns of titin isoforms in striated muscles and consequences for myofibrillar passive stiffness. J Muscle Res Cell Motil *24*, 175–189.

Nedrud, J., Labeit, S., Gotthardt, M., and Granzier, H. (2011). Mechanics on Myocardium Deficient in the N2B Region of Titin: The Cardiac-Unique Spring Element Improves Efficiency of the Cardiac Cycle. Biophys. J *101*, 1385–1392.

Neuhoff, V., Arold, N., Taube, D., and Ehrhardt, W. (1988). Improved staining of proteins in polyacrylamide gels including isoelectric focusing gels with clear background at nanogram sensitivity using Coomassie Brilliant Blue G-250 and R-250. Electrophoresis *9*, 255–262.

Neyroud, N., Richard, P., Vignier, N., Donger, C., Denjoy, I., Demay, L., Shkolnikova, M., Pesce, R., Chevalier, P., Hainque, B., et al. (1999). Genomic organization of the KCNQ1 K+ channel gene and identification of C-terminal mutations in the long-QT syndrome. Circ. Res *84*, 290–297.

Nishikawa, K.C., Monroy, J.A., Uyeno, T.E., Yeo, S.H., Pai, D.K., and Lindstedt, S.L. (2012). Is titin a "winding filament"? A new twist on muscle contraction. Proc. Biol. Sci. *279*, 981–990.

Oakley, C.E., Chamoun, J., Brown, L.J., and Hambly, B.D. (2007). Myosin binding protein-C: enigmatic regulator of cardiac contraction. Int. J. Biochem. Cell Biol *39*, 2161–2166.

Obermann, W.M., Gautel, M., Steiner, F., van der Ven, P.F., Weber, K., and Furst, D.O. (1996). The structure of the sarcomeric M band: localization of defined domains of myomesin, M-protein, and the 250-kD carboxy-terminal region of titin by immunoelectron microscopy. J Cell Biol *134*, 1441–1453.

Obermann, W.M., Gautel, M., Weber, K., and Furst, D.O. (1997). Molecular structure of the sarcomeric M band: mapping of titin and myosin binding domains in myomesin and the identification of a potential regulatory phosphorylation site in myomesin. EMBO J *16*, 211–220.

Ohlsson, M., Hedberg, C., Brådvik, B., Lindberg, C., Tajsharghi, H., Danielsson, O., Melberg, A., Udd, B., Martinsson, T., and Oldfors, A. (2012). Hereditary myopathy with early respiratory failure associated with a mutation in A-band titin. Brain *135*, 1682–1694.

Ohtsuka, H., Yajima, H., Maruyama, K., and Kimura, S. (1997). The N-terminal Z repeat 5 of connectin/titin binds to the C-terminal region of alpha-actinin. Biochem. Biophys. Res. Commun *235*, 1–3.

Opitz, C.A., Leake, M.C., Makarenko, I., Benes, V., and Linke, W.A. (2004). Developmentally regulated switching of titin size alters myofibrillar stiffness in the perinatal heart. Circ Res *94*, 967–975.

Ottenheijm, C.A.C., Knottnerus, A.M., Buck, D., Luo, X., Greer, K., Hoying, A., Labeit, S., and Granzier, H. (2009a). Tuning Passive Mechanics through Differential Splicing of Titin during Skeletal Muscle Development. Biophys. J *97*, 2277–2286.

Ottenheijm, C.A.C., Hidalgo, C., Rost, K., Gotthardt, M., and Granzier, H. (2009b). Altered contractility of skeletal muscle in mice deficient in titin's M-band region. J. Mol. Biol *393*, 10–26.

Palmio, J., Evilä, A., Chapon, F., Tasca, G., Xiang, F., Brådvik, B., Eymard, B., Echaniz-Laguna, A., Laporte, J., Kärppä, M., et al. (2014). Hereditary myopathy with early respiratory failure: occurrence in various populations. J. Neurol. Neurosurg. Psychiatr. *85*, 345–353.

Pan, H., Richards, A.A., Zhu, X., Joglar, J.A., Yin, H.L., and Garg, V. (2009). A novel mutation in LAMIN A/C is associated with isolated early-onset atrial fibrillation and progressive atrioventricular block followed by cardiomyopathy and sudden cardiac death. Heart Rhythm *6*, 707–710.

Park, D.S., Woodman, S.E., Schubert, W., Cohen, A.W., Frank, P.G., Chandra, M., Shirani, J., Razani, B., Tang, B., Jelicks, L.A., et al. (2002). Caveolin-1/3 double-knockout mice are viable, but lack both muscle and non-muscle caveolae, and develop a severe cardiomyopathic phenotype. Am J Pathol *160*, 2207–2217.

Paul, F.E., Hosp, F., and Selbach, M. (2011). Analyzing protein-protein interactions by quantitative mass spectrometry. Methods *54*, 387–395.

Peckham, M., Young, P., and Gautel, M. (1997). Constitutive and variable regions of Z-disk titin/connectin in myofibril formation: a dominant-negative screen. Cell Struct Funct *22*, 95–101.

Pelin, K., Ridanpää, M., Donner, K., Wilton, S., Krishnarajah, J., Laing, N., Kolmerer, B., Millevoi, S., Labeit, S., de la Chapelle, A., et al. (1997). Refined localisation of the genes for nebulin and titin on chromosome 2q allows the assignment of nebulin as a candidate gene for autosomal recessive nemaline myopathy. Eur. J. Hum. Genet *5*, 229–234.

Peng, J., Raddatz, K., Labeit, S., Granzier, H., and Gotthardt, M. (2006). Muscle atrophy in Titin M-line deficient mice. J Muscle Res Cell Motil 1–8.

Peng, J., Raddatz, K., Molkentin, J.D., Wu, Y., Labeit, S., Granzier, H., and Gotthardt, M. (2007). Cardiac hypertrophy and reduced contractility in hearts deficient in the titin kinase region. Circulation *115*, 743–751.

Perera, S., Holt, M.R., Mankoo, B.S., and Gautel, M. (2010). Developmental regulation of MURF ubiquitin ligases and autophagy proteins nbr1, p62/SQSTM1 and LC3 during cardiac myofibril assembly and turnover. Dev Biol.

Periasamy, M., Reed, T.D., Liu, L.H., Ji, Y., Loukianov, E., Paul, R.J., Nieman, M.L., Riddle, T., Duffy, J.J., Doetschman, T., et al. (1999). Impaired cardiac performance in heterozygous mice with a null mutation in the sarco(endo)plasmic reticulum Ca2+-ATPase isoform 2 (SERCA2) gene. J Biol Chem *274*, 2556–2562.

Pernigo, S., Fukuzawa, A., Bertz, M., Holt, M., Rief, M., Steiner, R.A., and Gautel, M. (2010). Structural insight into M-band assembly and mechanics from the titin-obscurin-like-1 complex. Proc Natl Acad Sci U S A.

Pfeffer, G., Povitz, M., Gibson, G.J., and Chinnery, P.F. (2014a). Diagnosis of muscle diseases presenting with early respiratory failure. J. Neurol.

Pfeffer, G., Barresi, R., Wilson, I.J., Hardy, S.A., Griffin, H., Hudson, J., Elliott, H.R., Ramesh, A.V., Radunovic, A., Winer, J.B., et al. (2014b). Titin founder mutation is a common cause of myofibrillar myopathy with early respiratory failure. J. Neurol. Neurosurg. Psychiatr. *85*, 331–338.

Pikkarainen, S., Tokola, H., Kerkela, R., Majalahti-Palviainen, T., Vuolteenaho, O., and Ruskoaho, H. (2003). Endothelin-1-specific activation of B-type natriuretic peptide gene via p38 mitogen-activated protein kinase and nuclear ETS factors. J Biol Chem *278*, 3969–3975.

Pizon, V., Iakovenko, A., van der Ven, P.F., Kelly, R., Fatu, C., Furst, D.O., Karsenti, E., and Gautel, M. (2002). Transient association of titin and myosin with microtubules in nascent myofibrils directed by the MURF2 RING-finger protein. J Cell Sci *115*, 4469–4482.

Pollazzon, M., Suominen, T., Penttilä, S., Malandrini, A., Carluccio, M.A., Mondelli, M., Marozza, A., Federico, A., Renieri, A., Hackman, P., et al. (2010). The first Italian family with tibial muscular dystrophy caused by a novel titin mutation. J. Neurol *257*, 575–579.

Prado, L.G., Makarenko, I., Andresen, C., Krüger, M., Opitz, C.A., and Linke, W.A. (2005). Isoform diversity of giant proteins in relation to passive and active contractile properties of rabbit skeletal muscles. J. Gen. Physiol *126*, 461–480.

Purcell, N.H., Darwis, D., Bueno, O.F., Muller, J.M., Schule, R., and Molkentin, J.D. (2004). Extracellular signal-regulated kinase 2 interacts with and is negatively regulated by the LIM-only protein FHL2 in cardiomyocytes. Mol Cell Biol *24*, 1081–1095.

Radke, M.H., Peng, J., Wu, Y., McNabb, M., Nelson, O.L., Granzier, H., and Gotthardt, M. (2007). Targeted deletion of titin N2B region leads to diastolic dysfunction and cardiac atrophy. Proc Natl Acad Sci U S A *104*, 3444–3449.

Rhee, D., Sanger, J.M., and Sanger, J.W. (1994). The premyofibril: evidence for its role in myofibrillogenesis. Cell Motil Cytoskeleton *28*, 1–24.

Richardson, P., McKenna, W., Bristow, M., Maisch, B., Mautner, B., O'Connell, J., Olsen, E., Thiene, G., Goodwin, J., Gyarfas, I., et al. (1996). Report of the 1995 World Health Organization/International Society and Federation of Cardiology Task Force on the Definition and Classification of cardiomyopathies. Circulation *93*, 841–842.

Rossi, E., Faiella, A., Zeviani, M., Labeit, S., Floridia, G., Brunelli, S., Cammarata, M., Boncinelli, E., and Zuffardi, O. (1994). Order of six loci at 2q24-q31 and orientation of the HOXD locus. Genomics *24*, 34–40.

Sanger, J.W., Ayoob, J.C., Chowrashi, P., Zurawski, D., and Sanger, J.M. (2000). Assembly of myofibrils in cardiac muscle cells. Adv Exp Med Biol *481*, 89–102.

Sanger, J.W., Sanger, J.M., and Franzini-Armstrong, C. (2004). Assembly of the skeletal muscle cell. In Myology, (New York, NY, USA: McGraw-Hill Professional), pp. 45–65.

Satoh, M., Takahashi, M., Sakamoto, T., Hiroe, M., Marumo, F., and Kimura, A. (1999). Structural analysis of the titin gene in hypertrophic cardiomyopathy: identification of a novel disease gene. Biochem Biophys Res Commun *262*, 411–417.

Schaffner, W., and Weissmann, C. (1973). A rapid, sensitive, and specific method for the determination of protein in dilute solution. Anal Biochem *56*, 502–514.

Schoenauer, R., Bertoncini, P., Machaidze, G., Aebi, U., Perriard, J.C., Hegner, M., and Agarkova, I. (2005). Myomesin is a molecular spring with adaptable elasticity. J Mol Biol *349*, 367–379.

Schoenauer, R., Lange, S., Hirschy, A., Ehler, E., Perriard, J.-C., and Agarkova, I. (2008). Myomesin 3, a novel structural component of the M-band in striated muscle. J. Mol. Biol *376*, 338–351.

Schultheiss, T., Lin, Z.X., Lu, M.H., Murray, J., Fischman, D.A., Weber, K., Masaki, T., Imamura, M., and Holtzer, H. (1990). Differential distribution of subsets of myofibrillar proteins in cardiac nonstriated and striated myofibrils. J Cell Biol *110*, 1159–1172.

Sebestyen, M.G., Fritz, J.D., Wolff, J.A., and Greaser, M.L. (1996). Primary structure of the kinase domain region of rabbit skeletal and cardiac muscle titin. J Muscle Res Cell Motil *17*, 343–348.

Seibenhener, M.L., Babu, J.R., Geetha, T., Wong, H.C., Krishna, N.R., and Wooten, M.W. (2004). Sequestosome 1/p62 is a polyubiquitin chain binding protein involved in ubiquitin proteasome degradation. Mol Cell Biol *24*, 8055–8068.

Shah, S.B., Peters, D., Jordan, K.A., Milner, D.J., Friden, J., Capetanaki, Y., and Lieber, R.L. (2001). Sarcomere number regulation maintained after immobilization in desmin-null mouse skeletal muscle. J Exp Biol *204*, 1703–1710.

Sheikh, F., Raskin, A., Chu, P.-H., Lange, S., Domenighetti, A.A., Zheng, M., Liang, X., Zhang, T., Yajima, T., Gu, Y., et al. (2008). An FHL1-containing complex within the cardiomyocyte sarcomere mediates hypertrophic biomechanical stress responses in mice. J Clin Invest *118*, 3870–3880.

Siebrands, C.C., Sanger, J.M., and Sanger, J.W. (2004). Myofibrillogenesis in skeletal muscle cells in the presence of taxol. Cell Motil. Cytoskeleton *58*, 39–52.

Smoot, M.E., Ono, K., Ruscheinski, J., Wang, P.-L., and Ideker, T. (2011). Cytoscape 2.8: new features for data integration and network visualization. Bioinformatics *27*, 431–432.

Song, Y., Xu, J., Li, Y., Jia, C., Ma, X., Zhang, L., Xie, X., Zhang, Y., Gao, X., Zhang, Y., et al. (2012). Cardiac ankyrin repeat protein attenuates cardiac hypertrophy by inhibition of ERK1/2 and TGF-β signaling pathways. PLoS ONE *7*, e50436.

Sorimachi, H., Kinbara, K., Kimura, S., Takahashi, M., Ishiura, S., Sasagawa, N., Sorimachi, N., Shimada, H., Tagawa, K., and Maruyama, K. (1995). Muscle-specific calpain, p94, responsible for limb girdle muscular dystrophy type 2A, associates with connectin through IS2, a p94-specific sequence. J Biol Chem *270*, 31158–31162.

Sorimachi, H., Freiburg, A., Kolmerer, B., Ishiura, S., Stier, G., Gregorio, C.C., Labeit, D., Linke, W.A., Suzuki, K., and Labeit, S. (1997). Tissue-specific expression and alpha-actinin binding properties of the Z-disc titin: implications for the nature of vertebrate Z-discs. J Mol Biol *270*, 688–695.

Tian, L.-F., Li, H.-Y., Jin, B.-F., Pan, X., Man, J.-H., Zhang, P.-J., Li, W.-H., Liang, B., Liu, H., Zhao, J., et al. (2006). MDM2 interacts with and downregulates a sarcomeric protein, TCAP. Biochem. Biophys. Res. Commun. *345*, 355–361.

Toro, C., Olivé, M., Dalakas, M.C., Sivakumar, K., Bilbao, J.M., Tyndel, F., Vidal, N., Farrero, E., Sambuughin, N., and Goldfarb, L.G. (2013). Exome sequencing identifies titin mutations causing hereditary myopathy with early respiratory failure (HMERF) in families of diverse ethnic origins. BMC Neurol *13*, 29.

Towbin, J.A., and Lorts, A. (2011). Arrhythmias and dilated cardiomyopathy common pathogenetic pathways? J. Am. Coll. Cardiol *57*, 2169–2171.

Trinick, J. (1996). Titin as a scaffold and spring. Cytoskeleton. Curr Biol *6*, 258–260.

Trinkle-Mulcahy, L., Boulon, S., Lam, Y.W., Urcia, R., Boisvert, F.-M., Vandermoere, F., Morrice, N.A., Swift, S., Rothbauer, U., Leonhardt, H., et al. (2008). Identifying specific protein interaction partners using quantitative mass spectrometry and bead proteomes. J. Cell Biol. *183*, 223–239.

Truett, G.E., Heeger, P., Mynatt, R.L., Truett, A.A., Walker, J.A., and Warman, M.L. (2000). Preparation of PCR-quality mouse genomic DNA with hot sodium hydroxide and tris (HotSHOT). BioTechniques *29*, 52, 54.

Tskhovrebova, L., and Trinick, J. (2003). Titin: properties and family relationships. Nat Rev Mol Cell Biol *4*, 679–689.

Tskhovrebova, L., and Trinick, J. (2004). Properties of titin immunoglobulin and fibronectin-3 domains. J. Biol. Chem *279*, 46351–46354.

Turnacioglu, K.K., Mittal, B., Dabiri, G.A., Sanger, J.M., and Sanger, J.W. (1997). An N-terminal fragment of titin coupled to green fluorescent protein localizes to the Z-bands in living muscle cells: overexpression leads to myofibril disassembly. Mol. Biol. Cell *8*, 705–717.

Valle, G., Faulkner, G., De Antoni, A., Pacchioni, B., Pallavicini, A., Pandolfo, D., Tiso, N., Toppo, S., Trevisan, S., and Lanfranchi, G. (1997). Telethonin, a novel sarcomeric protein of heart and skeletal muscle. FEBS Lett *415*, 163–168.

Vangheluwe, P., Tjwa, M., Van Den, B.A., Louch, W.E., Beullens, M., Dode, L., Carmeliet, P., Kranias, E., Herijgers, P., Sipido, K.R., et al. (2006). A SERCA2 pump with an increased Ca2+ affinity can lead to severe cardiac hypertrophy, stress intolerance and reduced life span. J Mol Cell Cardiol *41*, 308–317.

Vasli, N., Böhm, J., Le Gras, S., Muller, J., Pizot, C., Jost, B., Echaniz-Laguna, A., Laugel, V., Tranchant, C., Bernard, R., et al. (2012). Next generation sequencing for molecular diagnosis of neuromuscular diseases. Acta Neuropathol. *124*, 273–283.

Van der Ven, P.F., and Fürst, D.O. (1997). Assembly of titin, myomesin and M-protein into the sarcomeric M band in differentiating human skeletal muscle cells in vitro. Cell Struct. Funct. *22*, 163–171.

Van der Ven, P.F., Obermann, W.M., Weber, K., and Furst, D.O. (1996). Myomesin, M-protein and the structure of the sarcomeric M-band. Adv Biophys *33*, 91–99.

Van der Ven, P.F., Obermann, W.M., Lemke, B., Gautel, M., Weber, K., and Fürst, D.O. (2000). Characterization of muscle filamin isoforms suggests a possible role of gamma-filamin/ABP-L in sarcomeric Z-disc formation. Cell Motil. Cytoskeleton *45*, 149–162.

Vinkemeier, U., Obermann, W., Weber, K., and Furst, D.O. (1993). The globular head domain of titin extends into the center of the sarcomeric M band. cDNA cloning, epitope mapping and immunoelectron microscopy of two titin-associated proteins. J Cell Sci *106 (Pt 1)*, 319–330.

Wagner, S., Dybkova, N., Rasenack, E.C.L., Jacobshagen, C., Fabritz, L., Kirchhof, P., Maier, S.K.G., Zhang, T., Hasenfuss, G., Brown, J.H., et al. (2006). Ca2+/calmodulin-dependent protein kinase II regulates cardiac Na+ channels. J. Clin. Invest. *116*, 3127–3138.

Wang, K., and Wright, J. (1988). Architecture of the sarcomere matrix of skeletal muscle: immunoelectron microscopic evidence that suggests a set of parallel inextensible nebulin filaments anchored at the Z line. J. Cell Biol *107*, 2199–2212.

Wang, J., Sanger, J.M., and Sanger, J.W. (2005). Differential effects of Latrunculin-A on myofibrils in cultures of skeletal muscle cells: insights into mechanisms of myofibrillogenesis. Cell Motil. Cytoskeleton *62*, 35–47.

Wang, K., McClure, J., and Tu, A. (1979). Titin: major myofibrillar components of striated muscle. Proc Natl Acad Sci U S A *76*, 3698–3702.

Wang, S.M., Sun, M.C., and Jeng, C.J. (1991). Location of the C-terminus of titin at the Z-line region in the sarcomere. Biochem. Biophys. Res. Commun *176*, 189–193.

Wang, S.M., Jeng, C.J., and Sun, M.C. (1992). Studies on the interaction between titin and myosin. Histol. Histopathol *7*, 333–337.

Wang, S.M., Lo, M.C., Shang, C., Kao, S.C., and Tseng, Y.Z. (1998). Role of M-line proteins in sarcomeric titin assembly during cardiac myofibrillogenesis. J Cell Biochem *71*, 82–95.

Warren, C.M., Krzesinski, P.R., and Greaser, M.L. (2003). Vertical agarose gel electrophoresis and electroblotting of high-molecular-weight proteins. Electrophoresis *24*, 1695–1702.

Watanabe, Y., and Tanaka, M. (2011). p62/SQSTM1 in autophagic clearance of a non-ubiquitylated substrate. J. Cell. Sci. *124*, 2692–2701.

Watanabe, K., Nair, P., Labeit, D., Kellermayer, M., Greaser, M., Labeit, S., and Granzier, H. (2002). Molecular mechanics of cardiac titin's PEVK and N2B spring elements. J Biol Chem.

Wegner, A. (1979). Equilibrium of the actin-tropomyosin interaction. J. Mol. Biol *131*, 839–853.

Weinert, S., Bergmann, N., Luo, X., Erdmann, B., and Gotthardt, M. (2006). M line-deficient titin causes cardiac lethality through impaired maturation of the sarcomere. J Cell Biol *173*, 559–570.

Whiting, A., Wardale, J., and Trinick, J. (1989). Does titin regulate the length of muscle thick filaments? J. Mol. Biol *205*, 263–268.

Willis, M.S., Ike, C., Li, L., Wang, D.Z., Glass, D.J., and Patterson, C. (2007). Muscle Ring Finger 1, but not Muscle Ring Finger 2, Regulates Cardiac Hypertrophy In Vivo. Circ Res.

Witt, C.C., Burkart, C., Labeit, D., McNabb, M., Wu, Y., Granzier, H., and Labeit, S. (2006). Nebulin regulates thin filament length, contractility, and Z-disk structure in vivo. EMBO J *25*, 3843–3855.

Witt, S.H., Granzier, H., Witt, C.C., and Labeit, S. (2005). MURF-1 and MURF-2 target a specific subset of myofibrillar proteins redundantly: towards understanding MURF-dependent muscle ubiquitination. J. Mol. Biol. *350*, 713–722.

Wooldridge, A.A., Fortner, C.N., Lontay, B., Akimoto, T., Neppl, R.L., Facemire, C., Datto, M.B., Kwon, A., McCook, E., Li, P., et al. (2008). Deletion of the protein kinase A/protein kinase G target SMTNL1 promotes an exercise-adapted phenotype in vascular smooth muscle. J. Biol. Chem. *283*, 11850–11859.

Wu, C.-L., Cornwell, E.W., Jackman, R.W., and Kandarian, S.C. (2014). NF-κB but not FoxO sites in the MuRF1 promoter are required for transcriptional activation in disuse muscle atrophy. Am. J. Physiol., Cell Physiol. *306*, C762–C767.

Wu, Y., Labeit, S., LeWinter, M.M., and Granzier, H. (2002). Titin: an endosarcomeric protein that modulates myocardial stiffness in DCM. J Card Fail *8*, S276–S286.

Yamasaki, R., Berri, M., Wu, Y., Trombitas, K., McNabb, M., Kellermayer, M.S., Witt, C., Labeit, D., Labeit, S., Greaser, M., et al. (2001). Titin-actin interaction in mouse myocardium: passive tension modulation and its regulation by calcium/S100A1. Biophys J *81*, 2297–2313.

Yamasaki, R., Wu, Y., McNabb, M., Greaser, M., Labeit, S., and Granzier, H. (2002). Protein kinase A phosphorylates titin's cardiac-specific N2B domain and reduces passive tension in rat cardiac myocytes. Circ Res *90*, 1181–1188.

Yan, J., Seibenhener, M.L., Calderilla-Barbosa, L., Diaz-Meco, M.-T., Moscat, J., Jiang, J., Wooten, M.W., and Wooten, M.C. (2013). SQSTM1/p62 interacts with HDAC6 and regulates deacetylase activity. PLoS ONE *8*, e76016.

Yang, Z., Browning, C.F., Hallaq, H., Yermalitskaya, L., Esker, J., Hall, M.R., Link, A.J., Ham, A.-J.L., McGrath, M.J., Mitchell, C.A., et al. (2008). Four and a half LIM protein 1: a partner for KCNA5 in human atrium. Cardiovasc Res *78*, 449–457.

Young, P., Ferguson, C., Banuelos, S., and Gautel, M. (1998). Molecular structure of the sarcomeric Z-disk: two types of titin interactions lead to an asymmetrical sorting of alpha-actinin. EMBO J *17*, 1614–1624.

Young, P., Ehler, E., and Gautel, M. (2001). Obscurin, a giant sarcomeric Rho guanine nucleotide exchange factor protein involved in sarcomere assembly. J Cell Biol *154*, 123–136.

Zhou, D., Birkenmeier, C.S., Williams, M.W., Sharp, J.J., Barker, J.E., and Bloch, R.J. (1997). Small, membrane-bound, alternatively spliced forms of ankyrin 1 associated with the sarcoplasmic reticulum of mammalian skeletal muscle. J. Cell Biol *136*, 621–631.

Zou, P., Pinotsis, N., Lange, S., Song, Y.H., Popov, A., Mavridis, I., Mayans, O.M., Gautel, M., and Wilmanns, M. (2006). Palindromic assembly of the giant muscle protein titin in the sarcomeric Z-disk. Nature *439*, 229–233.

8 Abbreviations

ADP	adenosine di phosphate
AK	adenylate kinase
ANKRD2	muscle ankyrin repeat protein
APS	ammonium persulfate
AR	androgen receptor
AT	atria
ATP	adenosine tri phosphate
ATW	atria weight
BIN	bridging integrator protein
BKG	background
bp	base pair
BSA	bovine serum albumin
BW	body weight
CALM	calmodulin
cAMP	cyclic adenosine mono phosphate
CARP	cardiac ankyrin repeat protein
cDNA	complementary DNA
Chr	chromosome
CK	creatin kinase
CON	control
Cre	cre recombinase (causes recombination)
CREB	cAMP responsive element binding protein
CryAB	αB-Crystaline

Da	dalton
DARP	diabetes-related ankyrin repeat protein
DCM	dilated cardiomyopathy
ddH_2O	distilled water
DEPC	diethylpyrocarbonate
DMEM	Dulbecco's modified Eagle Medium
DMSO	dimethyl sulfoxide
DNA	deoxyribonucleic acid
DNase	deoxyribonuclease
dNTP	deoxynucleoside triphosphate
DTT	dithiothreitol
E	embryonic day post fertilization
ECL	enhanced chemiluminescence
EDL	extensor digitorum longus muscle
EDTA	ethylenediamine tetraacetic acid
EGTA	ethylene glycol-bis(2-aminoethylether)N,N,N′,N′tetraacetic acid
ELK	ETS domain containing protein
EM	electron microscopy
ES	embryonic stem cell
Ex	exon
F. C.	fold change
FA	formaldehyde
FAM	carboxyfluorescein
FBS	fetal bovine serum
FHL	four and a half LIM domain protein
Flp	flippase recombination enzyme

FN	fibronectin
for	forward
frt	flippase recognition target
GA	gastrocnemius
GATA	the GATA binding protein
HCM	hypertrophic cardiomyopathy
HE	heterozygous
HMERF	hereditary myopathy with early respiratory failure
HRP	horseradish peroxidase
Hsp	heat shock protein
HW	heart weight
Ig	immunoglobulin
IVC	individually ventilated cage
kDa	kilo Dalton
KO	knockout
LaGeSo	Animal Welfare of the German Society for Laboratory Animal Science
LGMD2A	limb-girdle muscular dystrophy type 2A
loxP-site	locus of crossing over-site
LV	left ventricle
LVW	left ventricle weight
MAPK/ERK	mitogen activated protein (MAP) kinase
MARP	muscle-ankyrin-repeat proteins

MCK	muscle creatin kinase
MDa	mega Dalton
MDC	Max-Delbrück-Centre
Mex	M-band exon
MHC	myosin heavy chain
MinK	potassium voltage-gated channel subfamily E member
MLC	myosin light chain
MLCK	myosin light-chain kinase
MLP	muscle LIM protein
mM	mili mol
mRNA	messenger RNA
MS	mass spectrometry
MURF	muscle-specific RING finger protein
MyBP	myosin binding protein
MYOM	myomesin
MYPN	myopalladin
NBR1	neighbor of Brca1 gene
Neo	neomycin
P.	polyacrylamide gel electrophoresis
PBS	phosphate buffered saline
PBS-T	PBS-Tween 20
PCR	polymerase chain reaction
PEVK	proline (P), glutamic acid (E), valine (V), and lysine (K) residues
PFA	paraformaldehyde
PFK	phospho fructo kinase
PKA	protein kinase A
PLN	phospholamban

PVDF	polyvinylidene difluoride
Q	quadriceps muscle
qMS	quantitative mass spectrometry
qRT-PCR	quantitative real-time PCR
rev	reverse
RNA	ribonucleic acid
RNase	ribonulease
rpm	revolution per minute
RT	room temperature
RT-PCR	reverse transcription PCR
RV	right ventricle
RVW	right ventricle weight
S100A	S100 calcium binding protein A
sANK	small ankyrin
SDS	sodium dodecyl sulfate
SEM	standard error of the mean
sHsp	small heat shock protein
SOL	soleus muscle
SQSTM/p62	sequestosome
SR	sarcoplasmic reticulum
SRF	serum response factor
TA	tibialis anterior muscle
TAE	tris-acetate EDTA
TAMRA	carboxytetramethylrhodamine
Taq	*Thermus aquaticus*

TBP	TATA-box binding protein
TBS-T	tris-buffered saline with Tween 20
T-CAP	titin cap or telethonin
TE	Tris-EDTA
TEMED	N, N, N′, N′-tetramethylethylendiamin
Ti	titin
TK	titin kinase
TMD	tibial muscular dystrophy
Tn	troponin
TPM	tropomyosin
Tris	tris(hydroxymethyl)-aminomethane
VAGE	vertical SDS-agarose gel electrophoresis
WB	Western blotting
WT	wild-type

9 List of figures

10 List of tables

Acknowledgement

First I would like to thank Prof. Dr. Michael Gotthardt for supervision. You gave me the opportunity to work in an excellently equipped laboratory on an exciting project. I'm very grateful for your encouragement and the freedom you gave me to explore research.

I thank Prof. Dr. Simone Spuler, leader of the MYOGRAD graduate school. You and MYOGRAD facilitated my studies and supported my education by allocation of so many instructive workshops, seminars, summer schools and retreats. It was a pleasure to be a part of MYOGRAD.

Furthermore I would like to thank the secretaries Sylvia Olbrich and Susanne Wissler for their kindness and helpfulness. You both helped me many times simplifying bureaucracy.

I am grateful to all the current and former members of the Gotthardt lab. I really enjoyed being your colleague and friend. I especially would like to thank the technicians Beate Golbrich Hannig and Carmen Judis. Your knowledge and technical assistance saved many time and rescued some experiments. Furthermore I would like to thank Mathias Pippow for his support in animal handling and making pictures. I know no better animal surgeon. I also would like to thank Franziska Rudolph for her help and expertise for fluorescence microscopy as well as Duoaa Megahed for her help and expertise in informatics. Thank you, Duoaa, for being the good soul of the lab.

I further would like to thank Dr. Michael Radke, Dr. Martin Liss and Dr. Peter Meinke for their support and supervision. Martin, I am very grateful for your constructive criticisms and your constitutive words at least during correction of my thesis. You're the best friend and colleague I know. Peter, I am happy about our friendship which survived your transmigration to Scotland. Thank you for being my friend and correction of my thesis.

Special thanks go to the animal caretakers Annika Ullmann and Mathias Grosser. Your regular observation of my mouse strains saved many time and fasted sample collection. I every time could rely on you if I was sick or in vacation.

I want to acknowledge Dr. Bettina Purfürst from the “Electron Microscopy Core Facility” for performing the EM analysis as well as Alina Dagane from the “Mass spectrometry facility” for performing quantitative MS analysis.

My family, but especially my parents Christine and Alexander Polack deserve special thanks for facilitating my studies. Without your love, support and encouragement I would never have come so far.

I also would like to thank my parents in law. Thank you for your support and your encouraging words.

Finally and over all I want to thank my wife Kathleen Polack. Thank you for your generous patience, encouragement, and endless faith in me and my work. Your unlimited love was the greatest support I had. I am so grateful to be your husband and a part of your life.

Curriculum vitae

For privacy protection the curriculum vitae is not included in online version.

Der Lebenslauf ist in der Online-Version aus Gründen des Datenschutzes nicht enthalten.